Spectroscopic Studies on the Molecular Structural Changes of Polymer Substrates and Polymer Adhesives Relevant to the Microelectronics Industry

by

Nathan W. Ulrich

A dissertation submitted in partial fulfillment
of the requirements for the degree of
Doctor of Philosophy
(Chemistry)
in the University of Michigan
2018

Doctoral Committee:

Professor Zhan Chen, Chair
Professor Jennifer Ogilvie
Professor Roseanne Sension
Professor Paul Zimmerman

nwulrich@umich.edu

ORCID iD: 0000-0003-1763-9268

DEDICATION

To my lovely wife Molly,

To Sam,

&

To Chauncey

ACKNOWLEDGEMENTS

I would like to thank my advisor, Professor Zhan Chen for his support on my PhD work. He gave me a somewhat stressful, somewhat frustrating, but mostly productive five years. He instructed and guided me towards my scientific accomplishment and academic targets. He supported me finically and granted me enough research freedom. The most important thing I learned from working with him was the interest in doing science, which is my future career goal upon graduation. I would like to thank professors Jennifer Ogilvie, Roseanne Sension, and Paul Zimmerman, for being on my thesis committee. I appreciate their time and effort for helping me achieve my doctoral degree.

I have met a lot of good people in the five years at Michigan. I appreciate the help from everybody in the Chen group. I want to sincerely thank all of the graduate students for helping me learn the techniques needed: Josh, Jesse, Jeanne, John, Chuan, Peipei, Yaoxin, Hao, Minyu; as well as all of the postdocs: Pei, Lei, Qiuming, Xingquan, Shuai, and Ganganath. I would like to especially thank my company members: Lirong, Wen, and John, who assisted in sample preparation and data collection.

I want to give my special thanks to my collaborators, without whom a large part of this thesis would not be possible. I appreciate Jaimal Williamson, Dr. Yuying Wei, and Dr. Yonghao Xiu, for their time and valuable discussion with me on my work.

I am grateful for the financial support from the Semiconductor Research Corporation. The funding supported me for parts of my graduate career as well as helped to supply me with the resources necessary to complete my work.

I want to thank my family, my sister, my father, mother, father-in-law, and mother-in-law. I especially want to thank my wife Molly, who had to put up with the long hours, high stress, and abysmal pay. Throughout the entire degree she has supported me both emotionally and financially. No matter how difficult things were, she was always there to reassure me that it would be ok and someday I would finally be finished.

I also had the privilege of making many new friends in graduate school. Whether it be commiseration, game-nights, or swimming days, they were always there for me. I especially want to thank Nick, Rachel, Brian, and Alicia who always provide interesting company. I also want to thank my original party members, Kyle W., Sam, Isabel, Kyle F., Jake, and Jacob. I also need to thank my favorite hot pot duo, Becky and Jieming. I also had the opportunity of getting to know Megan and Frances, two very dear friends that I will always treasure. This group of friends made graduate school bearable enough to continue and earn my PhD. I always could depend on them to lighten the mood and make my day better.

Nathan W. Ulrich

April 9th, 2018

TABLE OF CONTENTS

LIST OF FIGURES

LIST OF TABLES

LIST OF ABBREVIATIONS

AFM atomic force microscopy

ATMS (3-aminopropyl)trimethoxysilane

ATR-FTIR attenuated total-internal reflectance-Fourier transform infrared

BADGE bisphenol-A digylcidyl ether

d8-PMMA deuterated poly(methyl methacrylate)

d8-PS deuterated polystyrene

DETA diethylenetriamine

DFG difference frequency generation

OPA optical parametric amplification

OPG optical parametric generation

OTMS octadecyltrimethoxysilane

PCB printed circuit board

PEI polyethylenimine

PET poly(ethylene terephthalate)

PI polyimide

PMMA poly(methyl methacrylate)

PMT photomultiplier tube

PS polystyrene

γ-GPS (3-glycidoxypropyl) trimethoxysilane

SFG sum frequency generation

TIR total-internal reflection

TIR-SFG total-internal reflection SFG

TIRF total-internal reflection fluorescence

ABSTRACT

Microelectronic devices affect us every day; they are ubiquitously utilized in automotives, personal electronics, and biomedical devices. Adhesives are used in microchip assemblies to attach the chip to the printed circuit board, which greatly increases the lifetime of the microelectronic device. The focus of this thesis is to elucidate molecular interactions key to adhesion, how to improve adhesion, and how the molecular orientation at buried interfaces can affect macroscopic adhesion properties. In this work the intrinsically surface sensitive technique, sum frequency generation (SFG) vibrational spectroscopy, was utilized to noninvasively investigate buried interfaces *in situ*. By probing systems in their natural unperturbed state, we can deduce information that enables better design of adhesion systems. In this work, adhesion promoters, plasma treatment, real electronic devices, and flux residues were characterized and the molecular details of the buried interfaces were correlated to the macroscopic properties.

Epoxy based adhesives were modified with small amounts of adhesion promoters and they drastically improved the adhesion strength following accelerated stress testing; they were also capable of preventing interfacial water. This research demonstrates that molecular structural studies of buried epoxy interfaces during hygrothermal aging using SFG spectroscopy can greatly contribute to the overall understanding of moisture-induced failure mechanisms of adhesives found in microelectronic packaging.

Another method to improve the adhesion strength is plasma treatment, which is utilized to clean and activate the substrates prior to solder reflow and applying epoxy underfill. Two projects are outlined in this work, (1) plasma treatment of covered surfaces, and (2) plasma-based adhesion promotion. For (1), polymer surfaces were protected with a cover and exposed to various plasmas, to simulate the plasma processing steps found within the microelectronics industry. It was demonstrated that the middle and edge regions of the covered polymer surface behaved differently when exposed to various plasmas, which was determined both qualitatively and quantitatively. Next, project (2), focused on both the surface and the buried polymer/epoxy interface, and how plasmas treatment can improve the adhesion strength. The mechanism of this increase in adhesion

strength has not been thoroughly investigated at the molecular level *in situ* previously, because it is difficult to probe a buried interface where the adhesion occurs. To understand how plasma changes the surface and the corresponding buried interface, polymer surfaces were plasma treated and then put in contact with epoxy. It was found that the molecular structure of the buried interface of the pristine polymer/epoxy interface is drastically different from the plasma treated polymer/epoxy interface. The buried interface with plasma treated polymer surface was found to be very disordered and had much higher adhesion strength. The main mechanism for plasma-based adhesion when using He plasma was found to be disordering of the interface. This research elucidates the plasma treatment effects on structures and properties of buried polymer/epoxy interfaces, providing in-depth understanding on the mechanism of adhesion strength increase facilitated by plasma treatment.

In addition to the studies on various model systems, real devices manufactured from Texas Instruments were investigated. It is extremely difficult to examine molecular structures of buried interfaces in samples with multiple layers. In this work, real flip-chip (FC) devices were investigated. By milling down the FC and removing the Si wafer, three separate interfaces can be analyzed. New SFG metrology was developed to investigate this system, and methylene and methyl groups were detected from each of the three interfaces, and the orientation of methyl groups was determined at each interface. The SFG metrology developed in this research is general and can be applied to other real-world, complicated thick systems.

Flux materials are ubiquitously utilized in the microelectronics industry to clean and activate surfaces. However, flux residues can cause premature failure of the device, and they must be studied *in situ* at the buried interface to determine fundamental interactions and how they can be eliminated. Model flux residues were investigated at the surface and the buried epoxy interface with SFG spectroscopy. It was found that the flux residues greatly change the buried interface on both Cu and silica surfaces, which affects properties such as adhesion. It was also observed that the fluxes require long washing times before they are completely removed. This work will help the industry better understand molecular level details of commonly used techniques and improve processing conditions.

In this thesis, methods of adhesion promotion, real FC devices, and processing conditions were investigated. Using SFG spectroscopy, these systems were probed *in situ*, noninvasively. Data was generated from the interface, and molecular orientation was quantitatively determined and this was

correlated with adhesion strength. This work greatly adds to the understanding of how molecular structure at buried interfaces can determine the macroscale properties. By studying adhesion at a fundamental level we can design stronger ones that can prolong microelectronic device lifetimes.

Chapter 1: Introduction

1.1. Motivation

Microelectronic devices, ranging from cellphones to medical devices, are used in everyday life. The microelectronics field has rapidly developed over the past few decades and much research is being done to improve it even more. One of the biggest areas of research in microelectronics is packaging and materials, which focuses on how the devices are put together and what materials are used. Packaging focuses on the different methods of constructing microelectronic devices and how more transistors and connections can be packed in more tightly, giving the device more processing capabilities. Packaging research involves investigations on materials related to different substrates, adhesives, and processing chemicals that can make devices more resilient or processing more efficient. Adhesives are the most important packaging materials which connect to substrates to form buried interfaces. By understanding these interfaces on the molecular level we can design better, more resilient devices that can withstand greater stress and have longer lifetimes. There are many methods of analyzing these buried interfaces *ex situ*, but molecular interactions key to macroscopic properties, such as adhesion, may be altered with the *ex situ* studies. To understand the crucial interactions relevant to adhesion, *in situ* analysis at the buried interface is crucial and sum frequency generation (SFG) vibrational spectroscopy is an ideal metrology to do this.

In this work, SFG spectroscopy was utilized to investigate buried interfaces relevant to the microelectronics industry especially packaging and understand how various treatments can change such interfaces. Our goal was to develop SFG methods to investigate different kinds of systems to elucidate the molecular mechanisms of adhesion. Adhesion is a very complex interfacial property which is dictated by the molecular structures of the interface. Therefore to provide detailed understanding of adhesion, it is necessary to probe the buried interfaces *in situ* at the molecular level. SFG spectroscopy is a powerful technique that selectively probes interfaces with

submonolayer resolution and can provide molecular level structural information. Very few techniques have this level of surface sensitivity at atmospheric pressure. SFG signal is sensitive to the molecular structure (e.g., molecular orientation) and density of molecules or functional groups at the surface, which makes it capable of in depth analysis of interfaces.

Specifically, there are four aims of this thesis research. Aim 1 was to study how silane adhesion promoters affect the buried polymer/epoxy interface and determine if they can prevent interfacial moisture adsorption upon hygrothermal aging. Aim 2 was to investigate plasma effects on polymer surfaces and determine (a) how plasma affects covered surfaces and (b) how plasma increases adhesion strength. Aim 3 was to develop new metrology for investigating multiple buried interfaces in thick film samples by first polishing the samples and probing them. Aim 4 was to focus on flux residue analysis at surfaces and buried interfaces, in an effort to better understand common processing steps in the microelectronics industry.

1.2. Microelectronics Industry

The microelectronics industry has evolved rapidly with innovations such as the integrated circuit (IC), which revolutionized the field. Many innovations have developed over the past several decades that have allowed the miniaturization of technological devices, including using (1) adhesive materials and the (2) flip-chip on leadframe (FCOL) devices.[1, 2] For (1), there are two primary adhesives that are used, mold compound (MC) (overtop the device) and underfill (UF) (in between substrate/die), and both are used to increase the reliability and durability of devices. For (2), in flip-chip assemblies, a solder bump replaces wires used to connect die to substrates, which is currently the most space-efficient method for connecting an IC to a microchip (Figure 1.1). The density of inputs/outputs (IOs) or interconnects was greatly increased by using solder bumps instead of wires in FC devices. However, the solder bumps attached to the substrate are susceptible to shear stress in a temperature cycling environment, which can lead to device failure. Interfacial failures can be caused by interfacial peeling and delamination.[3] Any delamination that occurs at the underfill/die interface will propagate to the neighboring solder bumps and lead to solder joint fatigue and ultimately, device failure.

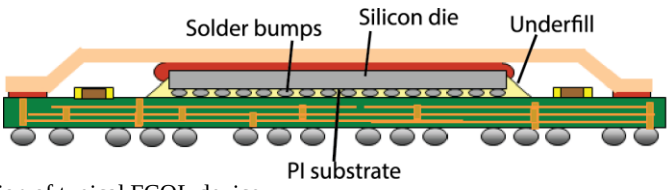

Figure 1.1: Illustration of typical FCOL device.

Flip-chip devices have an incredibly small footprint and by using MC and UF, the reliability of FCOL are greatly increased. Currently bisphenol-type epoxy adhesives are the most widely used underfill material in the microelectronics industry due to their fast curing times and excellent strength.[4, 5] Underfill material is still under much research to improve the performance and improving the adhesion at the UF/substrate interface is one method of increasing device lifetime.

1.3. Adhesion and Buried Interfaces

Adhesion has been well studied by many research groups over the years, but it is still a challenging area of research due to the complex and multidisciplinary approaches necessary to investigate it.[6-9] There are a litany of mechanisms that contribute to adhesion including interfacial hydrogen and chemical bonding, interfacial segregation, interfacial diffusion, electrostatic attraction, and mechanical interlocking.[10]

Because of the importance of underfill adhesion for the reliability of the flip-chip assembly, it has been studied extensively. However, most of the studies on such adhesion focused on the macroscale or on a mechanical level. To accurately understand the process of adhesion with molecular level detail, noninvasive probing must be performed at the buried interface. The issue is, the adhesive/substrate interface is a solid/solid buried interface that is inaccessible with traditional techniques. There are few instruments capable of probing these buried interface *in situ*. Typically buried interfaces, such as those in FCOL devices, are studied by breaking them apart (e.g., by separating the leadframe and die) and then performing *ex situ* analysis with SEM, XPS, etc. The issue with this strategy is that molecular interactions at interfaces that may be key to fully understand the system are greatly perturbed and may be vastly different from their native state. By investigating buried interfaces in devices *in situ* we could gain a better understanding of the molecular interactions at the interfaces. Such knowledge could greatly help us to improve adhesion by manipulating structures of adhesives and substrate surfaces.

To ensure the high quality of microelectronics, it is necessary to increase the strength and the resilience of adhesives used in packaging. There are primarily two methods of increasing the adhesion: (1) substrate surface modification and (2) adhesive modification. Adhesion promoting treatments can focus on modifying the substrate surface to promote chemical bonds, interfacial diffusion, or mechanical interlocking. Plasma treatment has been shown to modify the surface structure of polymer substrate materials, which leads to higher adhesion strength between polymer substrates and epoxy underfills.[11, 12] However, the detailed effects of plasma treatment on the buried interface between the plasma treated polymer surfaces in contact with epoxy and other underfill materials have not been studied *in situ* at a molecular level. Although plasma treatment typically improves the adhesion strength at polymer/epoxy and metal/epoxy interfaces, the mechanisms by which the adhesion is improved are not well understood and need to be investigated further.[13] Adhesive modification is a very common strategy to increase the adhesion strength at the substrate/adhesive interface. A popular class of additives is silane adhesion promoters (SAPs), which can increase the strength and prevent moisture induced failure. The interactions of the adhesive with SAPs must be understood on a fundamental level in order to design better adhesion systems. Both of the adhesion promoting strategies need to be understood at a molecular level and they need to be studied *in situ*, using a noninvasive technique, which will be performed in this thesis research using SFG spectroscopy as the primary technique.

1.4. Sum Frequency Generation (SFG) Vibrational Spectroscopy

In this thesis research, SFG is the primary method used for studying buried interfaces. A brief overview of the SFG background, theoretical groundwork, and experimental setup will be presented below.

1.4.1. SFG Background

Sum frequency generation (SFG) vibrational spectroscopy has been used extensively as a noninvasive analytical tool to study buried interfaces and surfaces, generating molecular-level detailed structure *in situ*.[14-24] SFG is an optical process thus, any interface that is accessible to visible and infrared light can be studied. Therefore, SFG can be used to study buried interfaces specifically *in situ*, without destroying the interface, as is necessary with standard surface sensitive techniques (e.g. XPS). SFG analysis is the best choice in this study because adhesion is related to the buried interfacial structure. SFG spectroscopy can be utilized to investigate surface and

interfacial chemical structure selectively, such as surface coverage, molecular orientation, and orientation distribution of interfacial functional groups. Interfacial molecular interactions such as interfacial diffusion and interfacial hydrogen bonding networks can be probed as well.[25-34] This technique has been extensively utilized to study polymer systems and buried polymer interfaces.[35-53] We have performed SFG spectroscopic studies on model and commercial epoxy systems typically used as underfill materials in the microelectronics industry.[54-56] It has also been shown that SFG can elucidate the structure-function relationship of complex systems noninvasively.[42, 57-64]

SFG is nonlinear optical vibrational spectroscopy. Vibrational spectroscopy (VS) is a label-free, noninvasive technique, capable of providing chemical identification for samples. VS has been widely used in materials, biological science, and medical research. Recent technological innovations have enabled lasers with high peak powers, and this has made it possible for nonlinear optical (NLO) vibrational techniques to emerge. NLO VS can have several advantages over traditional linear techniques, including: intrinsic surface sensitivity, coherent signal output (which makes collection easier), and fast label free imaging capabilities. The advancements of three areas of NLO are required for the field as a whole to progress: (1) theory and data analysis development, (2) instrumentation and upgrades made to current spectrometers and microscopes, and (3) applications to the fields of materials and biomedical research.

SFG VS is a second order nonlinear optical technique that is intrinsically surface specific with sub-monolayer sensitivity.[65-67] As a vibrational technique SFG provides spectra similar to FT-IR and Raman, but the source of the signal is exclusively from the interface. There are major advantages of SFG that are not found in other techniques, such as, operation at normal ambient conditions, which is not possible with techniques such as XPS and SEM. Another advantage is the signal is coherent, which facilitates easy collection of the signal. For both these reasons, SFG can probe various phases *in situ*, noninvasively, which sets it apart from other analytical techniques.

Below outlines the physical origins of SFG, starting with polarization and moving through to the selection rules of Raman and IR transitions. This material was adapted from Bain's work.[68] An approximation needs to be made, that the electron distribution in the molecule of interest responds harmonically to the induced electric field (E) of the incident light. The dipole moment μ, is defined as:

$$\mu = \mu^0 + \alpha E \qquad \text{Equation 1-1}$$

Here, μ^0 is the static dipole moment, α is the polarizability, and E is the electric field of the incident light. The induced dipole (αE) is a vector and α is a 3×3 tensor. In condensed phases the dipole moment per unit volume, or polarization, P, can be written as:

$$P = P^{(0)} + \varepsilon_0 \chi^{(1)} E \qquad \text{Equation 1-2}$$

For a material, the susceptibility will depend on the number of oscillators per unit volume, N, multiplied by the molecular polarizability average over all the orientations of the molecules in the material.

$$\chi^{(1)} = \frac{N\langle\alpha\rangle}{\varepsilon_0} \qquad \text{Equation 1-3}$$

The linear properties of isotropic materials are characterized by their complex refractive index.

$$n = \sqrt{1 + \chi^{(1)}} \qquad \text{Equation 1-4}$$

The real part determines the speed of light in the medium.

$$v = \frac{c}{Re(n)} \qquad \text{Equation 1-5}$$

The imaginary part determines the absorption coefficient, k,

$$k = \frac{4\pi}{\lambda_0} Im\sqrt{1 + \chi^{(1)}} \qquad \text{Equation 1-6}$$

where λ_0 is the wavelength of light in a vacuum.

In focused laser beams, the electric field is sufficiently high, such that the electrons are no longer able to respond harmonically and higher order terms must be included in the expression for the dipole moment to account for the anharmonicity.

$$\mu = \mu^0 + \alpha E + \beta : EE + \gamma \vdots EEE + \ldots \qquad \text{Equation 1-7}$$

The terms β and γ are known as the first and second hyperpolarizabilities, where $\beta : E$ denotes $\sum_{jk} \beta_{ijk} E_j E_k$. The polarization can now be written as

$$P = P^{(1)} + P^{(2)} + P^{(3)} + \ldots = \varepsilon_0 \chi^{(1)} E + \varepsilon_0 \chi^{(2)} : EE + \varepsilon_0 \chi^{(3)} \vdots EEE \ldots \quad \text{Equation 1-8}$$

Where $\chi^{(2)}$ is the second order nonlinear susceptibility, a third rank tensor, and $\chi^{(3)}$is a forth rank tensor known as the third order nonlinear susceptibility. We can set:

$$E(r,t) = E(r)\, cos(\omega t) \quad \text{Equation 1-9}$$

Substituting in and looking at just the second order term, we have:

$$P^{(2)} = \varepsilon_0 \chi^{(2)} : EE = \varepsilon_0 \chi^{(2)} E(r) E(r)\, cos^2(\omega t) \quad \text{Equation 1-10}$$

Rearranging the double angle trig identity

$$cos(2A) = 2\, cos^2(A) - 1 \quad \text{Equation 1-11}$$

$$cos^2(A) = \tfrac{1}{2} cos(2A) + 1 \quad \text{Equation 1-12}$$

And substituting back in we now have

$$P^{(2)} = \tfrac{1}{2} \varepsilon_0 \chi^{(2)} E(r) E(r) (1 + cos(2\omega t)) \quad \text{Equation 1-13}$$

As can be seen, light at 2ω can be generated and this process is known as second harmonic generation (SHG). SHG is a special case of SFG, where the two incident beams are of the same energy. If two laser beams at different frequencies interact at the sample, the polarization can be written as

$$P^{(2)} = \varepsilon_0 \chi^{(2)} : E_1(r) E_2(r)\, cos(\omega_1 t)\, cos(\omega_2 t) \quad \text{Equation 1-14}$$

Using the following trigonometric identity:

$$2\cos(A)\cos(B) = \cos(A - B) + \cos(A + B) \quad \text{Equation 1-15}$$

The polarization can be written as

$$P^{(2)} = \varepsilon_0 \chi^{(2)} : E_1(r) E_2(r) \tfrac{1}{2} [cos(\omega_1 - \omega_2) + cos(\omega_1 + \omega_2)] \quad \text{Equation 1-16}$$

As can be seen, light at the difference of the two frequencies, $\omega_1 - \omega_2$, can be generated and this process is known as Difference Frequency Generation (DFG). Also the sum of the two frequencies,

$\omega_1+\omega_2$, can be generated. This process is known as sum frequency generation. For our SFG research, experimentally ω_1 is in the visible frequency region, in our case 532.1 nm, and ω_2 is usually in the infrared frequency region, in our case tunable from 3-10 μm. SFG and DFG are both coherent processes. The direction of emission is determined by the conservation of momentum parallel to the surface (the wave matching condition).

$$k_{sum}\, sin(\theta_{sum}) = k_1\, sin(\theta_1) + k_2\, sin(\theta_2) \qquad \text{Equation 1-17}$$

Where k is the wave vector: $k = \frac{2\pi}{\lambda}$, θ_1 and θ_2 are the incident angles of the visible and IR beams. The intensity of the emitted light depends on $\left|\chi^{(2)}\right|^2$. An expression for $\chi^{(2)}$ can be found via second order perturbation theory as an infinite sum over the quantum states of the system. This has a complicated general solution, but some physical insight can be gained into SFG if the simplifications of ω_{sum} and ω_{vis} are not resonance with an electronic transition in the sample and the electric dipole approximation is considered.

Near a vibrational transition resonance, ω_0, in a molecule the hyperpolarizability of a vibrational mode, β, is given by:

$$\beta_{lmn}(\omega_{sum} = \omega_{vis} + \omega_{IR}) =$$
$$-\frac{1}{2\hbar}\sum_s \left\{\frac{\langle g|\mu_l|s\rangle\langle s|\mu_m|v\rangle}{\hbar(\omega_{sum}+\omega_{sg})} - \frac{\langle g|\mu_m|s\rangle\langle s|\mu_l|v\rangle}{\hbar(\omega_{vis}+\omega_{sg})}\right\} \times \left\{\frac{\langle v|\mu_n|g\rangle}{\omega_{IR}-\omega_0+i\Gamma}\right\}$$

Equation 1-18

$|g\rangle$ is the ground state, $|v\rangle$ is the excited vibrational state, $|s\rangle$ is any other state, Γ^{-1} is the relaxation time of the excited vibrational state, and μ is the electric dipole operator. The first bracket is the Raman polarizability and the second bracket is the infrared transition dipole moment. So a molecule is SFG active only if it is both infrared active and Raman active.

For a molecule to be infrared active the electric dipole moment of the molecule must change as the atoms are displaced relative to each other during the vibration. For example, homonuclear diatomic molecules are infrared inactive because their dipole moments remain zero no matter how long the bond is stretched.

For a molecule to be vibrational Raman active the selection rule is that the polarizability should change as the molecule vibrates. For example as a diatomic molecule expands and contracts, the molecular polarizability changes, thus they are Raman active.

1.4.2. SFG Selection Rule and Data Analysis

Now that polarization and selection rules for IR and Raman have been discussed, we can discuss SFG selection rules. A vibrational mode is only SFG active if it is both IR and Raman active. Equation 1-18 shows that SFG hyperpolarizability reaches maximum when $\omega_{IR} - \omega_0 = 0$. That is, when the infrared frequency is in resonance with the molecular vibrational frequency, a large enhancement occurs in SFG signal that we detect. The damping term Γ determines the line width of the resonance peak.

The SFG selection rule leads to the surface/interface sensitivity for SFG. Mathematically the intrinsic symmetry of $\chi^{(2)}$ forbids SFG in centrosymmetric materials. $\chi^{(2)}$ is a polar tensor of rank three, which changes sign under the inversion operation.

$$\chi^{(2)}(r) = -\chi^{(2)}(-r) \qquad \text{Equation 1-19}$$

A centrosymmetric material however is invariant under inversion thus:

$$\chi^{(2)}(r) = \chi^{(2)}(-r)$$
$$\rightarrow \chi^{(2)}(-r) = -\chi^{(2)}(-r) = 0 \qquad \text{Equation 1-20}$$

Thus, SFG by electric dipole mechanisms does not occur in a centrosymmetric material. It can occur by other mechanisms, such as magnetic dipole or electric quadrupole, but these are usually much weaker than the electric dipole mechanisms. Most bulk media possess inversion symmetry, therefore they do not generate SFG signal. At interfaces the inversion symmetry is broken and second order nonlinear optical phenomenon can occur. This is the source of the surface specificity that is cited for second harmonic and sum frequency generation. Thus it is possible to differentiate the functional groups that are at the surface from those in the same molecules in the bulk because those in the bulk do not generate SFG signals.

There has been much work on SFG theory including data analysis and many publications.[23, 59, 69] SFG signal can be define as:[16]

$$I_{SFG} \propto \left|\chi^{(2)}\right|^2 I_{IR} I_{vis} \qquad \text{Equation 1-21}$$

Here I_{IR}, I_{vis}, and $\chi_{eff}^{(2)}$ are the intensities of the IR and visible beams, and the effective second order nonlinear susceptibility as defined above, respectively. $\chi_{eff}^{(2)}$ can be described as a function of the resonant and nonresonant response:

$$\chi_{eff}^{(2)} = \chi_{NR}^{(2)} + \sum_q \frac{A_q}{\omega_{IR} - \omega_q + i\Gamma_q} \qquad \text{Equation 1-22}$$

In this expression $\chi_{NR}^{(2)}$ is the nonresonant signal contributed from the sample. The resonant portion of the nonlinear susceptibility can be modeled as the sum of Lorentzians with amplitude A_q, frequency ω_q, and line width Γ_q. This above equation is what is used to fit SFG peaks and determine orientation.

For an isotropic interface in the x-y plane, $\chi_{eff}^{(2)}$ can be related to $\chi^{(2)}$ defined in the lab fixed coordinate system via local field correction factors, i.e., Fresnel Factors.[16]

$$\chi_{eff,ssp}^{(2)} = L_{yy}(\omega_{SF}) L_{yy}(\omega_{Vis}) L_{zz}(\omega_{IR}) \sin\theta_{IR}\, \chi_{yyz} \qquad \text{Equation 1-23}$$

$$\chi_{eff,sps}^{(2)} = L_{yy}(\omega_{SF}) L_{zz}(\omega_1) L_{yy}(\omega_2) \sin\theta_{Vis}\, \chi_{zyy} \qquad \text{Equation 1-24}$$

$$\chi_{eff,pss}^{(2)} = L_{zz}(\omega_{SF}) L_{yy}(\omega_1) L_{yy}(\omega_2) \sin\theta_{SF}\, \chi_{zyy} \qquad \text{Equation 1-25}$$

$$\chi_{eff,ppp}^{(2)} = \begin{matrix} -L_{xx}(\omega_{SF}) L_{xx}(\omega_{Vis}) L_{zz}(\omega_{IR}) \cos\theta_{SF} \cos\theta_{Vis} \sin\theta_{IR}\, \chi_{xxz} \\ -L_{xx}(\omega_{SF}) L_{zz}(\omega_{Vis}) L_{xx}(\omega_{IR}) \cos\theta_{SF} \sin\theta_{Vis} \cos\theta_{IR}\, \chi_{xzx} \\ +L_{zz}(\omega_{SF}) L_{xx}(\omega_{Vis}) L_{xx}(\omega_{IR}) \sin\theta_{SF} \cos\theta_{Vis} \cos\theta_{IR}\, \chi_{zxx} \\ +L_{zz}(\omega_{SF}) L_{zz}(\omega_{Vis}) L_{zz}(\omega_{IR}) \sin\theta_{SF} \sin\theta_{Vis} \sin\theta_{IR}\, \chi_{zzz} \end{matrix} \qquad \text{Equation 1-26}$$

In these expressions, $\chi_{IJK}^{(2)}$ (IJK = x, y, z) is a local nonlinear second order optical susceptibility component of the materials at the interface defined in the lab-fixed coordinate system.[59] Here θ_{IR} and θ_{Vis} are the angles of incidence from the surface normal of the incoming infrared and visible beams, respectively (). The SFG output angle is defined as θ_{SF}. L_{ii} (i = x, y, z) is the Fresnel coefficient, which is a function of refractive indices, beam input angles, and the linear reflection and transmission coefficients.[16] ω_{SF}, ω_{Vis}, ω_{IR} are the frequencies of the sum frequency, visible,

and IR beams, respectively. There are four polarization combinations typically used in SFG data collection, ssp, sps, pss, and ppp ('ssp' means s-polarized SF, s-polarized visible, and p-polarized IR). There are two systems that the F factors can be calculated for (a) 2-media system (1 interface-interface I) or (b) 3-media system (2 interfaces-interface I and II) (Figure 1.2). System (a) consists of air/solid support interface and System (b) has a thin film present on a solid support, forming a buried interface. For System (b), SFG signal can be generated at both interface I and Interface II. The linear reflection and transmission coefficients for s- and p-polarized light at the plane boundary separating media i and j are given by1:

$$r_{ij}^{p} = \frac{n_j \cos(\theta_i) - n_i \cos(\theta_j)}{n_j \cos(\theta_i) + n_i \cos(\theta_j)} \qquad \text{Equation 1-27}$$

$$r_{ij}^{s} = \frac{n_i \cos(\theta_i) - n_j \cos(\theta_j)}{n_i \cos(\theta_i) + n_j \cos(\theta_j)} \qquad \text{Equation 1-28}$$

$$t_{ij}^{p} = \frac{2n_i \cos(\theta_i)}{n_j \cos(\theta_i) + n_i \cos(\theta_j)} \qquad \text{Equation 1-29}$$

$$t_{ij}^{s} = \frac{2n_i \cos(\theta_i)}{n_i \cos(\theta_i) + n_j \cos(\theta_j)} \qquad \text{Equation } \textit{1-30}$$

where n_i and n_j are the refractive indices of media i and j, respectively, and θ_i and θ_j are the incident angle in medium i and the transmitted angle into medium j, respectively. The local field factors (L factors) at interface I (polymer/air) are given by[2-4]:

$$L_{xx}^{I}(\omega) = \frac{t_{12}^{p}}{1 + r_{12}^{p} r_{23}^{p} e^{2i\beta}} (1 - r_{23}^{p} e^{2i\beta}) \frac{\cos\theta_2}{\cos\theta_1} \qquad \text{Equation 1-31}$$

$$L_{yy}^{I}(\omega) = \frac{t_{12}^{s}}{1 + r_{12}^{s} r_{23}^{s} e^{2i\beta}} (1 + r_{23}^{s} e^{2i\beta}) \qquad \text{Equation 1-32}$$

$$L_{zz}^{I}(\omega) = \frac{t_{12}^{p}}{1 + r_{12}^{p} r_{23}^{p} e^{2i\beta}} (1 + r_{23}^{p} e^{2i\beta}) \frac{n_1 n_2}{n_{m,12}^{2}} \qquad \text{Equation 1-33}$$

$$\beta = \frac{2\pi}{\lambda} n_2 d \cos\theta_2 \qquad \text{Equation 1-34}$$

where λ is the wavelength of the beam in nm, ω is the beam frequency, and θ_1 and θ_2 are the beam incident angles in medium 1 and medium 2, respectively. The thickness of the polymer film d is

in nm and $n_{m,12}$ is the refractive index of the interface. The local field factors at interface II (solid support/polymer) are given by[2-4]:

$$L_{xx}^{II}(\omega) = e^{i\Delta}\frac{t_{12}^{p}}{1+r_{12}^{p}r_{23}^{p}e^{2i\beta}}(1-r_{23}^{p}e^{2i\beta})\frac{cos\theta_2}{cos\theta_1} \quad \text{Equation 1-35}$$

$$L_{yy}^{II}(\omega) = e^{i\Delta}\frac{t_{12}^{s}}{1+r_{12}^{s}r_{23}^{s}e^{2i\beta}}(1+r_{23}^{s}) \quad \text{Equation 1-36}$$

$$L_{zz}^{II}(\omega) = e^{i\Delta}\frac{t_{12}^{p}}{1+r_{12}^{p}r_{23}^{p}e^{2i\beta}}(1+r_{23}^{p}e^{2i\beta})\frac{n_1 n_2}{n_{m,23}^{2}} \quad \text{Equation 1-37}$$

where

$$\Delta_{SFG} = \frac{2\pi n_{2,SFG}d}{\lambda_{SFG}cos\theta_{2,SFG}} \quad \text{Equation 1-38}$$

$$\Delta_{VIS} = \frac{2\pi n_{2,VIS}d}{\lambda_{VIS}cos\theta_{2,VIS}} - \frac{2\pi n_{1,VIS}d}{\lambda_{VIS}}(tan\theta_{2,VIS}+tan\theta_{2,SFG})sin\theta_{1,VIS} \quad \text{Equation 1-39}$$

$$\Delta_{IR} = \frac{2\pi n_{2,IR}d}{\lambda_{IR}cos\theta_{2,IR}} - \frac{2\pi n_{1,IR}d}{\lambda_{VIS}}(tan\theta_{2,IR}+tan\theta_{2,SFG})sin\theta_{1,IR} \quad \text{Equation 1-40}$$

Using the above equations, quantitative data analysis on SFG spectra collected can be performed to determine orientations of various function groups on surfaces and at interfaces, which will be discussed in more detail below.

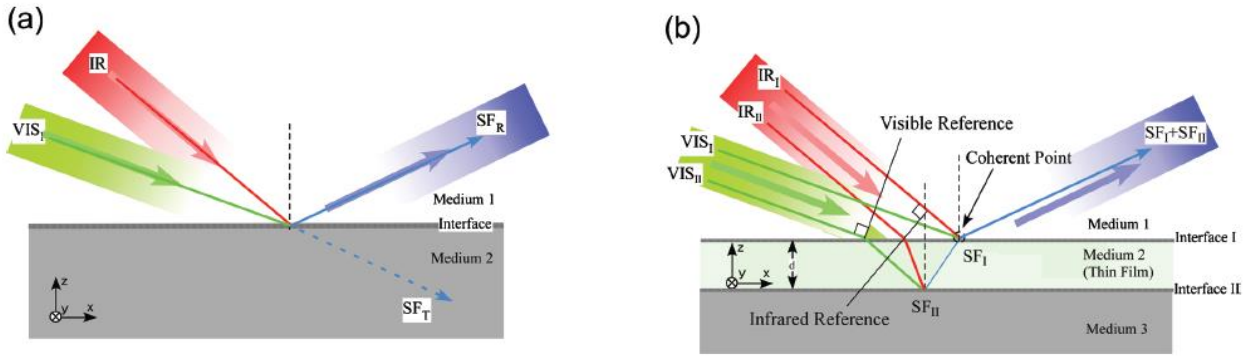

Figure 1.2: a. Schematic for SFG from an interface between media 1 and 2. b. A general interference model for SFG from a thin-film system on a solid substrate medium 3 consisting of two interfaces. For simplification, multiply reflected beams are not shown in the figure. Reproduce with permission from ref. [70].

1.4.3. SFG Experimental Setup and Geometries

To generate SFG data a complicated laser spectroscopic system is necessary, due to the required frequency tunable IR beam. There are four unique components of the spectrometer in out lab: (1)

the Nd:YAG laser, (2) the harmonics unit, (3) the optical parametric oscillator/optical parametric amplifier (OPO/OPA) and difference frequency generation (DFG) system, and (4) the signal collection, see Figure 1.3 for spectrometer setup. For (1), a Nd:YAG picosecond laser (1064 nm) was utilized for generating input beams for SFG experiments. Several different SFG spectrometers were used for collecting data in this research, with the laser output pulse duration of ~25 ps with a repetition rate of 20, 40, or 50 Hz. The 1064 nm laser output beam was guided to (2) the harmonics unit (HU). A portion of the 1064 nm beam is guided through a Potassium Dihydrogen Phosphate crystal and through the second harmonic process, a 532 nm beam is generated and sent to the sample as the visible input light. The remaining portion of the 1064 nm beam is split again and a 1064 nm beam is sent to the (3) DFG crystal and the other portion of the 1064 nm is frequency doubled and sent to the OPG/OPA system. After the OPG/OPA and DFG, a frequency tunable mid-IR beam is generated. (4) The two laser beams (visible and frequency tunable IR beams) are overlapped spatially and temporally on the sample surface and then the SFG beam is guided through a monochrometer to a gated PMT for detection.

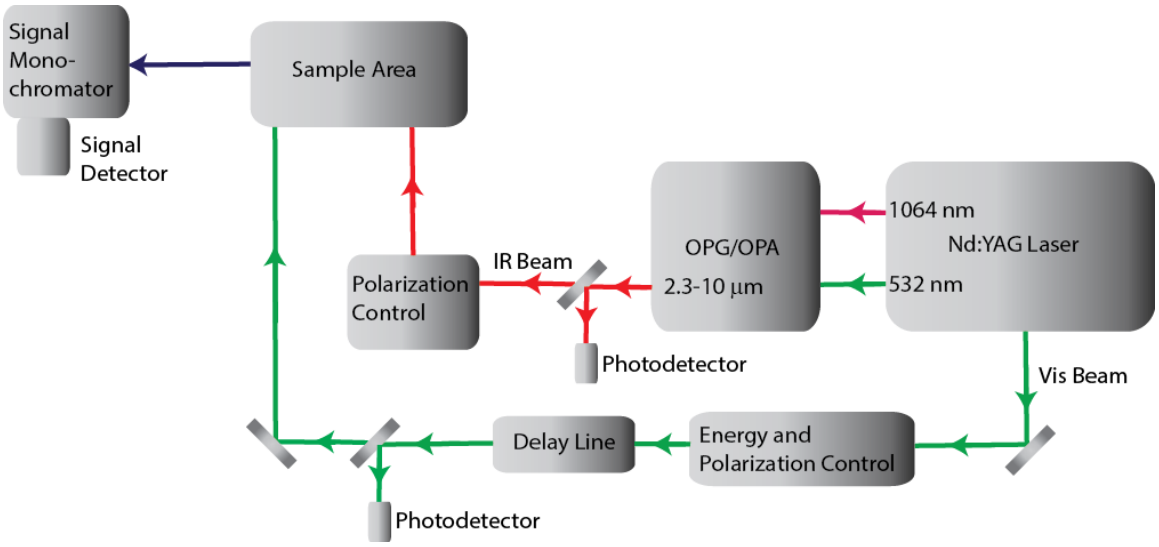

Figure 1.3: SFG spectrometer setup, adapted from the eksla.com website.

There are two main types of data collection experimental geometries that were used in this work, prism and window (face up and face down) (Figure 1.4). Prism geometry uses total internal reflection (TIR), which means the laser beams come through the side of the prism and then directly reflect off the bottom side with no transmission.

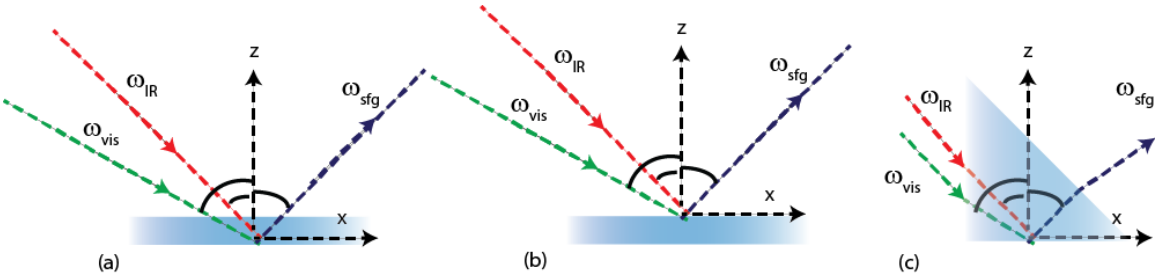

Figure 1.4: SFG experimental geometries (a) window face-down, (b) window face-up, and (c) prism.

1.4.4. Molecular Orientation Calculation of Various Functional Groups

$\chi^{(2)}$ is related to molecular hyperpolarizability β (thus the symmetry of the functional group) and molecular orientation of the functional group. More detailed relationships between $\chi^{(2)}$ and β will be given in later sections. In general, in such relationships the molecular orientation can be characterized by orientation angles. For certain functional groups, only the tile angle θ (the angle from the surface normal) is needed to define the orientation, and SFG can measure such orientations though $\langle \cos\theta \rangle$ and $\langle \cos^3\theta \rangle$ ("< >" indicates averaging). In a randomly oriented ensemble of molecules the odd moments of the orientational distribution vanish and so does $\chi^{(2)}$. An interface must induce a net polar orientation at the interface for it to be SFG active. Thus the magnitude of $\chi^{(2)}$, and hence the magnitude of the detected SFG signal is very sensitive to the degree of orientational order.

$\chi^{(2)}$ is a tensor and can be defined in the lab-fixed coordination system with the surface as x-y plane and z as the surface normal. For a surface that is isotropic (like a spin cast polymer) there are only four independent nonzero components of $\chi^{(2)}$: $\chi_{zzz}, \chi_{xxz} = \chi_{yyz}, \chi_{xzx} = \chi_{yzy}, \chi_{zzx} = \chi_{zyy}$. For experiments that are conducted away from electronic resonances of the sample there is a further simplification known as the Kleinmann symmetry where: $\chi_{xzx} = \chi_{zxx}$. These nonzero tensor components can be probed by varying the polarizations of the input/output light beams in the SFG experiment. With s-polarized visible and infrared (E in the y direction) only χ_{zyy} contributes, giving rise to p-polarized sum frequency emission. With s-polarized visible and p-polarized IR, only χ_{yyz} contributes and gives rise to s-polarized sum frequency emission. With p-polarized visible and p polarized infrared all four components contribute with their relative importance determined by the electric fields at the surface. As presented above, we defined the $\chi^{(2)}$ probed using different laser polarizations as effective nonlinear optical susceptibility with

components such as χ_{ssp} (s-polarized SFG signal, s-polarized visible, and p-polarized IR, in order of decreasing energy, the polarization combinations are ordered signal, visible, and infrared). The relationships between effective nonlinear optical susceptibility components and the components of the $\chi^{(2)}$ defined in the lab coordinate system were discussed above, and will be further discussed below.

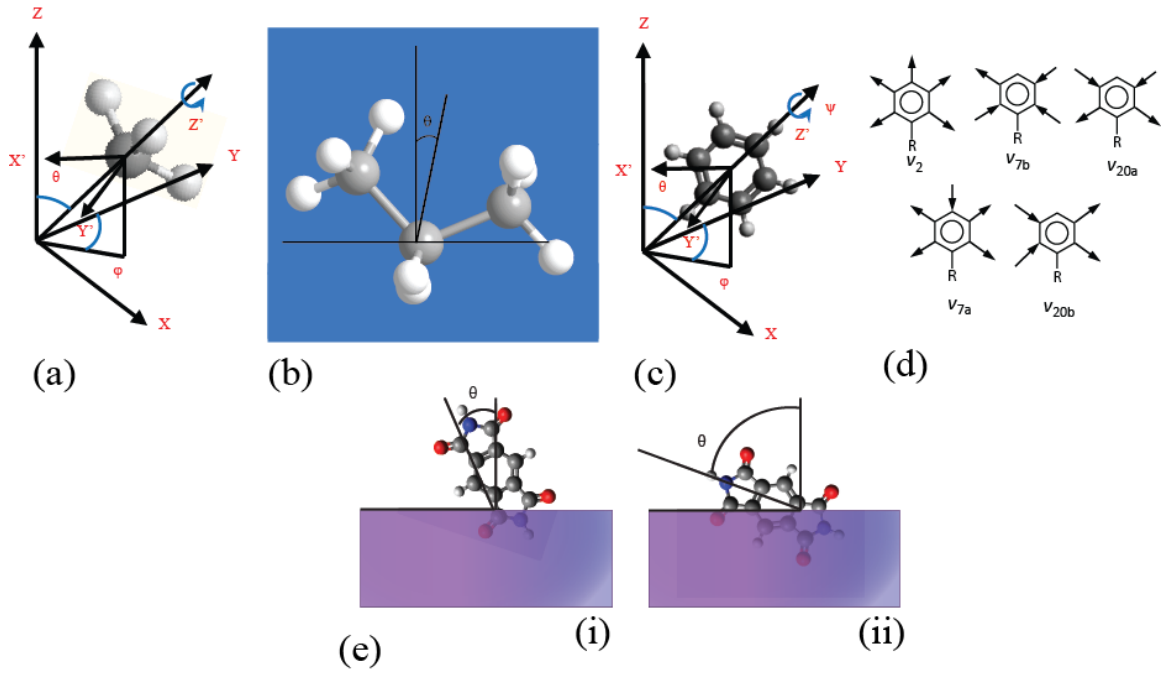

Figure 1.5: Molecular coordinates for functional groups probed in this work: (a) methyl, (b) isopropyl, (c) phenyl, (d) phenyl stretching modes, (e) polyimide, with (i) low tilt and (ii) high tilt.

1.4.4.1. Methyl Functional Group

SFG has been extensively used to study orientations of various functional groups and molecules according to the transformations discussed above. According to the symmetry of the molecule or functional group, such transformations can be simplified. Taking the methyl functional group for example, here the relationships between the measured χ_{ijk} components and hyperpolarizability tensor components (β_{abc}) are presented below:[16, 71]

For the symmetric methyl C-H stretch:

$$\chi^{(2)}_{xxz,s} = \chi^{(2)}_{yyz,s} = \frac{1}{2}N\beta^{(2)}_{ccc}[(1+r)\langle cos\theta\rangle - (1-r)\langle cos^3\theta\rangle] \quad \text{Equation 1-41}$$

$$\chi^{(2)}_{xzx,s} = \chi^{(2)}_{yzy,s} = \chi^{(2)}_{zxx,s} = \chi^{(2)}_{zyy,s} = \frac{1}{2}N\beta^{(2)}_{ccc}(1-r)[\langle cos\theta\rangle - \langle cos^3\theta\rangle] \quad \text{Equation 1-42}$$

$$\chi^{(2)}_{zzz,s} = N\beta^{(2)}_{ccc}[r\langle cos\theta\rangle + (1-r)\langle cos^3\theta\rangle] \quad \text{Equation 1-43}$$

For the asymmetric C-H stretch:

$$\chi^{(2)}_{xxz,as} = \chi^{(2)}_{yyz,as} = -\frac{1}{2}N\beta^{(2)}_{caa}[\langle cos\theta\rangle - \langle cos^3\theta\rangle] \quad \text{Equation 1-44}$$

$$\chi^{(2)}_{xzx,as} = \chi^{(2)}_{yzy,as} = \chi^{(2)}_{zxx,as} = \chi^{(2)}_{zyy,as} = \frac{1}{2}N\beta^{(2)}_{caa}\langle cos^3\theta\rangle \quad \text{Equation 1-45}$$

$$\chi^{(2)}_{zzz,as} = N\beta^{(2)}_{caa}[\langle cos\theta\rangle - \langle cos^3\theta\rangle] \quad \text{Equation 1-46}$$

The Gaussian distribution has been used extensively to represent the orientation angle distribution.[72, 73] Using a Gaussian distribution, we have:

$$f(\theta) = Cexp\left[-\frac{(\theta-\theta_0)^2}{2\sigma^2}\right] \quad \text{Equation 1-47}$$

$$\langle cos\,\theta\rangle = \int_0^\pi cos\,\theta\, f(\theta)\, sin\,\theta\, d\theta \quad \text{Equation 1-48}$$

$$\langle cos^3\theta\rangle = \int_0^\pi cos^3\theta f(\theta)\, sin\,\theta\, d\theta \quad \text{Equation 1-49}$$

In addition to methyl (CH_3),[16, 71, 74] orientation analysis of other functional groups such as methylene (CH_2), [66, 75] aromatic C-H stretch,[37, 76-79] [80, 81] α-helical, and β-sheet [82, 83], has also been reported.

1.4.4.2. Phenyl Functional Group

Another common functional group to perform orientation analysis on is the phenyl C-H stretching vibrational modes, for polymer such as PS. There are both A_1 type and B_1 type modes. For simplicity, we assume a delta orientation angle distribution for a phenyl group for data analysis. To determine the orientation of a phenyl group on an isotropic surface, both tilt and twist angles need to be deduced. In the following we will perform analysis on both cases: (1) we will deduce the tilt angle by averaging the twist angle; (2) we will deduce both the tilt and the twist angles. From the fitting results of the SFG ssp and sps spectra, we could deduce χ_{yyz} and χ_{yzy}.

1. Ignoring the twist angle ψ (by averaging ψ)

For the ν_2 mode:

$$\frac{\chi_{ssp,\nu_2}}{\chi_{sps,\nu_2}} = \frac{9.83\cos\theta - \cos 3\theta}{\cos\theta - \cos 3\theta} \quad \text{Equation 1-50}$$

For ν_{7b} mode:

$$\frac{\chi_{ssp,\nu_{7b}}}{\chi_{sps,\nu_{7b}}} = \frac{\cos 3\theta - \cos\theta}{3\cos\theta + \cos 3\theta} \quad \text{Equation 1-51}$$

After considering the Fresnel coefficients, we have:

$$\frac{\chi_{yyz,\nu_2}}{\chi_{yzy,\nu_2}} = 0.8443\,\frac{9.83\cos\theta-\cos 3\theta}{\cos\theta-\cos 3\theta} \quad \text{Equation 1-52}$$

$$\frac{\chi_{yyz,\nu_{7b}}}{\chi_{yzy,\nu_{7b}}} = 0.8443\,\frac{\cos 3\theta-\cos\theta}{3\cos\theta+\cos 3\theta} \quad \text{Equation 1-53}$$

2. With considering the twist angle ψ

$$\frac{\chi_{ssp,\nu_2}}{\chi_{sps,\nu_2}} = \frac{9.83\cos\theta-\cos 3\theta-4.01\cos\theta\sin^2\theta\cos 2\psi}{(\cos\theta-\cos 3\theta)(1-\cos 2\psi)} \quad \text{Equation 1-54}$$

$$\frac{\chi_{eff,ssp,\nu_{7b}}}{\chi_{eff,sps,\nu_{7b}}} = \frac{(\cos 3\theta-\cos\theta)(1+\cos 2\psi)}{4\cos\theta-(\cos\theta-\cos 3\theta)(1+\cos 2\psi)} \quad \text{Equation 1-55}$$

After considering the Fresnel coefficients and with the experimentally measured data, we have:

$$\frac{\chi_{yyz,\nu_2}}{\chi_{yzy,\nu_2}} = 0.8443\,\frac{9.83\cos\theta-\cos 3\theta-4.01\cos\theta\sin^2\theta\cos 2\psi}{(\cos\theta-\cos 3\theta)(1-\cos 2\psi)} \quad \text{Equation 1-56}$$

$$\frac{\chi_{eff,ssp,\nu_{7b}}}{\chi_{eff,sps,\nu_{7b}}} = 0.8443\,\frac{(\cos 3\theta-\cos\theta)(1+\cos 2\psi)}{4\cos\theta-(\cos\theta-\cos 3\theta)(1+\cos 2\psi)} \quad \text{Equation 1-57}$$

By using each of the ν_2 or ν_{7b} vibrational mode, we could deduce the tilt angle after averaging the twist angle. Likely if the two tilt angles deduced using two modes are same, it is reasonable to average the twist angle. Otherwise it is necessary to deduce the twist angle. By using the data analysis results for both vibrational modes, we can deduce the tilt and twist angles simultaneously.

1.4.4.3. Isopropyl Functional Group

The orientation of the methyl groups on epoxy molecules which will be studied in this thesis can be deduced using SFG spectra collected using different polarization combinations and the nonlinear susceptibility components of the vibrational modes. The two methyl groups on bisphenol A diglycidyl ether have been previously modeled as an isopropyl group, which means the entire $(CH_3)_2C$ unit is treated as a single unit, rather than two methyl groups.[84] The two methyl groups have a fixed angle $2\alpha = 112°$ and it was assumed that the methyl groups can freely rotate, which

means the $(CH_3)_2C$ group has quasi-C_{2v} symmetry. The results of the nonvanishing components of the second-order nonlinear susceptibility, $\chi^{(2)}$, are:

$$\chi_{yyz,sym} = N(\beta_{aac}-\beta_{ccc})[\{(cos\,\alpha - cos^3\,\alpha) \times (5 + 3\,cos\,2\psi) - 2\,cos\,\alpha\}(cos\,\theta - cos^3\,\theta) - 2(cos\,\alpha - cos^3\,\alpha)\,cos\,\theta] + 2N\beta_{aac}\,cos\,\alpha\,cos\,\theta$$ Equation 1-58

$$\chi_{yzy,sym} = N(\beta_{aac}-\beta_{ccc})\{(\cos\alpha - \cos^3\alpha) \times (5 + 3\cos 2\psi)\,(\cos\theta - \cos^3\theta) + 2\cos\alpha\cos\theta\,(\cos^2\alpha + \cos^2\theta - 2)\}$$

Equation 1-59

$$\chi_{zzz,sym} = N(\beta_{aac}-\beta_{ccc})[(\cos\alpha - \cos^3\alpha)\{2\cos^3\theta - 3(1 + \cos 2\psi)(\cos\theta - \cos^3\theta)\} - 2\cos\alpha\cos^3\theta] + 2N\beta_{aac}\cos\alpha\cos\theta$$

Equation 1-60

$$\chi_{yyz,asym} = N\beta_{caa}[(\cos\alpha - \cos^3\alpha)\{-2\cos\theta + 3(\cos\theta - \cos^3\theta)(1 + \cos 2\psi)\} - 2\cos^3\alpha\,(\cos\theta - \cos^3\theta)]$$ Equation 1-61

$$\chi_{yzy,asym} = N\beta_{caa}[3(\cos\alpha - \cos^3\alpha) \times (\cos\theta - \cos^3\theta)(1 + \cos 2\psi) + 2\cos^3\alpha\cos^3\theta]$$

Equation 1-62

$$\chi_{zzz,asym} = 2N\beta_{caa}[(\cos\alpha - \cos^3\alpha)\{2\cos\theta - 3(\cos\theta - \cos^3\theta)(1 + \cos 2\psi)\} + 2\cos^3\alpha\,(\cos\theta - \cos^3\theta)]$$ Equation 1-63

where β_{aac}, β_{caa}, and β_{ccc} are elements of the hyperpolarizability tensor and have the values of 3.4, 1.9, and 1, respectively, and N is the number density of isopropyl groups at the interface. By detecting and fitting SFG signals collected in different polarization combinations, ratios of the $\chi^{(2)}$ elements can be calculated and used to determine values of the tilt and twist angles, θ and ψ, respectively. In this study, the twist angle, ψ, was assumed to have free rotation and thus was averaged.[85] For these studies, the ratios of $\chi_{yyz,sym}/\chi_{yzy,asym}$ and $\chi_{yyz,asym}/\chi_{yzy,asym}$ were utilized to determine the tilt angle of the methyl groups.[84]

1.4.4.4. Polyimide Functional Group

Two orientation analysis methods were adopted to study PI surface imide ring orientations for two tilt angle ranges: a large tile 60°-90° and a small tilt, 0°-60°. In the former case the two carbonyl

groups that are perpendicular to the backbone chain of the polymer oscillate and in the latter case the two carbonyls that are parallel to the polymer backbone chain oscillate. The $\chi^{(2)}$ expressions for the large tilt (60°-90°) are:

$$\chi_{yyz,as} = -N_s(a_{as})_{X'X'Y'}\langle sin^3\theta\rangle\langle cos\psi\rangle - (a_{as})_{Y'Y'Y'}(\langle sin\theta\rangle\langle sin^2\psi cos\psi\rangle + \langle sin\theta cos^2\theta\rangle\langle cos^3\psi\rangle) \quad \text{Equation 1-64}$$

$$\chi_{yyz,s} = -N_s(a_s)_{X'X'Y'}\langle sin^3\theta\rangle\langle cos\psi\rangle - (a_s)_{Y'Y'Y'}(\langle sin\theta\rangle\langle sin^2\psi cos\psi\rangle + \langle sin\theta cos^2\theta\rangle\langle cos^3\psi\rangle) \quad \text{Equation 1-65}$$

For the smaller tilt (0°-60°) the $\chi^{(2)}$ expressions are:

$$\chi_{yyz,as} = N_s\{(a_{as})_{X'Y'Y'}\langle sin^2\theta cos\theta\rangle\langle cos^2\psi\rangle\} \quad \text{Equation 1-66}$$

$$\chi_{yyz,ss} = \frac{N_s}{2}\{(a_s)_{X'X'X'}\langle sin^2\theta cos\theta\rangle + (a_s)_{Y'Y'X'}(\langle cos\theta\rangle\langle sin^2\psi\rangle + \langle cos^3\theta\rangle\langle cos^2\psi\rangle)\} \quad \text{Equation 1-67}$$

where α_s and α_{as} are the hyperpolarizability components for the symmetric and antisymmetric vibrational modes of C=O groups coupled to PI imide ring, θ is the tilt angle, and ψ is the twist angle. For the high tilt angle condition, the values of the hyperpolarizability components are: $\alpha_{asY'Y'Y'}$ = 1.13, $a_{asX'X'Y'}$=1.00, $a_{ssY'Y'Y'}$= 1.25, and $a_{ssX'X'Y'}$=1.00.[86-88] For the low tilt orientation, the values of the hyperpolarizability components are: $\alpha_{asX'Y'Y'}$=1.80, $\alpha s_{sX'X'X'}$=1.00, $\alpha_{ssY'Y'X'}$=2.50.[86-88]

1.5 Presented Research

There are four projects that will be outlined in this thesis: (1) Hygrothermal treatment of buried polymer epoxy interfaces with silane additives; (2) Plasma treatment to determine (a) what effects they can have on adhesion promotion and (b) how covered surfaces behave in the presence of plasma treatment; (3) New metrology developed to study buried interfaces of thick polymer/adhesive films; (4) Flux residue analysis, to see how these residues can change the molecular structure at the interface and how this can change the macroscopic properties. All of these projects were performed to obtain a better understanding of fundamental molecular interactions common in the microelectronics industry. By primarily using nonlinear optical

techniques we can gain a better understanding of the fundamental physics that determine properties of these systems and probe systems that are not available for probing with other techniques.

In chapter 2, hygrothermal treatments of polymer/epoxy systems were investigated with SFG, FT-IR, and lap shear analysis. To the epoxy systems, small amounts of silane adhesion promoters (SAP) were added, to see if they can prevent moisture induced fatigue. The polymers polyethylene terephthalate (PET) and polystyrene (PS) were utilized and function as a hydrophilic and hydrophobic surface, respectively. By investigating the interfacial, bulk, and mechanical properties, strong conclusions were drawn about these systems and how SAPs can prevent interfacial moisture, which translate to increased mechanical properties.

In chapter 3, plasma effects were systematically investigated to see how polymer surfaces can be modified. There are two projects contained within this chapter, (a) plasma effects on covered surfaces, and (b) adhesion promotion by plasma treatment. The project (a), investigated how covered polymer surfaces behave in the presence of various plasmas, and project (b), investigated the ability of plasma treatment to improve the adhesion strength of polymer/epoxy systems. For (a) covered polymer surfaces were investigated to simulate a common processing step in which covered polymer surfaces are plasma treated prior to underfill dispensing. This processing step activates the surface and causes better wetting and bonding of the adhesive underfill material to the polymer surface, but it is not known if the plasma treatment is homogeneous or heterogeneous, i.e., if the plasma uniformly affects the polymer surface or not. The gap between the surface and the cover is typically on the order of tens of microns. This investigation proved the heterogeneous nature of plasma treatment on covered surfaces, which has important implications for processing condition parameters. Part (b) focused on the mechanism of plasma induced adhesion promotion. Plasma treatment is a very common processing technique, but the detailed chemical structural changes induced by plasma are not well known. We investigated PS and PI surfaces before and after He plasma treatment and showed how disordered polymer surfaces cause disordered buried interfaces when in contact with epoxy. This disordered buried interface showed a strong increase in adhesion strength. By studying both covered surface plasma effects and plasma-based adhesion promotion we can obtain a better understanding on how plasma modifies surfaces.

Chapter 4 focused on new metrology development to study buried interfacial structures of thick polymer films. In the majority of our research, model systems are investigated, where

simplifications are made to make SFG analysis possible. In this work, real flip-chips on lead frames (FCOL) were prepared from Texas Instruments (TI) and then the die was polished away, exposing the organic layers of the device. By polishing the samples, SFG analysis was possible and the organic layers were probed and information was obtained on the surface and the buried interface. Many layers are present in FCOL and each interface was probed, and orientation analysis was performed for each. By developing metrology that is capable of investigating real microelectronic samples we have drastically propelled the capabilities of SFG and made it a more viable instrument for real samples.

Chapter 5 focused on flux residue analysis. Flux mixtures are utilized in the microelectronics industry to remove oxides from metals prior to solder reflow. Flux residues can cause device failure during accelerated stress testing. By preventing the residue, we will be able to prevent device failure and increase device lifetime. To model this complicated issue, we look at a reactive and inert surface, before and after flux treatment, at the surface and the buried epoxy interface. Washing treatments were performed to determine how difficult it is to remove flux. It was found, through SFG, that the flux residue can remain on the surface after washing and be difficult to remove on the inert, silica, surface. On the more reactive Cu surface, flux residue can be more easily reacted, and removed. The flux residue greatly changes the buried interface, making it more ordered. In addition to SFG measurements, lap shear analysis was also performed, in order to understand how the molecular orientation can affect the macroscopic mechanical properties. This chapter uses SFG to provide valuable information to an industrially relevant problem, and in doing so, proves the efficacy of SFG to provide real answers that were not previously answerable.

In summary, polymer surfaces and polymer/epoxy buried interfaces have been investigated with SFG, FT-IR, and mechanical testing. Adhesion modifiers and processing conditions were probed with these techniques and a better understanding was obtained. The work further develops SFG into a powerful technique to study important buried interfaces in microelectronics.

1.6 References

[1] H.-M. Tong, "Microelectronics packaging: present and future," *Mater. Chem. Phys.*, vol. 40, pp. 147-161, 1995.

[2] C. P. Wong, "Recent advances in hermetic equivalent flip-chip hybrid IC packaging of microelectronics," *Mater. Chem. Phys.*, vol. 42, pp. 25-30, 1995.

[3] Z. Q. Jiang, Y. Huang, and A. Chandra, "Thermal Stresses in Layered Electronic Assemblies," *J. Electron. Packaging,* vol. 119, pp. 127-132, 1997.

[4] S. Luo, T. Yamashita, and C. P. Wong, "Study on Property of Underfill Based on Epoxy Cured with Acid Anhydride for Flip Chip Application," *J. Electron. Manuf.*, vol. 10, pp. 191-200, 2000.

[5] K. C. Yung and H. Liem, "Enhanced thermal conductivity of boron nitride epoxy-matrix composite through multi-modal particle size mixing," *J. Appl. Polym. Sci.*, vol. 106, pp. 3587-3591, 2007.

[6] B. G. Yacobi, S. Martin, K. Davis, A. Hudson, and M. Hubert, "Adhesive bonding in microelectronics and photonics," *Journal of Applied Physics,* vol. 91, pp. 6227-6262, 2002.

[7] B.-m. Z. Newby, M. K. Chaudhury, and H. R. Brown, "Macroscopic Evidence of the Effect of Interfacial Slippage on Adhesion," *Science,* vol. 269, pp. 1407-1409, September 8, 1995 1995.

[8] M. N. Sathyanarayana and M. Yaseen, "Role of promoters in improving adhesions of organic coatings to a substrate," *Progress in Organic Coatings,* vol. 26, pp. 275-313, 9// 1995.

[9] P. H. Harding and J. C. Berg, "The adhesion promotion mechanism of organofunctional silanes," *Journal of Applied Polymer Science,* vol. 67, pp. 1025-1033, 1998.

[10] A. J. Kinloch, *Adhesion and adhesives: Science and technology*. London: John Wiley & Sons, Ltd, 1988.

[11] S. Bhattacharya, A. Datta, J. M. Berg, and S. Gangopadhyay, "Studies on surface wettability of poly(dimethyl) siloxane (PDMS) and glass under oxygen-plasma treatment and correlation with bond strength," *Journal of Microelectromechanical Systems,* vol. 14, pp. 590-597, 2005.

[12] D. Hegemann, H. Brunner, and C. Oehr, "Plasma treatment of polymers for surface and adhesion improvement," *Nuclear Instruments and Methods in Physics Research Section B: Beam Interactions with Materials and Atoms,* vol. 208, pp. 281-286, 8// 2003.

[13] F. Awaja, M. Gilbert, G. Kelly, B. Fox, and P. J. Pigram, "Adhesion of polymers," *Prog. Polym. Sci.*, vol. 34, pp. 948-968, **2009**.

[14] Y. R. Shen, "Optical Second Harmonic Generation at Interfaces," *Annual Review of Physical Chemistry,* vol. 40, pp. 327-350, 1989.

[15] K. B. Eisenthal, "Liquid Interfaces Probed by Second-Harmonic and Sum-Frequency Spectroscopy," *Chemical Reviews,* vol. 96, pp. 1343-1360, 1996.

[16] X. Zhuang, P. Miranda, D. Kim, and Y. Shen, "Mapping molecular orientation and conformation at interfaces by surface nonlinear optics," *Physical Review B,* vol. 59, pp. 12632-12640, 1999.

[17] Z. Chen, Y. R. Shen, and G. A. Somorjai, "Studies of polymer surfaces by sum frequency generation vibrational spectroscopy," *Annual review of physical chemistry,* vol. 53, pp. 437-465, 2002.

[18] B. Li, J. Zhou, X. Xu, J. Yu, W. Shao, Y. Fang, *et al.*, "Solvent quality affects chain conformational order at the polymer surface revealed by sum frequency generation vibrational spectroscopy," *Polymer,* vol. 54, pp. 1853-1859, 2013.

[19] X. Lu, B. Li, P. Zhu, G. Xue, and D. Li, "Illustrating consistency of different experimental approaches to probe the buried polymer/metal interface using sum frequency generation vibrational spectroscopy," *Soft Matter,* vol. 10, pp. 5390-5397, 2014.

[20] Y. Fang, B. Li, J. Yu, J. Zhou, X. Xu, W. Shao, *et al.*, "Probing surface and interfacial molecular structures of a rubbery adhesion promoter using sum frequency generation vibrational spectroscopy," *Surface Science,* vol. 615, pp. 26-32, 2013.

[21] A. Perry, C. Neipert, B. Space, and P. B. Moore, "Theoretical Modeling of Interface Specific Vibrational Spectroscopy: Methods and Applications to Aqueous Interfaces," *Chemical Reviews,* vol. 106, pp. 1234-1258, 2006.

[22] X. Chen, W. Hua, Z. Huang, and H. C. Allen, "Interfacial Water Structure Associated with Phospholipid Membranes Studied by Phase-Sensitive Vibrational Sum Frequency Generation Spectroscopy," *Journal of the American Chemical Society,* vol. 132, pp. 11336-11342, 2010.

[23] Y. R. Shen, "Basic Theory of Surface Sum-Frequency Generation," *The Journal of Physical Chemistry C,* vol. 116, pp. 15505-15509, 2012.

[24] C. Tian, S. J. Byrnes, H.-L. Han, and Y. R. Shen, "Surface Propensities of Atmospherically Relevant Ions in Salt Solutions Revealed by Phase-Sensitive Sum Frequency Vibrational Spectroscopy," *The Journal of Physical Chemistry Letters,* vol. 2, pp. 1946-1949, 2011.

[25] C. Chen, J. Wang, C. L. Loch, D. Ahn, and Z. Chen, "Demonstrating the Feasibility of Monitoring the Molecular-Level Structures of Moving Polymer/Silane Interfaces during Silane Diffusion Using SFG," *J. Am. Chem. Soc.,* vol. 126, pp. 1174-1179, 2004.

[26] M. A. Sánchez, T. Kling, T. Ishiyama, M.-J. van Zadel, P. J. Bisson, M. Mezger, *et al.*, "Experimental and theoretical evidence for bilayer-by-bilayer surface melting of crystalline ice," *Proceedings of the National Academy of Sciences,* vol. 114, pp. 227-232, 2017.

[27] M. Bonn, H. J. Bakker, Y. Tong, and E. H. G. Backus, "No Ice-Like Water at Aqueous Biological Interfaces," *Biointerphases,* vol. 7, p. 20, 2012.

[28] R. Pandey, K. Usui, R. A. Livingstone, S. A. Fischer, J. Pfaendtner, E. H. G. Backus, *et al.*, "Ice-nucleating bacteria control the order and dynamics of interfacial water," *Science Advances,* vol. 2, 2016.

[29] M. Bonn, C.-S. Hsieh, L. Piatkowski, H. J. Bakker, and Z. Zhang, "Ultrafast dynamics of water at the water-air interface studied by femtosecond surface vibrational spectroscopy," *EPJ Web of Conferences,* vol. 41, 2013.

[30] S. Nihonyanagi, P. C. Singh, S. Yamaguchi, and T. Tahara, "Two-Dimensional Heterodyne-Detected VSFG Spectroscopy of Water Molecules at Charged Interfaces," *EPJ Web of Conferences,* vol. 41, 2013.

[31] Q. Du, E. Freysz, and Y. R. Shen, "Vibrational spectra of water molecules at quartz/water interfaces," *Physical Review Letters,* vol. 72, pp. 238-241, 1994.

[32] J. A. McGuire and Y. R. Shen, "Ultrafast Vibrational Dynamics at Water Interfaces," *Science,* vol. 313, pp. 1945-1948, 2006.

[33] X. Su, L. Lianos, Y. R. Shen, and G. A. Somorjai, "Surface-Induced Ferroelectric Ice on Pt(111)," *Physical Review Letters,* vol. 80, pp. 1533-1536, 1998.

[34] C.-S. Tian and Y. R. Shen, "Isotopic Dilution Study of the Water/Vapor Interface by Phase-Sensitive Sum-Frequency Vibrational Spectroscopy," *Journal of the American Chemical Society,* vol. 131, pp. 2790-2791, 2009.

[35] X. Lu, M. L. Clarke, D. Li, X. Wang, G. Xue, and Z. Chen, "A Sum Frequency Generation Vibrational Study of the Interference Effect in Poly(n-butyl methacrylate) Thin Films Sandwiched between Silica and Water," *J. Phys. Chem. C,* vol. 115, pp. 13759-13767, 2011.

[36] S. J. Kweskin, K. Komvopoulos, and G. A. Somorjai, "Conformational changes at polymer gel interfaces upon saturation with various liquids studied by infrared-visible sum frequency generation vibrational spectroscopy," *Appl. Phys. Lett.,* vol. 88, p. 134105, 2006.

[37] G. P. Harp, H. Rangwalla, M. S. Yeganeh, and A. Dhinojwala, "Infrared-Visible Sum Frequency Generation Spectroscopic Study of Molecular Orientation at Polystyrene/Comb-Polymer Interfaces," *J. Am. Chem. Soc.,* vol. 125, pp. 11283-11290, 2003.

[38] M. Xiao, X. Zhang, Z. J. Bryan, J. Jasensky, A. J. McNeil, and Z. Chen, "Effect of Solvent on Surface Ordering of Poly(3-hexylthiophene) Thin Films," *Langmuir,* vol. 31, pp. 5050-5056, 2015.

[39] Q. Li, R. Hua, and K. C. Chou, "Electronic and Conformational Properties of the Conjugated Polymer MEH-PPV at a Buried Film/Solid Interface Investigated by Two-Dimensional IR−Visible Sum Frequency Generation," *J. Phys. Chem. B,* vol. 112, pp. 2315-2318, 2008.

[40] S. J. Kweskin, K. Komvopoulos, and G. A. Somorjai, "Molecular Restructuring at Poly(n-butyl methacrylate) and Poly(methyl methacrylate) Surfaces Due to Compression by a Sapphire Prism Studied by Infrared−Visible Sum Frequency Generation Vibrational Spectroscopy," *Langmuir,* vol. 21, pp. 3647-3652, 2005.

[41] H. Ye, A. Abu-Akeel, J. Huang, H. E. Katz, and D. H. Gracias, "Probing Organic Field Effect Transistors In Situ during Operation Using SFG," *J. Am. Chem. Soc.,* vol. 128, pp. 6528-6529, 2006.

[42] N. W. Ulrich, J. N. Myers, and Z. Chen, "Characterization of polymer/epoxy buried interfaces with silane adhesion promoters before and after hygrothermal aging for the elucidation of molecular level details relevant to adhesion," *RSC Advances,* vol. 5, pp. 105622-105631, 2015.

[43] P. T. Wilson, L. J. Richter, W. E. Wallace, K. a. Briggman, and J. C. Stephenson, "Correlation of molecular orientation with adhesion at polystyrene/solid interfaces," *Chemical Physics Letters,* vol. 363, pp. 161-168, 2002.

[44] G. Li, A. Dhinojwala, and M. S. Yeganeh, "Interference Effect from Buried Interfaces Investigated by Angular-Dependent Infrared−Visible Sum Frequency Generation Technique," *The Journal of Physical Chemistry C,* vol. 115, pp. 7554-7561, 2011.

[45] S. Ye, S. Morita, G. Li, H. Noda, M. Tanaka, K. Uosaki, *et al.*, "Structural Changes in Poly(2-methoxyethyl acrylate) Thin Films Induced by Absorption of Bisphenol A. An Infrared and Sum Frequency Generation (SFG) Study," *Macromolecules,* vol. 36, pp. 5694-5703, 2003/07/01 2003.

[46] Y. Li, I. Ciofi, L. Carbonell, N. Heylen, J. Van Aelst, M. R. Baklanov, *et al.*, "Influence of absorbed water components on SiOCH low-k reliability," *Journal of Applied Physics,* vol. 104, p. 034113, 2008.

[47] P. T. Wilson, K. A. Briggman, W. E. Wallace, J. C. Stephenson, and L. J. Richter, "Selective study of polymer/dielectric interfaces with vibrationally resonant sum frequency generation via thin-film interference," *Applied Physics Letters,* vol. 80, pp. 3084-3086, 2002.

[48] K. Kunal, C. G. Robertson, S. Pawlus, S. F. Hahn, and A. P. Sokolov, "Role of Chemical Structure in Fragility of Polymers: A Qualitative Picture," *Macromolecules,* vol. 41, pp. 7232-7238, 2008.

[49] S. Roke, "Nonlinear Optical Spectroscopy of Soft Matter Interfaces," *ChemPhysChem,* vol. 10, pp. 1380-1388, 2009.

[50] N. Ji, V. Ostroverkhov, C.-Y. Chen, and Y.-R. Shen, "Phase-Sensitive Sum-Frequency Vibrational Spectroscopy and Its Application to Studies of Interfacial Alkyl Chains," *Journal of the American Chemical Society,* vol. 129, pp. 10056-10057, 2007.

[51] Z. Chen, R. Ward, Y. Tian, S. Baldelli, A. Opdahl, Y.-R. Shen, *et al.*, "Detection of Hydrophobic End Groups on Polymer Surfaces by Sum-Frequency Generation Vibrational Spectroscopy," *Journal of the American Chemical Society,* vol. 122, pp. 10615-10620, 2000.

[52] S. H. Kim, A. Opdahl, C. Marmo, and G. A. Somorjai, "AFM and SFG studies of pHEMA-based hydrogel contact lens surfaces in saline solution: adhesion, friction, and the presence of non-crosslinked polymer chains at the surface," *Biomaterials,* vol. 23, pp. 1657-1666, 2002.

[53] A. Opdahl and G. A. Somorjai, "Solvent Vapor Induced Ordering and Disordering of Phenyl Side Branches at the Air/Polystyrene Interface Studied by SFG," *Langmuir,* vol. 18, pp. 9409-9412, 2002.

[54] C. Zhang, J. Hankett, and Z. Chen, "Molecular Level Understanding of Adhesion Mechanisms at the Epoxy/Polymer Interfaces," *ACS Appl. Mater. Interfaces,* vol. 4, pp. 3730-3737, 2012.

[55] Z. Chen, "Investigating buried polymer interfaces using sum frequency generation vibrational spectroscopy," *Prog. Polym. Sci.,* vol. 35, pp. 1376-1402, 2010.

[56] C. Zhang, N. E. Shephard, S. M. Rhodes, and Z. Chen, "Headgroup effect on silane structures at buried polymer/silane and polymer/polymer interfaces and their relations to adhesion," *Langmuir,* vol. 28, pp. 6052-9, 2012.

[57] M. Xiao, J. Jasensky, X. Zhang, Y. Li, C. Pichan, X. Lu, *et al.*, "Influence of the side chain and substrate on polythiophene thin film surface, bulk, and buried interfacial structures," *Physical Chemistry Chemical Physics,* vol. 18, pp. 22089-22099, 2016.

[58] L. Shen, N. W. Ulrich, C. M. Mello, and Z. Chen, "Determination of conformation and orientation of immobilized peptides and proteins at buried interfaces," *Chemical Physics Letters,* vol. 619, pp. 247-255, 2014.

[59] X. Lu, C. Zhang, N. Ulrich, M. Xiao, Y.-H. Ma, and Z. Chen, "Studying Polymer Surfaces and Interfaces with Sum Frequency Generation Vibrational Spectroscopy," *Analytical Chemistry,* vol. 89, pp. 466-489, 2016.

[60] X. Zou, S. Wei, J. Jasensky, M. Xiao, Q. Wang, C. L. Brooks, *et al.*, "Molecular Interactions between Graphene and Biological Molecules," *Journal of the American Chemical Society,* 2017.

[61] C. Hess, M. Wolf, S. Roke, and M. Bonn, "Femtosecond time-resolved vibrational SFG spectroscopy of CO/Ru(001)," *Surface Science,* vol. 502, pp. 304-312, 2002.

[62] H. Wang, J. Jasensky, N. W. Ulrich, J. Cheng, H. Huang, Z. Chen, *et al.*, "Capsaicin-Inspired Thiol–Ene Terpolymer Networks Designed for Antibiofouling Coatings," *Langmuir,* vol. 33 (47), pp. 13689-13698, 2017.
[63] C. Zhang, J. N. Myers, and Z. Chen, "Molecular Behavior at Buried Epoxy/Poly(ethylene terephthalate) Interface," *Langmuir,* vol. 30, pp. 12541-50, 2014.
[64] N. W. Ulrich, J. Andre, J. Williamson, K.-W. Lee, and Z. Chen, "Plasma treatment effect on polymer buried interfacial structure and property," *Physical Chemistry Chemical Physics,* vol. 19, pp. 12144-12155 2017.
[65] A. G. Lambert, P. B. Davies, and D. J. Neivandt, "Implementing the Theory of Sum Frequency Generation Vibrational Spectroscopy: A Tutorial Review," *Applied Spectroscopy Reviews,* vol. 40, pp. 103-145, 2005.
[66] C. Hirose, N. Akamatsu, and K. Domen, "Formulas for the analysis of surface sum - frequency generation spectrum by CH stretching modes of methyl and methylene groups," *The Journal of Chemical Physics,* vol. 96, pp. 997-1004, 1992.
[67] J. Löbau and K. Wolfrum, "Sum-frequency spectroscopy in total internal reflection geometry: signal enhancement and access to molecular properties," *Journal of the Optical Society of America B,* vol. 14, pp. 2505-2512, 1997/10/01 1997.
[68] R. Braun, B. D. Casson, and C. D. Bain, "A sum-frequency study of the two-dimensional phase transition in a monolayer of undecanol on water," *Chemical Physics Letters,* vol. 245, pp. 326-334, 1995.
[69] C. Hirose, N. Akamatsu, and K. Domen, "Formulas for the Analysis of the Surface SFG Spectrum and Transformation Coefficients of Cartesian SFG Tensor Components," *Appl. Spectrosc.,* vol. 46, pp. 1051-1072, 1992.
[70] Y. Tong, Y. Zhao, N. Li, M. Osawa, P. B. Davies, and S. Ye, "Interference effects in the sum frequency generation spectra of thin organic films. I. Theoretical modeling and simulation," *The Journal of Chemical Physics,* vol. 133, p. 034704, 2010.
[71] J. Wang, C. Chen, S. M. Buck, and Z. Chen, "Molecular chemical structure on poly(methyl methacrylate) (PMMA) surface studied by sum frequency generation (SFG) vibrational spectroscopy," *J. Phys. Chem. B,* vol. 105, pp. 12118-12125, 2001.
[72] X. Wei, X. Zhuang, S.-C. Hong, T. Goto, and Y. R. Shen, "Sum-Frequency Vibrational Spectroscopic Study of a Rubbed Polymer Surface," *Physical Review Letters,* vol. 82, pp. 4256-4259, 05/24/ 1999.
[73] G. J. Simpson and K. L. Rowlen, "An SHG Magic Angle: Dependence of Second Harmonic Generation Orientation Measurements on the Width of the Orientation Distribution," *Journal of the American Chemical Society,* vol. 121, pp. 2635-2636, 1999/03/01 1999.
[74] C. Hirose, H. Yamamoto, N. Akamatsu, and K. Domen, "Orientation analysis by simulation of vibrational sum frequency generation spectrum: CH stretching bands of the methyl group," *The Journal of Physical Chemistry,* vol. 97, pp. 10064-10069, 1993/09/01 1993.
[75] J. Wang, S. E. Woodcock, S. M. Buck, C. Chen, and Z. Chen, "Different Surface-Restructuring Behaviors of Poly(methacrylate)s Detected by SFG in Water," *J. Am. Chem. Soc.,* vol. 123, pp. 9470-9471, 2001/09/01 2001.
[76] D. C. Duffy, P. B. Davies, and C. D. Bain, "Surface Vibrational Spectroscopy of Organic Counterions Bound to a Surfactant Monolayer," *The Journal of Physical Chemistry,* pp. 15241-15246, 1995.

[77] K. S. Gautam, A. D. Schwab, A. Dhinojwala, D. Zhang, S. M. Dougal, and M. S. Yeganeh, "Molecular Structure of Polystyrene at Air/Polymer and Solid/Polymer Interfaces," *Physical Review Letters,* vol. 85, pp. 3854-3857, 10/30/ 2000.

[78] X. Lu, J. Han, N. Shephard, S. Rhodes, A. D. Martin, D. Li, *et al.*, "Phenolic Resin Surface Restructuring upon Exposure to Humid Air: A Sum Frequency Generation Vibrational Spectroscopic Study," *J. Phys. Chem. B,* vol. 113, pp. 12944-12951, 2009/10/01 2009.

[79] X. Lu, S. A. Spanninga, C. B. Kristalyn, and Z. Chen, "Surface Orientation of Phenyl Groups in Poly(sodium 4-styrenesulfonate) and in Poly(sodium 4-styrenesulfonate):Poly(3,4-ethylenedioxythiophene) Mixture Examined by Sum Frequency Generation Vibrational Spectroscopy," *Langmuir,* vol. 26, pp. 14231-14235, 2010/09/07 2010.

[80] X. Chen, J. Wang, A. P. Boughton, C. B. Kristalyn, and Z. Chen, "Multiple Orientation of Melittin inside a Single Lipid Bilayer Determined by Combined Vibrational Spectroscopic Studies," *Journal of the American Chemical Society,* vol. 129, pp. 1420-1427, 2007/02/01 2007.

[81] K. T. Nguyen, S. V. Le Clair, S. Ye, and Z. Chen, "Orientation determination of protein helical secondary structures using linear and nonlinear vibrational spectroscopy," *The journal of physical chemistry. B,* vol. 113, pp. 12169-12180, 2009.

[82] K. T. Nguyen, J. T. King, and Z. Chen, "Orientation Determination of Interfacial β-Sheet Structures in Situ," *The Journal of Physical Chemistry B,* vol. 114, pp. 8291-8300, 2010/07/01 2010.

[83] J. Wang, X. Chen, M. L. Clarke, and Z. Chen, "Detection of chiral sum frequency generation vibrational spectra of proteins and peptides at interfaces in situ," *Proceedings of the National Academy of Sciences of the United States of America,* vol. 102, pp. 4978-4983, 2005.

[84] S. Kataoka and P. S. Cremer, "Probing molecular structure at interfaces for comparison with bulk solution behavior: Water/2-propanol mixtures monitored by vibrational sum frequency spectroscopy," *J. Am. Chem. Soc.*, vol. 128, pp. 5516-5522, 2006.

[85] S. Roy, K.-K. Hung, U. Stege, and D. K. Hore, "Rotations, Projections, Direction Cosines, and Vibrational Spectra," *Applied Spectroscopy Reviews,* vol. 49, pp. 233-248, 2014.

[86] J. N. Myers and Z. Chen, "Surface plasma treatment effects on the molecular structure at polyimide/air and buried polyimide/epoxy interfaces," *Chin. Chem. Lett.*, vol. 26, p. 449, 2015.

[87] J. Sung, D. Kim, C. N. Whang, M. Oh-e, and H. Yokoyama, "Sum-Frequency Vibrational Spectroscopic Study of Polyimide Surfaces Made by Spin Coating and Ionized Cluster Beam Deposition," *The Journal of Physical Chemistry B,* vol. 108, pp. 10991-10996, 2004/07/01 2004.

[88] D. Kim, M. Oh-e, and Y. R. Shen, "Rubbed Polyimide Surface Studied by Sum-Frequency Vibrational Spectroscopy," *Macromolecules,* vol. 34, pp. 9125-9129, 2001/12/01 2001.

Chapter 2: Hygrothermal Treatment of Model Underfill Systems with Silane Adhesion Promoters

2.1. Introduction

One method of characterizing the resilience of an epoxy underfill is to perform hygrothermal aging and then analyze the samples to see how they change in the presence of stress. Hygrothermal treatments are performed by exposing the samples to high heat and humidity, which can decrease the strength of adhesion [1] by disrupting the interfacial interactions.[2] The bulk of the research on epoxy underfills for microelectronic packaging has focused on bulk and surface analysis *ex situ*. Techniques such as adhesion strength testing,[3] scanning acoustic microscopy (SAM),[4] thermogravimetric analysis,[5] moiré interferometry,[6] Fourier transform infrared spectroscopy (FTIR),[1] scanning electron microscopy (SEM),[1, 5] and X-ray photoelectron spectroscopy (XPS)[4] have all been utilized to investigate epoxy underfills and determine how they behave with the hygrothermal treatment. Techniques such as SAM, moiré interferometry, SEM, and XPS, can provide structural or elemental information, but they cannot provide chemical or interfacial functional group orientation information. Delamination can be monitored by techniques such as SAM, but this technique is incapable of determining molecular-level interactions relevant to adhesion, which are primarily determined by the structures of the molecules at the interface.[7] One substantial issue with all of these methods is that none of them are capable at looking at the molecular-level detail *in situ* at the buried interface, which is relevant where the die is connected to a substrate via an underfill (Figure 1.1). Buried interfaces provide a substantial challenge for researchers due to a lack of techniques available that can probe these regions and provide chemical information. Buried interfaces have been traditionally studied by breaking apart the two substrates, characterizing the resulting surfaces, and then attempting to extrapolate the molecular structure at the buried interface from the *ex situ* measurements on the two exposed surfaces. The problem with this method is that the molecular interactions that may determine the strength of adhesion at the interface could be destroyed when the substrates are separated and analyzed, thus the measured

results are not the same as what we want while the system is in its native state. In order to fully elucidate how hygrothermal testing affects delamination of epoxy underfills at buried interfaces, a technique must be utilized that can provide chemical specific information, and make *in situ* measurements, nondestructively.

In this chapter the effects of silane adhesion promoters (SAPs) and hygrothermal (HT) aging were implemented to better understand how to increase adhesion and how stress testing changes the buried interface. Hygrothermal aging is also presented to show how adhesion promoters can reduce moisture content at the interface, which improves adhesion strength. Polymers are put in contact with epoxy adhesives to simulate substrate/underfill buried interfaces. These systems are then treated with adhesion promoters and hygrothermal aging, to see how the buried polymer/epoxy interface changes. The main technique utilized to probe these systems is SFG vibrational spectroscopy. This research further demonstrates the capabilities of SFG to probe buried polymer/epoxy systems *in situ*, which provides a much better understanding of adhesion relevant to the microelectronics industry.

SFG spectroscopy was employed to investigate how polymer/epoxy interfaces behave in the presence of high temperature and humidity and to determine if silane adhesion promoters can prevent or delay the effects of hygrothermal aging. Specifically, we studied the deuterated polystyrene (dPS)/epoxy, and deuterated poly(ethylene terephthalate) (dPET)/epoxy buried interfaces with and without silane adhesion promoters before and after hygrothermal aging. The deuterated polymers were used in this study to avoid spectral confusion between the polymer and the epoxy (with or without silanes added). The polymers polystyrene and poly-(ethylene terephthalate) are excellent examples of hydrophobic and relative hydrophilic substrates, respectively, which serve as good models for polymer substrates in the microelectronics industry. SFG and attenuated total internal reflectance-Fourier transform infrared spectroscopy (ATR-FTIR) spectra of these interfaces were collected before and after hygrothermal aging in order to elucidate the interfacial molecular structure and provide a possible mechanism for adhesion loss. In addition to the control systems (without added silanes), three different silanes adhesion promoters were utilized: (3-aminopropyl)-trimethoxysilane (ATMS), (3-glycidoxypropyl) trimethoxysilane (γ-GPS), and octadecyltrimethoxysilane (OTMS), to determine what effect the

promoters have and if they can prevent some water uptake at the interface. Lap shear adhesion tests were then performed on the same systems to correlate macroscopic adhesion changes during hygrothermal aging to changes observed in the spectral data, in order to understand the structure-function relationship of the buried polymer/epoxy interfaces and to understand adhesion on a more fundamental level. The success of such investigations will ultimately lead to more robust underfills that can withstand greater stress.

2.2. Materials and Methods

2.2.1. Materials

Right angle fused silica prism substrates (Altos Photonics, Inc., Bozeman, MT) were utilized for all SFG experiments as solid supports for polymer thin film deposition. The polymer PET, with a deuterated aliphatic chain (d4-PET or dPET), and deuterated polystyrene (d8-PS or dPS) were both purchased from Polymer Science, Inc., Monticello, IN. Two solutions (2.0 weight %) were made by dissolving dPET in 2-chlorophenol (Sigma-Aldrich, St. Louis, MO, >99%) and dPS in chloroform (Sigma-Aldrich, St. Louis, MO, >99.8%). Three different silanes were utilized: (3-glycidoxypropyl) trimethoxysilane (γ-GPS), (3-Aminopropyl)-trimethoxysilane (ATMS), and octadecyltrimethoxysilane (OTMS), were all purchased from Sigma-Aldrich (St. Louis, MO) and 1.5 weight % of each silane was added to an epoxy sample prior to curing. Commercial epoxy resin 3302 (CE3302) was obtained from Epoxies Etc., Cranston, RI. CE3302 base is a proprietary blend, composed predominantly of bisphenol A-(epichlorohydrin) and trace amounts of bis(1,2,2,6,6-pentamethyl-4 piperidinyl)-sebacate and 4-nonylphenol. The CE3302 hardener used was poly(oxypropylenediamine). Bisphenol A digylcidyl ether (BADGE) is produced in the curing process and then reacts further with poly(oxypropylenediamine) to produce a cross-linked structure.[8] All chemical structures can be found in Figure 2.1.

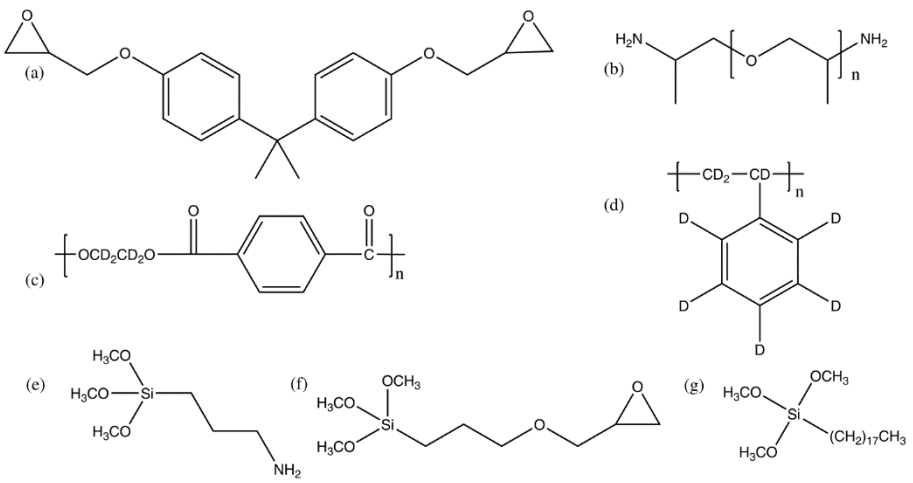

Figure 2.1: Chemicals used in the experiment: A. bisphenol A diglycidyl ether (BADGE), B. poly(oxypropylenediamine), C. poly(ethylene terephthalate) with aliphatic chain deuterated (d4-PET, we refer to it as dPET in this chapter), D. deuterated polystyrene (d8-PS), E. (3-Aminopropyl)trimethoxysilane (ATMS), F. (3-glycidoxypropyl) trimethoxysilane (γ-GPS), and G. octadecyltrimethoxysilane (OTMS).

2.2.2. Sample Preparation

Silica prisms were cleaned first in a concentrated sulfuric acid bath saturated with potassium dichromate followed by a rinse of deionized water and then they were finally dried under a stream of nitrogen. Following the acid cleaning, the substrates were exposed to air plasma (PE-50, Plasma Etch) for 2 minutes prior to polymer film deposition. Polymer solutions were spin-cast on the fused silica substrates at 2500 rpm for 30 s using a P-6000 spin coater (Speedline Technologies). In order to remove solvent residue, the samples were covered and placed overnight in the fume hood. For epoxy curing, the mixing ratio for resin to hardener was 2:1 by mass. After vigorously mixing the resin and hardener together, the epoxy was cured on top of the spin-cast polymer films according to manufacturer specifications (2 hours at 52°C).[8] After epoxy curing, the samples were exposed to 85°C and 100% relative humidity (RH) environmental conditions for defined periods of time by placing the samples above liquid water in a home-built, sealed container. Right angle silicon prisms were used in all ATR-FTIR experiments as solid supports. Silicon substrates were cleaned and samples prepared using the same methods for the silica samples.

2.2.3. SFG and ATR-FTIR

Both SFG and single bounce ATR-FTIR were utilized in this work. Spectra were collected from the buried interface between the polymer and epoxy after curing, after 24 hours hygrothermal treatment, and after 48 hours hygrothermal treatment. Because the aliphatic group deuterated PET and deuterated PS were used in this study, no aliphatic C−H signals were generated from the

polymer at the buried polymer/substrate interface (in the spectral region scanned). The use of prism substrates and the adoption of the experimental geometry shown in Figure 2.2 greatly enhanced SFG signals compared to the use of the previous experimental geometry utilizing window substrates.[9-11] ATR-FTIR measurements were performed using a Nicolet 6700 FT-IR spectrometer controlled by OMNIC software. The input angle was approximately 45° vs. the sample surface. Single-bounce ATR-FTIR measurements with a silicon prism internal reflection element as a solid support was utilized due to its spectral transparency in the 2500−3500 cm^{-1} region (Figure 2.2).

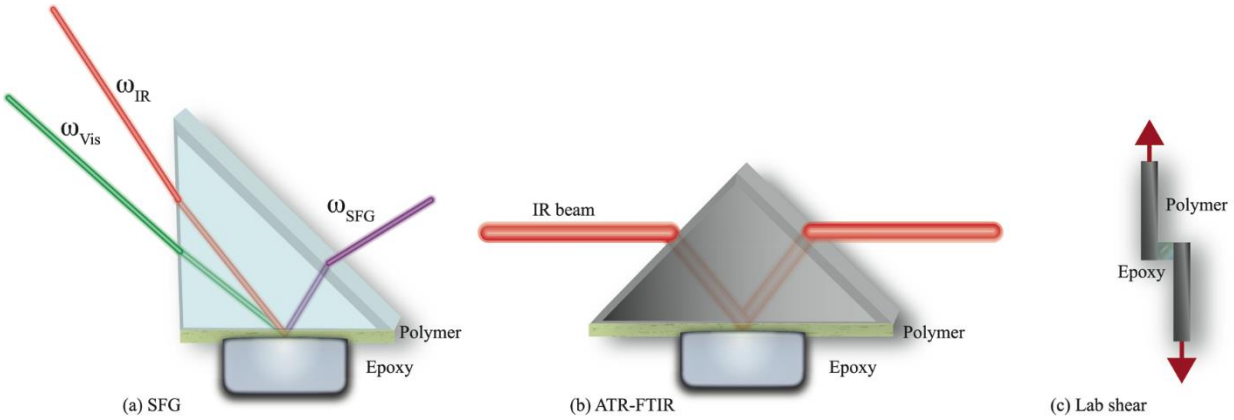

Figure 2.2: A. SFG, B. ATR-FTIR, and B. lap shear experimental geometry utilized to research the epoxy buried interfaces.

2.2.4. Lap Shear Adhesion Testing

Adhesion lap shear tests were performed at room temperature after the specified hygrothermal aging time using a method based on ASTM D3163 (Figure 2.2). After the sheets were completely separated, an abrupt drop in adhesion strength was observed. The maximum adhesion strength observed before the sudden drop in force was utilized for all reported adhesion strength measurements. All adhesion failures were primarily adhesive failure at the interface as determined by a visual comparison of the delaminated area and a control region that was not exposed to epoxy adhesive, which shows that the interfacial molecular structures reported are related to the interfacial adhesive properties.

2.3 Results and Discussion

2.3.1 Previous Investigations

In previous work, in order to understand how moisture affects the buried polymer/epoxy interface, samples were prepared and exposed to 85°C/100% R.H.[12] Two polymers were investigated, polystyrene (PS) and polyethylene terephthalate (PET); and one epoxy, bis-phenyl diglycidyl ether (BADGE). The SiO_2/epoxy interface was also investigated, as a model for a Si surface. These systems were investigated with SFG spectroscopy, ATR-FTIR spectroscopy, and lap shear analysis. The samples were investigated before and after hygrothermal aging (24 and 48 hours).

For the previously investigated three systems, dPS/epoxy, dPET/epoxy, and SiO_2/epoxy interfaces mentioned above, deuterated polymers were used to avoid spectral confusion with the epoxy. The dPS surface is very hydrophobic, the dPET surface is less hydrophobic, and the SiO_2 surface is hydrophilic. By comparing these three surfaces we can understand if the hydrophobicity of the surface has a role in moisture uptake at the buried interface. SFG spectroscopy is sensitive to the ordering at interfaces, with more ordering causing higher intensity. The dPS/epoxy gave very strong SFG signal, showing that the buried interface is well ordered, following hygrothermal aging of 24 and 48 hours there was no observable change in the SFG spectra. The dPET/epoxy interface was less ordered than the dPS/epoxy interface. Following hygrothermal treatment there was interfacial water detected at the buried interface. This shows that the hydrophobicity of the surface matters and water can migrate to the buried interface and form an ordered lattice for less hydrophobic dPET interface after the hygrothermal treatment. The SiO_2/epoxy showed similar results to the dPET/epoxy, very ordered structure and following hygrothermal aging, ordered water was detected at the interface. In addition to SFG measurements, the same systems were probed with ATR-FTIR, which penetrates ~800 nm into the sample, so the ATR-FTIR spectra generated contain information about both the polymer film and the epoxy in the interfacial region. It was found that in all three systems, bulk water was detected. Lap shear analysis was performed on the PS/epoxy and PET/epoxy interfaces. The adhesion strength of the PS/epoxy system decreased by 30%, after 24 hours of hygrothermal aging and PET/epoxy decreased by 70%.

The SFG data clearly shows that the hydrophobicity of the polymer surface determines if water can penetrate to the interface and form an ordered network at the buried interface. All systems had bulk water, but on the hydrophilic surfaces had interfacial water present after hygrothermal aging.

It was also shown that after hygrothermal aging the adhesion strength for both PS/epoxy and PET/epoxy decreased, but the PET/epoxy system decreased much more, which is due to the interfacial water. This work suggests that if we can prevent interfacial water from forming, we will have a system that is more resilient to hygrothermal aging.

A ubiquitous method of increasing the adhesion of epoxy based materials is to use SAPs. These silanes can greatly increase the adhesion and resilience to accelerated stress testing, but the mechanisms by which they increase the adhesion is not known. In previous work,[8] SAPs were investigated on dPET and dPS in contact with various epoxy materials. By using SFG spectroscopy it was determined that these silanes can migrate to the interface to increase the adhesion strength by promoting interfacial diffusion. It was also found that more ordered methyl groups of some silane molecules at the buried interface are correlated with lower adhesion.

As discussed above, strong adhesion loss is seen when interfacial water is formed and SAPs could migrate to the interface. In order to see if silanes can prevent interfacial water from forming, polymer/epoxy systems were investigated with 1.5% silanes added to epoxy, before and after hygrothermal aging. In this work, there were two systems investigated, dPS/epoxy and dPET/epoxy interfaces, along with three SAPs, (3-glycidoxypropyl) trimethoxysilane (γ-GPS), (3-Aminopropyl) trimethoxysilane (ATMS), octadecyltrimethoxysilane (OTMS). ATMS and γ-GPS were utilized because they have an amine and an epoxide ring that can further react, respectively, and OTMS is an unreactive control with a terminated methyl group.

2.3.2 dPET/epoxy Interface

In order to fully understand the hygrothermal effect, the first system that was investigated is the control dPET/epoxy interface, with no additional silane adhesion promoters added to the commercial epoxy. There is one weak peak present in the SFG spectrum collected from the dPET/epoxy control prior to hygrothermal aging at 2940 cm^{-1}, which can be assigned to the Fermi resonance of the epoxy methyl group (Figure 2.3: a1). After 24 hours of hygrothermal treatment, there was an additional peak at 3150 cm^{-1}, which can be assigned to interfacial strongly hydrogen bonded water. After 48 hours of hygrothermal treatment, the same two peaks were present, but the water peak grew in intensity relative to the methyl peak. We believe that this is evidence that the interfacial region greatly changes after hygrothermal aging. The selection rule of SFG determines that SFG can only detect ordered water at the interface. Here ordered water was detected in the

SFG spectra, which shows the water molecules migrated to the interface, strongly hydrogen bonded, and adopted some ordering. Since there is water detected after hygrothermal treatment at the interface, we believe that the adhesion strength will decrease, which we will show below.

To understand how silane adhesion promoters affect water uptake, dPET/epoxy interfaces in the presence of the three silane adhesion promoters, ATMS, γ-GPS, and OTMS, mixed into the epoxy (Figure 2.3: a2, a3, and a4, respectively) were investigated. For the ATMS and γ-GPS systems, no SFG signal was detected before or after hygrothermal aging, showing that the system is disordered at the interface and remains disordered at the interface throughout the aging process, which means water vapor is not moving to the interface and forming an ordered structure through a hydrogen bonding network. This shows that ATMS and γ-GPS are capable of preventing structural changes and ordered water uptake at the interface. As we indicated above, only 1.5 % of the silane was added to the epoxy bulk.

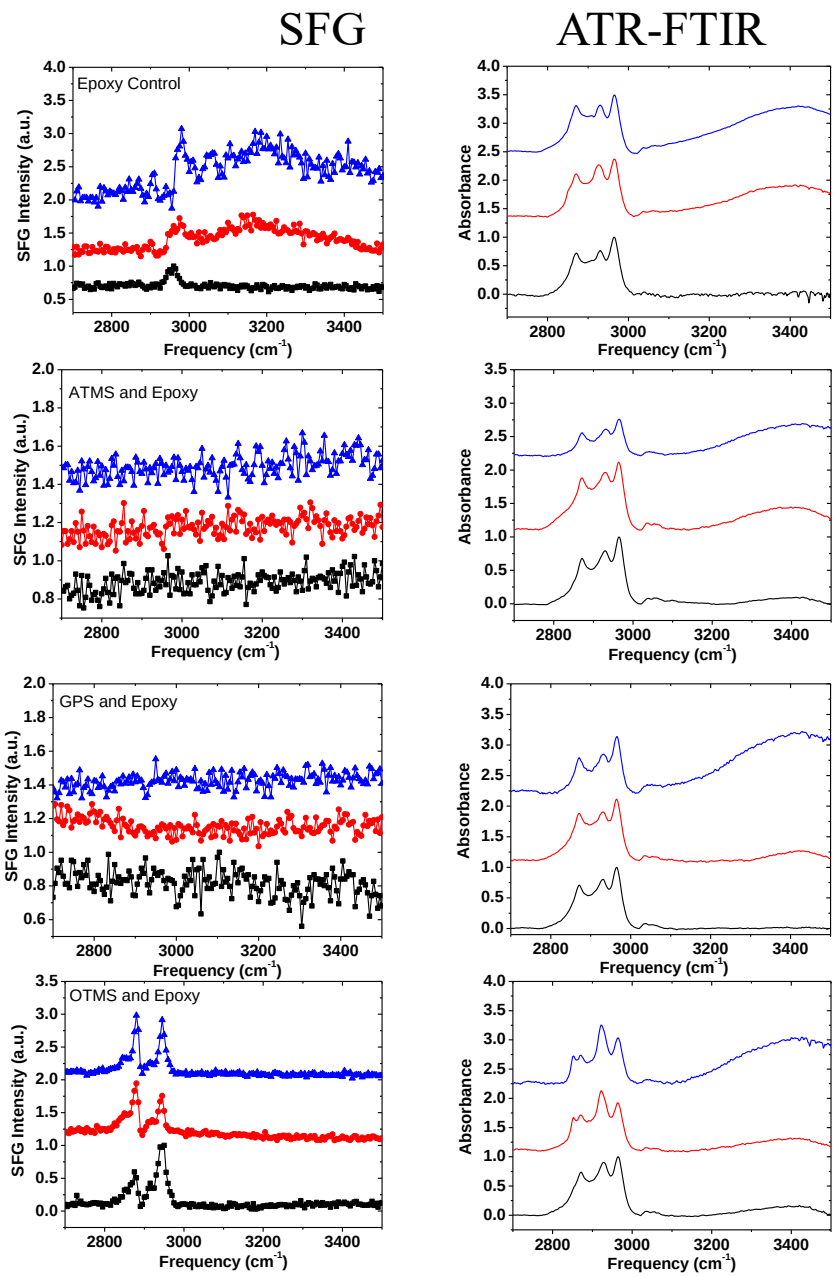

Figure 2.3: SFG (a) (first column) and ATR-FTIR (second column)(b) spectra collected from the interfaces or interfacial regions between dPET and (1) epoxy, (2) epoxy with ATMS, (3) epoxy with GPS, and (4) epoxy with OTMS. Black (bottom) spectra are at time zero, red (middle) spectra are at after 24 hours hygrothermal treatment, and blue (top) spectra are after 48 hours hygrothermal treatment.

Here it is clearly shown that a small amount of the silane in the epoxy bulk can greatly vary the interfacial structure between the polymer and epoxy. As we reported before,[8] the absence of the SFG signal from the polymer/epoxy (with silane) interface is likely due to the interfacial diffusion, and such interfacial diffusion could enhance the interfacial adhesion. We believe that after adding ATMS or γ-GPS, they can segregate to the interface and diffuse through the interface. Therefore we believe that the adhesion at such interfaces should be relatively stronger, which will be further discussed below. For the OTMS system, the methyl group symmetric stretch and Fermi resonance are present in the SFG spectra throughout the aging process and no interfacial water is detected, however the two peaks change in intensity relative to each other. Such methyl signals can be contributed from both epoxy and OTMS. This study shows that with only 1.5 % OTMS molecules in the epoxy bulk, they are capable of preventing interfacial water, but the methyl groups are still reorienting during the aging process, indicated by the peak ratio changing. In the past, we demonstrated that the interfacial methyl groups detected by SFG may be related to weak adhesion, which will be discussed further below while we present the adhesion testing data. In summary, here SFG studies clearly show that the small amount of silane added to epoxy can effectively minimize/reduce the interfacial ordered water layer formation.

To observe if water can move into the dPET/epoxy system, a supplementary technique ATR-FTIR was utilized in this study. The theoretical penetration depth of the infrared evanescent wave used for the ATR-FTIR study here was calculated as 800 nm. The dPET thin-film is approximately 100 nm, which means that this technique can probe 700 nm into the epoxy region (this region, relative to SFG, is considered to be the bulk or interfacial region).[13] In all three spectra (pretreatment, 24 hours, 48 hours hygrothermal aging) for each of the four systems (control or dPET/epoxy without silane added, or dPET/epoxy incorporated with ATMS, or γ-GPS, and or OTMS), there are three peaks present in the C-H stretching frequency region (Figure 2.3: b1, b2, b3, and b4) at 2870, 2930, and 2965 cm^{-1}, which can be assigned to the epoxy methyl symmetric stretch, methylene antisymmetric stretch, and methyl antisymmetric stretch, respectively.[14] Since ATR-FTIR detects signals from the bulk material, and we only added 1.5 % of silanes to the epoxy bulk, we therefore believe that these signals are dominated by the contributions from the epoxy. Subsequent to the 24 hour hygrothermal aging, there was a new peak that emerged at 3400 cm^{-1}, which can be assigned to O–H stretch of water from the interfacial region of the epoxy. This signal is contributed by the weakly hydrogen bonded water molecules. Therefore different from the

ordered water molecules at the interface, here the water molecules in the bulk or interfacial region of epoxy are mostly weakly hydrogen bonded. After 48 hours, the water absorbance peak grew in intensity relative to the 24 hour spectrum, indicating that water continued to diffuse into the epoxy bulk with increased aging.

In order to correlate the molecular-level detail to the macroscopic properties, lap shear adhesion testing was performed before and after 24 hours of hygrothermal aging, see Figure 2.4. For all four systems, there was a decrease in adhesion strength, which matches the literature for systems at 100% R.H.[15] The control system had the biggest drop in adhesion, going from 8.1 MPa to 1.9 MPa, a decrease of 76%. For the epoxy materials with added adhesion promoters, the interface between dPET and epoxy with ATMS added had the smallest decrease in adhesion, from 10.6 MPa to 7.5 MPa (decrease of 29%), followed by the adhesion of the interface between dPET and epoxy with added γ-GPS, from 8.2 MPa to 5.4 MPa (decrease of 34%). The dPET/epoxy with OTMS added interface had the largest decrease in adhesion strength, which went from 7.7 MPa to 4.3 MPa (decrease of 44%). For all three interfaces between dPET and epoxy with silanes added, the adhesion after hygrothermal aging is more than twice of the control. These results show that silane adhesion promoters have the ability to prevent some loss in adhesion strength after hygrothermal aging.

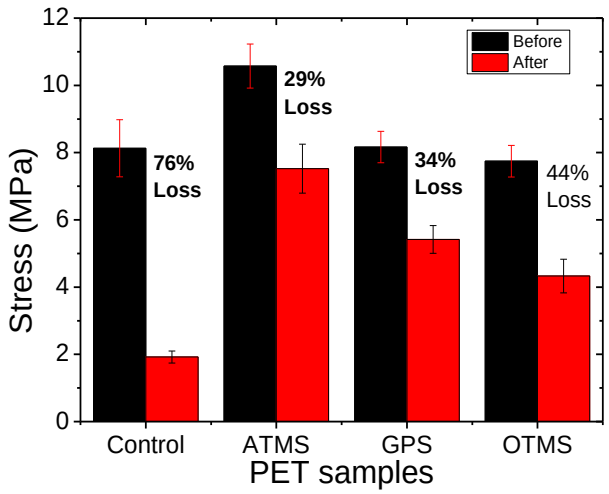

Figure 2.4: Adhesion testing results of dPET/epoxy without and with silane samples. Adhesion strength is the maximum adhesion force/contact area. The black bars are before hygrothermal aging and the red bars are after 24 hours of aging. The error bars are the standard error.

Figure 2.3b shows similar ATR-FTIR spectra for different samples under similar condition, but adhesion-testing results indicated that they have very different adhesion strength. This shows that the interfacial structure plays an important role in adhesion. PET is a relatively polar polymer, which means it is energetically favorable for water to form a hydrogen-bonding structure at the interface, and this is what is seen in the SFG spectrum for the control system. After hygrothermal aging, there is a peak assigned to water, which shows that water can migrate to the interface and form bonding interactions with the polymer. For the control system, there is water detected at both the interface with SFG and bulk (or interfacial region) with ATR-FTIR, which is what one would expect considering the fact that no adhesion promoters were added. The lap shear results show a big decrease in adhesion for the control sample but smaller decreases for the systems with silane adhesion promoters. This shows that if there is ordered water detected by SFG (along the bulk water detected by ATR-FTIR), the adhesion strength will be drastically reduced (decrease of 71% for the control sample).

In contrast from the control sample, all the SFG spectra collected from the interfaces between dPET and epoxy with silane added do not exhibit substantial water contribution. As we discussed previously,[8] ordered methyl groups at an interface should yield lower adhesion strength. For the situations both before and after hygrothermal aging, the control and OTMS incorporated systems have ordered methyl groups, shown in the SFG spectra. The adhesion strengths of these systems are lower than the ATMS and γ-GPS incorporated systems, which have disordered interfaces between dPET and epoxy with silanes added and higher adhesion strengths. The measured adhesion of the dPET/epoxy (without silane or control) interface is higher than that of the dPET/epoxy with OTMS added interface. This is reasonable because stronger signal in the SFG spectrum from the later interface was observed, showing that the methyl groups are more ordered at the interface than the control sample. We showed previously that ordered interfacial methyl groups reduce the adhesion.

The dPET/epoxy systems with γ-GPS, ATMS, and OTMS have been investigated previously (without hygrothermal aging) and the spectra presented in this work match the literature, with no signal coming from the γ-GPS and ATMS systems and strong methyl signal coming from the OTMS system.[8] After the hygrothermal treatment, no water signal was detected form any of the three interfaces. This shows that the adhesion promoters are capable of preventing water migration

to the interface. Silanes have been shown to move to the interface,[8] and there is water present in the bulk.

The promoters ATMS and γ-GPS are good at reducing water because the amine in ATMS and the epoxide ring in γ-GPS can further react with the epoxy matrix once they migrate to the interface and become chemically immobilized, which then prevents the water molecules from becoming ordered because the water molecules cannot form an ordered structure. OTMS makes the interface more nonpolar, but it cannot react further with the epoxy matrix, so it decreases the water uptake but it does not increase the level of adhesion strength by reacting further. Thus, OTMS prevents loss of adhesion strength due to the prevention of interfacial ordered water formation, but it does not increase the adhesion strength by reacting further with the epoxy matrix like the reaction γ-GPS is capable of undergoing. Nevertheless, all the three silane added system could prevent water from getting into the interface to form a ordered water layer. Therefore they could greatly reduce the adhesion loss compared to the control sample after hygrothermal aging. The measured adhesion strengths reduced somehow, even though SFG spectra from the interfaces between PET and epoxy with ATMS or γ-GPS are similar before and after hygrothermal treatment. This decrease should be due to the effect of bulk (or interfacial region) water in epoxy detected by ATR-FTIR after the hygrothermal aging.

2.3.3 dPS/epoxy Interface

As we discussed above, PET has a relative hydrophilic surface compared to many other polymers. In order to see if a more hydrophobic interface behaves differently from PET (dPET/epoxy), the dPS/epoxy interface was investigated. The effects of hygrothermal aging was examined by collecting the SFG spectrum from the dPS/epoxy interface, see Figure 2.5: a1. There are two peaks present in the SFG spectrum of dPS/epoxy control prior to hygrothermal aging at 2870 cm^{-1} and 2940 cm^{-1}, which can be assigned to the epoxy methyl group symmetric stretching and the Fermi resonance of the epoxy methyl group. After 24 hours and 48 hours of hygrothermal treatment the peak ratios in the spectra fluctuate slightly, but there is no interfacial water detected. We believe that this is evidence that the interfacial region does not change greatly after hygrothermal aging. Ordered water was not detected, which shows the water molecules are not present or not capable of forming ordered structures at this hydrophobic interface.

To investigate if silane adhesion promoters can change how water responds at a hydrophobic interface, the same three silane adhesion promoters were added to the dPS/epoxy system (Figure 2.5: a2, a3, and a4). For all three silane promoter systems, there are two peaks present in each of the SFG spectrum at 2870 cm^{-1} and 2940 cm^{-1}, which can be assign to the symmetric stretching and the Fermi resonance of the epoxy methyl group, respectively. No substantial changes were observed in the spectra throughout hygrothermal aging.

To confirm that water can move into the bulk (or interfacial region) of the dPS/epoxy systems, ATR-FTIR was used again to study all the dPS/epoxy systems. In all three spectra (pretreatment, 24 hours, 48 hours hygrothermal aging) for each of the four systems (control sample, samples with ATMS, γ-GPS, or OTMS in epoxy) there are three peaks present in the C-H stretching frequency region (Figure 2.5: b1, b2, b3, and b4, respectively) at 2870, 2930, and 2965 cm^{-1}, which can be assigned to the epoxy methyl symmetric stretch, methylene antisymmetric stretch, and methyl antisymmetric stretch, respectively.[14] Subsequent to the 24 hour hygrothermal aging there was a new broad peak that emerged centered at 3400 cm^{-1}, which can be assigned to O–H stretch of water from the bulk region of the epoxy. After 48 hours the water absorbance peak grew in intensity relative to the 24 hour spectrum, indicating that water continued to diffuse into the epoxy bulk with increased aging.

Lap shear adhesion testing was performed for the dPS/epoxy systems before and after 24 hour hygrothermal aging, see Figure 2.6. For all four systems there was some decrease in the level of adhesion strength. The control system went from 7.4 MPa to 3.0 MPa (decrease of 59%). For the adhesion promoters, ATMS incorporated sample had the smallest decrease, from 8.7 MPa to 4.4 MPa (decrease of 50%), followed by γ-GPS incorporated sample, from 8.2 MPa to 3.7 MPa (decrease of 55%), and the largest decrease in adhesion strength was OTMS incorporated sample, which went from 7.6 MPa to 2.7 MPa (decrease of 64%). These results show that ATMS and γ-GPS have the ability to prevent some loss of adhesion strength after hygrothermal aging, while OTMS actually makes the decrease in adhesion strength larger.

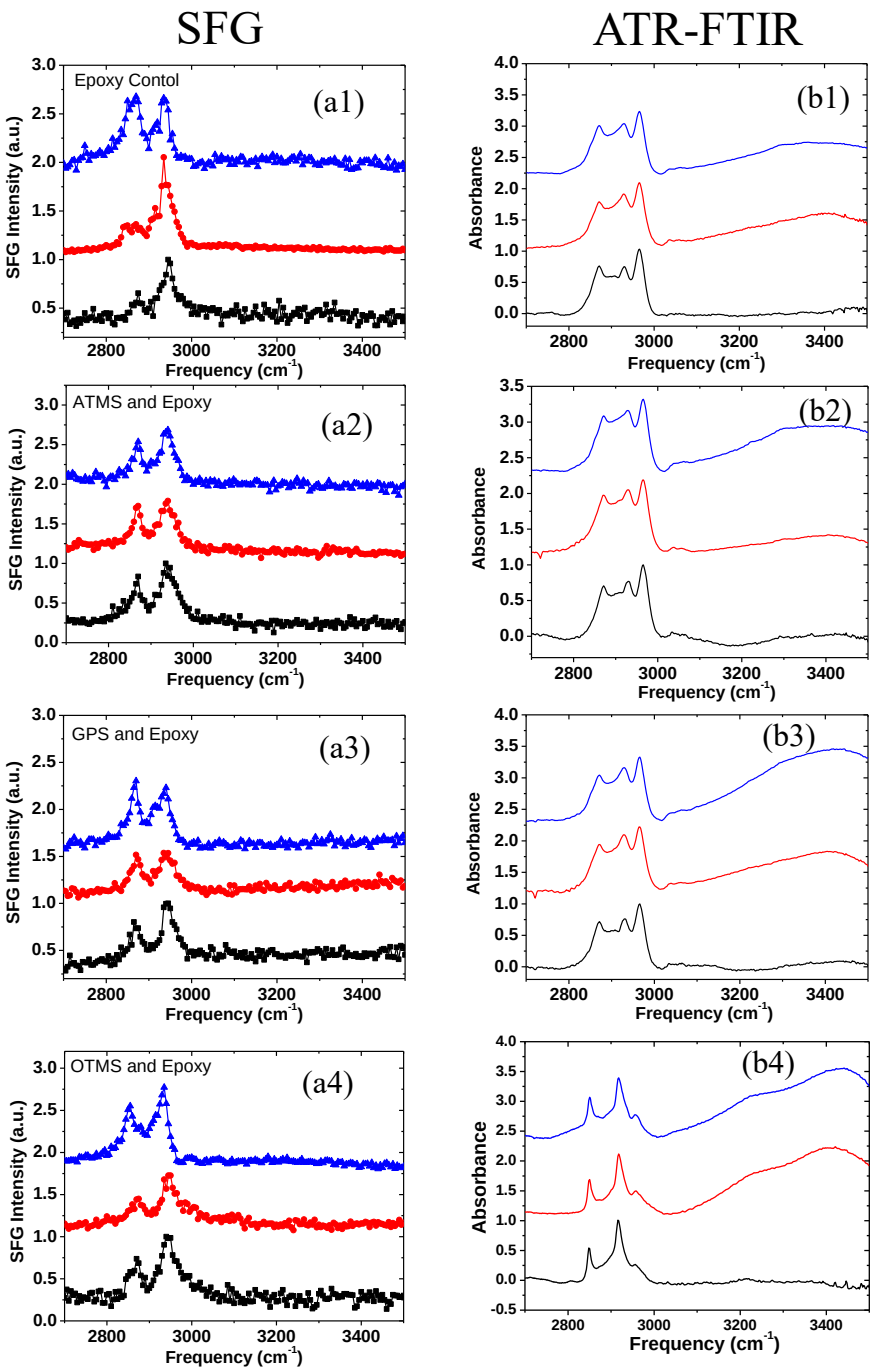

Figure 2.5: SFG (left) and ATR-FTIR (right) of dPS (A.) control, (B.) ATMS, (C.) GPS, and (D.) OTMS. Black (bottom) spectra are at time zero, red (middle) spectra are at after 24 hours hygrothermal treatment, and blue (top) spectra are after 48 hours hygrothermal treatment.

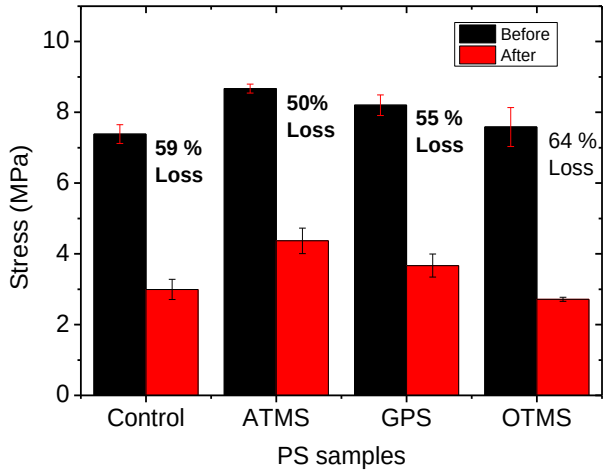

Figure 2.6: Adhesion testing results of dPS/epoxy interface and the interfaces between dPS and epoxy with silane added. The black bars are before hygrothermal aging and the red bars are after 24 hours of aging. The error bars are the standard error.

The polymer PS is a relatively nonpolar material, which means water cannot form a hydrogen-bonding structure at the interface easily, and this is what is seen in the SFG spectrum for the control system. No ordered water is detected after the hydrothermal aging. Similar results were found from the other three silane incorporated epoxy in contact with dPS. This shows that the control and all three adhesion promoters are capable of preventing water ordering at the interface after hygrothermal treatment. However, we observed in the ATR-FTIR spectra that there is water present in the bulk, even though no water is detected at the interface with SFG. The lap shear results show the measured adhesion strengths for all the samples decrease, showing that the water in the bulk may play an important role in adhesion reduction for the PS system. The interfaces between dPS and epoxy with added ATMS and γ-GPS have less adhesion reduction, because the amine in ATMS and the epoxide ring in γ-GPS can further react with the epoxy in the bulk as well as at the interface once they migrate to the interface. For the control sample and the sample with OTMS, the adhesion decreases are larger. For OTMS, it was found in a previous investigation,[8] that it is energetically favorable for it to segregate to the interface and order, leading to weaker adhesion. It is interesting to see in the ATR-FTIR spectra, all the spectra are similar except those from the dPS/epoxy interface with OTMS before and after 24 hours hygrothermal treatment, therefore the signals seen in the spectrum originate from OTMS molecules, which are clearly seen, showing that they can segregate to the interfacial region (800 nm range from the interface).

2.4 Conclusions

In this study, molecular structures at buried polymer/epoxy interfaces were investigated *in situ* before and after hygrothermal aging using SFG and ATR-FTIR. The dPET/epoxy (without silane) interface prior to aging has higher adhesion strength than that of the dPS/epoxy (without silane) interface. This is due to the more ordered interfacial methyl groups at dPS/epoxy interface, evidenced by the stronger SFG methyl signals detected from the dPS/epoxy interface. However, after the hygrothermal treatment, the dPS/epoxy (without silane) has stronger adhesion than that of the dPET/epoxy (without silane) interface. This is because PET is more hydrophilic, and ordered water layer can be formed at the dPET/epoxy interface, reducing adhesion. In contrast, dPS is more hydrophobic, and no ordered water was detected from the dPS/epoxy interface.

We added three different silanes to the epoxy in the dPET/epoxy system. Even though the silane amount added is very small, all three silane adhesion promoters were capable of preventing interfacial water segregation and ordering throughout hygrothermal aging. No ordered water was detected from the interfaces between dPET and epoxy (with added silane). The adhesion loss was observed to be much smaller compared to the control sample.

For all four dPS/epoxy samples, there were no substantial changes detected throughout hygrothermal aging. This lack of change could be due to the hydrophobic property of dPS, which prevents water from forming an ordered water layer at the interface. There was bulk water detected in all eight systems, which shows how silane adhesion promoters are not capable of preventing the bulk water absorption, and the adhesion decreased in all the systems after hygrothermal aging.

For the dPET/epoxy systems the control sample (with no added silane in epoxy) had the biggest decrease in adhesion strength after aging, while the interfaces between dPET and epoxy with added ATMS or γ-GPS had the smallest adhesion reduction. This is because of the ability of these two silanes to react further once they have migrated to the interface. The introduction of OTMS to epoxy did not increase the adhesion strength of the dPET/epoxy (with OTS added) interface after testing, which could be due to its inability to undergo further reactions at the interface. For the dPS/epoxy systems, the highest adhesion strength after hygrothermal aging was the samples with added ATMS and γ-GPS in epoxy, while the control and OTMS added epoxy had the lowest adhesion strength to dPET.

From this work it is clear that relatively hydrophilic surfaces can have initial higher adhesion, but through hygrothermal aging the strength of the adhesion is drastically reduced, but this can be mitigated by using a silane adhesion promoter that is capable of undergoing further reactions at the interface or in the bulk. The hydrophobic polymer has lower adhesion strength prior to hygrothermal treatment, but can handle the treatment better than its polar counterpart. The adhesion promoters can be utilized to increase the strength of adhesion and reduce adhesion loss after hygrothermal treatment of PS, but the effects are not as substantial as the PET.

To our knowledge, this is the first investigation on molecular-level structural changes that occur at buried epoxy interfaces with additional silane adhesion promoters present *in situ* during hygrothermal aging. Understanding the mechanism of hygrothermal aging affects the molecular structure and orientation at buried interfaces *in situ* will contribute to the understanding of moisture-induced failure mechanisms in microelectronic packages and help facilitate better design and development of more robust underfills that can withstand greater stress testing compared to their predecessors.

2.5 References

[1] W. K. Chiang, Y. C. Chan, B. Ralph, and A. Holland, "Adhesive strength of flip chip packages," *Int. J. Adhes. Adhes.*, vol. 28, pp. 109-119, 2008.

[2] B. M. Sharratt, L. C. Wang, and R. H. Dauskardt, "Anomalous debonding behavior of a polymer/inorganic interface," *Acta Materialia*, vol. 55, pp. 3601-3609, 2007.

[3] S. Luo and C. P. Wong, "Influence of temperature and humidity on adhesion of underfills for flip chip packaging," *IEEE Trans. Compon. Packag. Technol.*, vol. 28, pp. 88-94, 2005.

[4] K.-W. G. Lee, M. A.; Duchesne, E, "Chip-Underfill Interfaces of Flip Chip Plastic Ball Grid Array Packages," *Electron. Mater. Lett.*, vol. 2, pp. 171-174, 2006.

[5] L. K. Teh, M. Teo, E. Anto, C. C. Wong, S. G. Mhaisalkar, P. S. Teo, *et al.*, "Moisture-induced failures of adhesive flip chip interconnects," *IEEE Compon. Packag. Technol.*, vol. 28, pp. 506-516, 2005.

[6] P. Jin-Hyoung, J. Kyung-Woon, P. Kyung-Wook, and L. Soon-Bok, "A Study of Hygrothermal Behavior of ACF Flip Chip Packages With Moire Interferometry," *IEEE Trans. Compon. Packag. Technol.*, vol. 33, pp. 215-221, 2010.

[7] F. Awaja, M. Gilbert, G. Kelly, B. Fox, and P. J. Pigram, "Adhesion of polymers," *Prog. Polym. Sci.*, vol. 34, pp. 948-968, **2009**.

[8] C. Zhang, J. Hankett, and Z. Chen, "Molecular Level Understanding of Adhesion Mechanisms at the Epoxy/Polymer Interfaces," *ACS Appl. Mater. Interfaces*, vol. 4, pp. 3730-3737, 2012.

[9] C. Ohe, H. Kamijo, M. Arai, M. Adachi, H. Miyazawa, K. Itoh, *et al.*, "Sum Frequency Generation Spectroscopic Study on Photoinduced Isomerization of Poly(vinyl alcohol) Containing Azobenzene Side Chain at the Air−Water Interface," *J. Phys. Chem. C*, vol. 112, pp. 172-181, 2008.

[10] A. V. Vázquez, N. E. Shephard, C. L. Steinecker, D. Ahn, S. Spanninga, and Z. Chen, "Understanding molecular structures of silanes at buried polymer interfaces using sum frequency generation vibrational spectroscopy and relating interfacial structures to polymer adhesion," *J. Colloid Interface Sci.*, vol. 331, pp. 408-16, 2009.

[11] C. Zhang, N. E. Shephard, S. M. Rhodes, and Z. Chen, "Headgroup effect on silane structures at buried polymer/silane and polymer/polymer interfaces and their relations to adhesion," *Langmuir*, vol. 28, pp. 6052-9, 2012.

[12] J. N. Myers, X. Zhang, Y. Xiu, Y. Wei, J. M. Williamson, K. W. Lee, *et al.*, "Nondestructive Characterization of Molecular Structures at Buried Copper/Epoxy Interfaces and Their Relationship to Locus of Failure Analysis," *IEEE Transactions on Components, Packaging and Manufacturing Technology*, vol. 5, pp. 1432-1440, 2015.

[13] J. N. Myers, C. Zhang, K.-W. Lee, J. Williamson, and Z. Chen, "Hygrothermal Aging Effects on Buried Molecular Structures at Epoxy Interfaces," *Langmuir*, vol. 30, pp. 165-171, 2014.

[14] B. Stuart, *Infrared spectroscopy fundamentals and applications*. Chichester, Eng.; Hoboken, N.J.: J. Wiley, 2004.

[15] E. H. Wong, R. Rajoo, T. B. Lim, and Y.-W. Mai, "Swelling and Time-Dependent Subcritical Debonding of Underfill During Temper- ature-Humidity Aging of Flip Chip Packages," *IEEE Transactions on Components and Packaging Technologies*, vol. 28, pp. 862-868, 2005.

Chapter 3: Plasma Effects on Polymer Surfaces

3.1 Introduction

Promoting the adhesion between adhesive compounds and polymers or metal surfaces is a key area of research in the microelectronics industry, especially for packaging. In addition to SAPs (discussed in the previous chapter), plasma treatment is also frequently utilized to enhance adhesion.[1] Plasma treatments focus on modifying the surface to promote chemical bonds, interfacial diffusion, and better wetting. It has been shown that plasma treatment can modify the surface structure of polymer materials, which leads to higher adhesion strength.[2, 3] However, the detailed effects of plasma treatment on the buried interface between the plasma treated polymer surfaces in contact with underfill materials has not been studied *in situ* at a molecular level.

In order to protect the electrical circuitry, epoxy resin is dispensed via capillary action in to protect the moisture sensitive interface. But, prior to dispensing the epoxy resin into the space between the substrate and die, the device is exposed to plasma in order to increase the adhesion strength of the epoxy by activating the involved surface and causing it to be more reactive.[4] Two questions are important for such plasma treatment but are not answered in the literature: 1. Does the plasma treatment of covered surfaces affect the entire surface heterogeneously due to the cover between the substrate and die?[5] and 2. How can plasma treatment increase adhesion and cause better wetting? In this chapter, these two areas of plasma treatment are investigated with SFG spectroscopy, FT-IR, and lap shear analysis to see how plasma can affect polyimide (PI) and polystyrene (PS).

Polyimide has been widely used in many applications due to its excellent chemical resistance, high glass transition temperature, and outstanding mechanical properties.[19-22] In many of these applications, the surface or interfacial properties such as adhesion, interfacial-diffusion, and wettability of PIs are crucial.[23] For example, there are extensive investigations to improve the adhesion of PI to metal surfaces.[24] Specifically, poor adhesion at the PI and epoxy interface, in flip-chip packages (Figure 1.1), can lead to the propagation of cracks, moisture diffusion, and

corrosion of solder bumps (metallic interconnections).[25-27] Although PIs typically have poor adhesion to epoxies, they are ubiquitously utilized as microchip passivation layers and polymeric substrates in microelectronic packaging due to their remarkable aforementioned properties.

This chapter outlines two projects: (1) plasma effects on polymer surfaces with cover and (2) plasma adhesion promotion. For (1), the polymer PI has been studied in the presence of plasma in the literature,[6] but to the best of our knowledge, no investigation has been performed on the sandwich geometry (e.g., polymer surface with a cover) to determine if when covered the middle and edge regions of a polymer are affected differently by plasma treatment. Due to the structure of the interface being of utmost importance to the adhesion strength,[1, 7, 8] the entire surface including the middle and edge regions must be investigated to determine how the plasma affects each position on the surface. It is not known if the plasma treatment affects the entire interface homogenously or if there is some distribution of plasma effects on the surface due to the cover between the substrate and die with a gap being on the order of tens of microns.[5] For (2), in the second part of this chapter, plasma treatment as a method of adhesion promotion was investigated. The mechanism of plasma-based adhesion promotion has not been studied in detail previously with molecular level details. In this study, the effects of air, helium and oxygen plasma treatments were investigated at the PS and PI surfaces.

In the first section, two polymer surfaces, PS and PI, were studied before and after various plasma treatments. A sandwiched geometry was utilized during the plasma exposure in order to simulate minute spacers relevant in the microelectronics industry. It is well known that the PS surface structure could be vastly changed after plasma treatment,[9] therefore, here we studied PS surface under cover after plasma treatment as a model. The polymer PI was then implemented due to its ubiquitous use in the microelectronics industry. SFG spectra were taken before and after plasma exposure and SFG orientation analysis on surface functional groups was performed on both the PS and PI systems, before and after exposure to air, O_2, or He plasmas. In conjunction with SFG spectroscopy, the bulk technique FT-IR spectroscopy was also used in order to determine if the differences detected by SFG originate solely from the surface or if some bulk structural change is also present.

In the second section, SFG and ATR-FTIR spectroscopies were implemented to probe buried interfaces between a commercial epoxy and two polymers, PS and PI. Pristine and He plasma

treated polymer surfaces were investigated as well as buried polymer (before and after plasma treatment)/epoxy interfaces. In addition to spectroscopic analysis, adhesion testing experiments were performed to measure the adhesion strengths between epoxies and polymers to understand if the plasma treatment increased the adhesion strength. The adhesion measurement data can be interpreted by the molecular structures of the buried interfaces deduced from the SFG results. Contact angle measurements were also performed to see if the polymer surfaces become more hydrophilic after plasma treatment.

3.2 Materials and Methods

3.2.1 Materials

Calcium fluoride (CaF_2) and fused silica prisms (SiO_2) were ordered from Altos Photonics, Inc. (Bozeman, MT). ACS reagent grade toluene (>99.5%) and ACS reagent grade ethanol (>99.5%) were purchased from Sigma-Aldrich (St. Louis, MO). Contrex powdered labware detergent was bought from Decon Labs (King of Prussia, PA). N-Methyl-2-pyrrolidone (NMP) and Poly(pyromellitic dianhydride-co-4,40-oxydianiline) amic acid solution (polyamic acid) as a ~13 wt% solution in solvent were purchased from Sigma-Aldrich (St. Louis, MO). The deuterated polystyrene (d8-PS or dPS) was purchased from Polymer Science, Inc. (Monticello, IN), and a solution (2.0 weight %) was made by dissolving it in toluene. Commercial epoxy resin 3302 (CE3302) was obtained from Epoxies Etc. (Cranston, RI). CE3302 base is a proprietary blend, composed predominantly of bisphenol A digylcidyl ether and trace amounts of bis(1,2,2,6,6-pentamethyl-4 piperidinyl)-sebacate and 4-nonylphenol. The CE3302 hardener used was poly(oxypropylenediamine). Bisphenol A digylcidyl ether (BADGE) is produced in the curing process and then reacts further with poly(oxypropylenediamine) to produce a cross-linked structure.[10] All pertinent chemical structures can be found in Figure 2.1. Compressed He (>99.99%) was obtained from Metro Welding (Detroit, MI). High Impact Polystyrene (HIPS) Standard Tolerance, ASTM D1892 and PEI (Polyetherimide), Standard Tolerance, ASTM D5205 were both purchased (Amazon, Seattle, WA) and utilized for lap shear analysis. Because PS is very brittle, we used HIPS in the adhesion tests. The water contact angle on HIPS (114^o) is similar to that measured on the pure PS film surface. We believe that HIPS can serve as a model for PS in the adhesion testing experiment. Optical fiber polishing paper was purchased from Thorlabs (Newtown, NJ) (30 µm, 6 µm, 3 µm, 1 µm, and 0.02 µm grit).

3.2.2 Sample Preparation

Silica or CaF_2 prisms were used for SFG experiments. Silica prisms were cleaned first in a concentrated sulfuric acid bath saturated with potassium dichromate followed by a rinse of deionized water and then they were finally dried under a stream of nitrogen. Following the acid cleaning, the substrates were exposed to air plasma (Plasma Etch, Inc., PE-50, Carson City, NV) for 2 minutes prior to polymer film deposition. CaF_2 prisms were cleaned by soaking in toluene for 72 hours, rinsing with ethanol, washing with detergent, rinsing with DI water, and then finally exposed to air plasma for 2 minutes. A polymer solution (2% by mass PS in toluene) was spin-cast on the fused silica or CaF_2 substrates at 2500 rpm for 30 s using a P-6000 spin coater (Speedline Technologies, Franklin, MA). In order to remove solvent residue, the samples were heated at 50°C for 2 hours. For ATR-FTIR measurements, CaF_2 prisms were utilized and cleaned as specified above. For the PMDA-ODA film, a poly(pyromellitic dianhydride-co-4,40-oxydianiline) solution was diluted 1:3 by weight in NMP. Polyimide thin films were deposited by spin casting the diluted poly(pyromellitic dianhydride-co-4,40-oxydianiline) solution on prisms at 3000 RPM for 30 s. Cross-linked polyimide films were prepared by curing the poly(pyromellitic dianhydride-co-4,40-oxydianiline) film in a vacuum furnace (STT-1200C-6-12 High Temperature Tube Furnace, Sentro Tech Corp., Strongsville, OH) at 260°C for 60 minutes, which then produces the cross-linked poly(pyromellitic dianhydride-*co*-4,4′-oxydianiline) (PMDA/ODA), referred to as PI, see Figure 3.1 for curing reaction. The prepared PS and PI polymer surfaces were then exposed to He plasma for 100s and then put in contact with the epoxy. For epoxy curing, the mixing ratio for resin to hardener was 2:1 by mass. After vigorously mixing the resin and hardener together, the epoxy was cured on top of the spin-coated polymer surface and cured for 2 hours at 60°C.

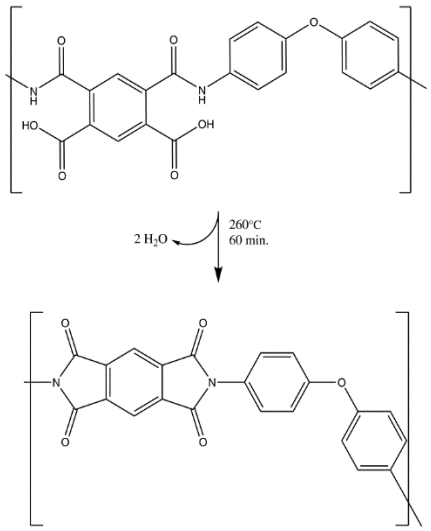

Figure 3.1: PI curing reaction

For plasma treatment, a sandwiched geometry was utilized, with a silica window and 56 μm spacers (Figure 3.2), and then the polymer surfaces were exposed to air, O_2, or He plasma for 10 s. This was done to simulate the packaging conditions found within the microelectronics industry, where the chip/die interfaces are soldered together and then plasma is used as a pretreatment to epoxy resin dispensing. Experimental SFG geometry and positions probed are also found in Figure 3.2.

Lap shear samples were prepared by sanding a portion of the surface (25mm x 10mm) of the adherent (30mm x 50mm x 10mm) with optical fiber polishing paper, going from 30 μm, 6 μm, 3 μm, 1 μm, and finally to 0.02 μm, which should yield a surface that has a roughness on the order of tens of nanometers. Following sanding some of the lap shear adherents were plasma treated for 100s in helium. Following plasma treatment an edge of the polymer adherent was coated with a ~3mm x ~25mm rectangle of epoxy prepared as described above. Another polymer adherent was placed on top of the epoxied adherent. The samples were then placed in an oven and cured as described above. All adhesion failures were determined to be adhesive failure at the epoxy/polymer interface, which was determined by a visual comparison of the delaminated area and a control region, which was not exposed to the adhesive.

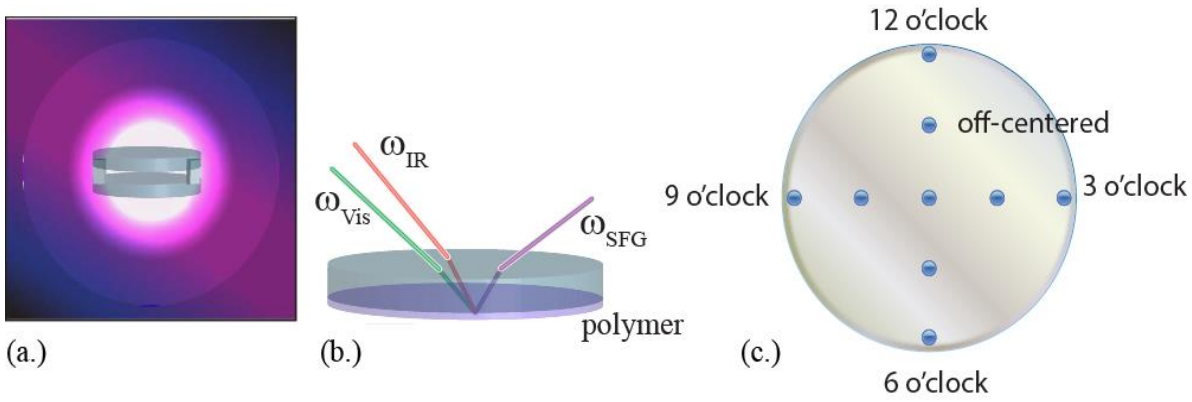

Figure 3.2: (a.) sandwich of sample and protective layer in plasma chamber. (b.) SFG facedown experimental geometry, and (c.) sample positions probed by SFG and FT-IR, there are four edge positions, 4 off-centered positions, and one middle position.

3.2.3 Lap Shear Adhesion Testing

Adhesion lap shear tests were performed at room temperature using a method based on ASTM D3163, using the Instron 5544. When the adherents were completely separated, an abrupt drop in adhesion strength was observed. The maximum adhesion strength observed before the sudden drop in force was utilized for all reported adhesion strength measurements. The adherents utilized were made of PS or PI. All results are the average of eight or more samples being tested.

3.2.4 Contact Angle Measurement

Contact angle measurements were also performed on the two polymer surfaces to see if the plasma treatment affects the hydrophilicity/hydrophobicity of the surface. Static water contact angles were measured using a CAM 100 optical contact meter (KSV Instruments). The PS and PI surfaces were the same surfaces used in lap shear measurements, and they were prepared the same way as previously stated.

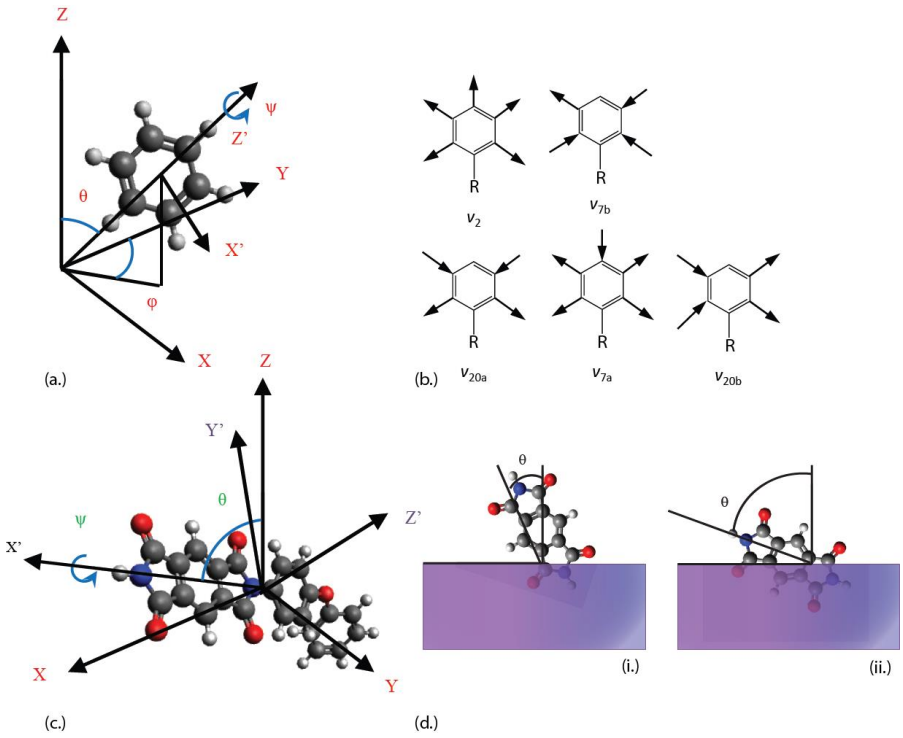

Figure 3.3: (a.) Axes defined in phenyl moiety in PS, where ψ is the twist angle, φ is the azimuthal angle, and θ is the tilt angle. (b.) The vibrational stretching modes of the phenyl moiety. (c.) Axes defined in PI core moiety, where ψ is the twist angle and θ is the tilt angle. (d.) The two possible orientations for the PI core, I: the two carbonyls that are parallel to the polymer chain oscillate and II: the two carbonyl groups that are perpendicular to the chain of the polymer oscillate.

3.3 Covered Plasma Effect

3.3.1 Results and Discussion

3.3.1.1 Investigation of the Polystyrene Surface

In order to better understand how plasma affects covered hydrophobic polymer surfaces, PS was investigated before and after exposure to air, He, and O_2 plasmas. To verify that the middle, off-centered, and edge regions behave differently in the presence of plasma due to the effect of the cover, SFG spectra were taken from all three regions: one in the middle, four off-centered between the middle and the edge, and four on the edge, before and after 10 s of air plasma (Figure 3.2). Figure 3.4 displays the collected SFG spectra. The off-centered and the edge positions each comprises four sites for data collection: positions at 12 o'clock, 3 o'clock, 6 o'clock, and 9 o'clock. Strong SFG signals were detected from all positions on the PS surface prior to plasma. The signals at 3023 cm^{-1}, 3036 cm^{-1}, 3055 cm^{-1}, and 3066 cm^{-1} can be assigned to the phenyl C-H stretching vibrational modes of v_{20b}, v_{7a}, v_{7b}, and v_2, respectively (see Table 3.1 for fitting results and

complete assignment). These same peaks are found in all SFG spectra collected from all the positions (middle, off-centered, and edge) on the pristine PS surface and they have very similar spectral profiles. After 10 s of air plasma treatment, the SFG spectrum collected from the PS surface middle position is mostly unchanged. The SFG spectra collected from the off-centered positions after 10 s air plasma treatment still have the same spectral profile, but the intensities decreased. The SFG spectra collected from the edge positions greatly change after 10 s air plasma treatment and the intensities greatly decreased.

Table 3.1: Fitting parameters for PS before and after air plasma treatment at the middle and edge positions.

Middle before				Middle after		
ω_i (cm^{-1})	Γ_i (cm^{-1})	A_q (ssp)	A_q (sps)	A_q (ssp)	A_q (ssp)	assignment
3022	6.0	0.14	-0.04	.14	-0.025	ν_{20b} (as)
3040	5.0	-0.09	-0.02	-0.09	-0.02295	ν_{7a} (s)
3055	7.0	0.05	-0.08	0.05	-0.08	ν_{7b} (as)
3066	6.0	0.3	0.04	0.27	0.035	ν_2 (s)
Edge before				Edge after		
ω_i (cm^{-1})	Γ_i (cm^{-1})	A_q (ssp)	A_q (sps)	A_q (ssp)	A_q (ssp)	assignment
3022	6.0	0.14	-0.04	0.2	-0.02	ν_{20b} (as)
3040	5.0	-0.09	-0.02295	-0.063	-0.02	ν_{7a} (s)
3055	7.0	0.05	-0.08	0.18	-0.057	ν_{7b} (as)
3066	6.0	0.3	0.04	0.08	0.028	ν_2 (s)

The similar SFG spectra collected from the middle position before and after air plasma treatment on the PS surface indicate that the middle position is mostly unaffected by the plasma treatment

and the cover is preventing the plasma from reaching the middle efficiently. The off-centered positions were affected somewhat but not entirely by the plasma, which is expected if the plasma is travelling through the sandwich, from the edge to the middle. There is a similar spectral profile, although the intensity is reduced, as compared with the pristine surface. The edge positions were greatly perturbed by the plasma treatment and the detected SFG intensities from the edge positions greatly decreased, which shows the plasma strongly affects the edge surface structure. The reduction in SFG signal could be a result of a surface disordering, surface functional group orientation change, or the plasma treatment is completely removing the PS and the decrease of signal stems from a lack of PS. To determine which explanation is correct, bulk analysis is required in order to verify if there is any PS film left on the substrate at different positions after plasma exposure. Before we present the bulk results, we want to validate the trend that plasma affects the edge differently than the middle.

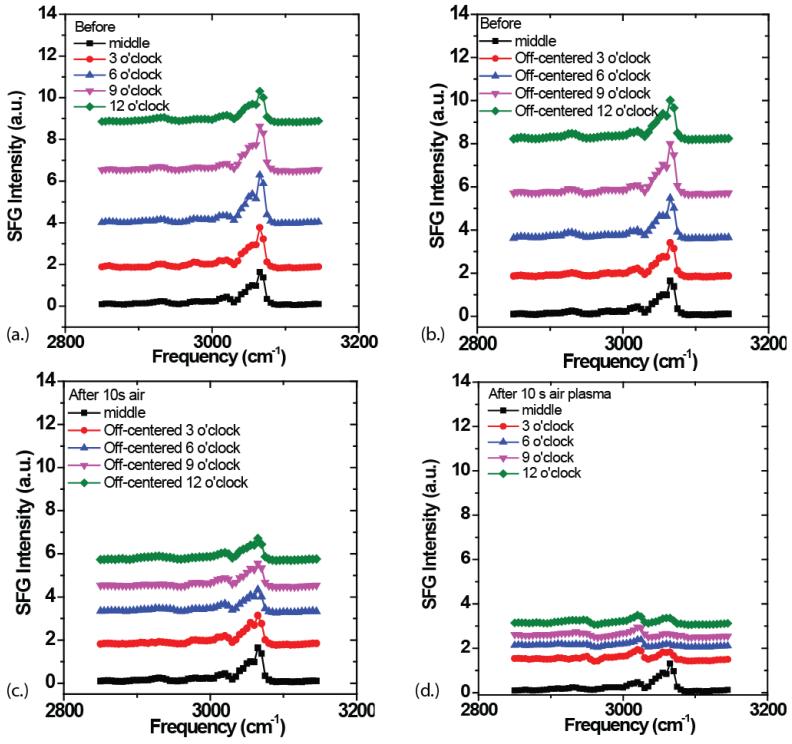

Figure 3.4: SFG spectra collected from (a.) PS before air plasma, middle and four off-center spots, (b.) PS before air plasma, middle and four edge spots, (c.) PS after 10 seconds of air plasma, four spots, middle and four off-center spots, (d.) PS after 10 seconds of air plasma, four spots, middle and four edge spots.

To further substantiate the claim that air plasma affects the edges more than the middle of the PS surface, a sample was analyzed before and after air plasma and SFG intensity collected at every

1.5 mm moving from the edge to the middle of the window with the same cover. the spectral intensity decreasing slightly, while the edge position generates a drastically different spectrum and the intensity greatly diminishes. The same is true for the O2 plasma experiment; the middle is almost unperturbed with the spectrum intensity slightly decreasing, while the edge greatly changes. Comparing the two plasma treatment effects, the O2 plasma seems to reduce the SFG signal intensity of the PS to a greater extent than the He plasma. There are several possibilities for SFG intensity decreasing, either the surface phenyl ring coverage changes, or the phenyl groups reorient (e.g., lie down more), or they adopt a more random distribution. Before we discuss the surface phenyl orientation, we want to know whether the plasma treatment only affects the PS surface or if it influences the PS bulk structure as well.

shows the intensity plots at 3065 cm^{-1} before and after 1 s, 5 s, 10 s, and 20 s air plasma treatment. Prior to plasma treatment, each spot on the sample generates very similar SFG signal intensity at 3065 cm^{-1}. All plots were normalized with the highest measured intensity within the individual plots and the scales for all plots were made constant. After plasma treatment, there is a dramatic decrease in the edge SFG signal intensity as compared with the middle SFG signal intensity, where the SFG signal detected from the PS surface edge has the lowest intensity and that from the PS surface middle has the highest intensity, which is a similar result that was observed previously. As the plasma time increases, the plasma effects are detected closer to the middle position, indicating that the cover is protecting the polymer surface and longer treatment times are necessary to plasma treat the middle position. This further confirms that the plasma is moving in from the edge towards the middle of the sample.

The intensities of the SFG spectra collected from the pristine surface for all positions on the sample are very similar, while the post-plasma treatment SFG signal intensities greatly vary, with the edge positions giving weaker SFG signal and the middle position still generating very strong signal. This experiment shows that edge and middle are affected differently and the plasma is moving through the space between the sample and the cover. The above presented two experiments are consistent with each other, demonstrating that the edge regions experience more of the plasma effect and the plasma perturbs these regions more efficiently than the middle of the surface.

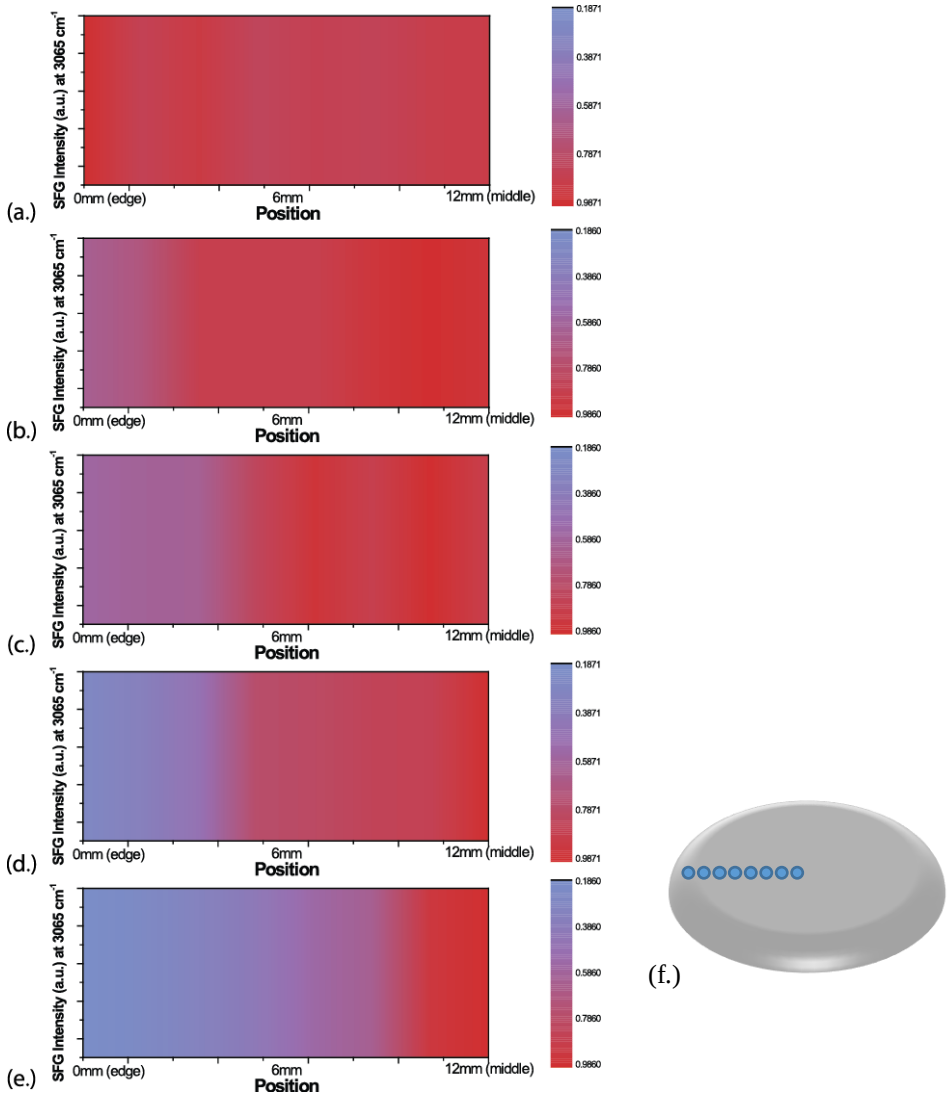

Figure 3.5: SFG intensity collected at 3065 cm^{-1} every 1.5 mm moving from the edge (spot 1) to the center of the window (spot 8) before (a.) and after 1 s air plasma (b.), 5 s (c.), 10 s (d.), and 20 s (e.). In (f.), the 8 positions analyzed are shown, scanning from the edge position to the middle position.

To even further understand how plasma affects the PS surface, both He and O_2 plasmas were utilized to see if they would affect the PS surface differently than air plasma. For this set of experiments there were three positions on the samples that SFG spectra were collected from, the middle and two edge positions. Representative SFG spectra collected from the middle and the edge positions are presented in Figure 3.6. Similar to the air plasma experiments, both the edge and the middle of a pristine surface generate the same SFG spectral profile and intensity. After the sample was treated by the He plasma for 10 s, the middle position generates a very similar spectrum, with

the spectral intensity decreasing slightly, while the edge position generates a drastically different spectrum and the intensity greatly diminishes. The same is true for the O_2 plasma experiment; the middle is almost unperturbed with the spectrum intensity slightly decreasing, while the edge greatly changes. Comparing the two plasma treatment effects, the O_2 plasma seems to reduce the SFG signal intensity of the PS to a greater extent than the He plasma. There are several possibilities for SFG intensity decreasing, either the surface phenyl ring coverage changes, or the phenyl groups reorient (e.g., lie down more), or they adopt a more random distribution. Before we discuss the surface phenyl orientation, we want to know whether the plasma treatment only affects the PS surface or if it influences the PS bulk structure as well.

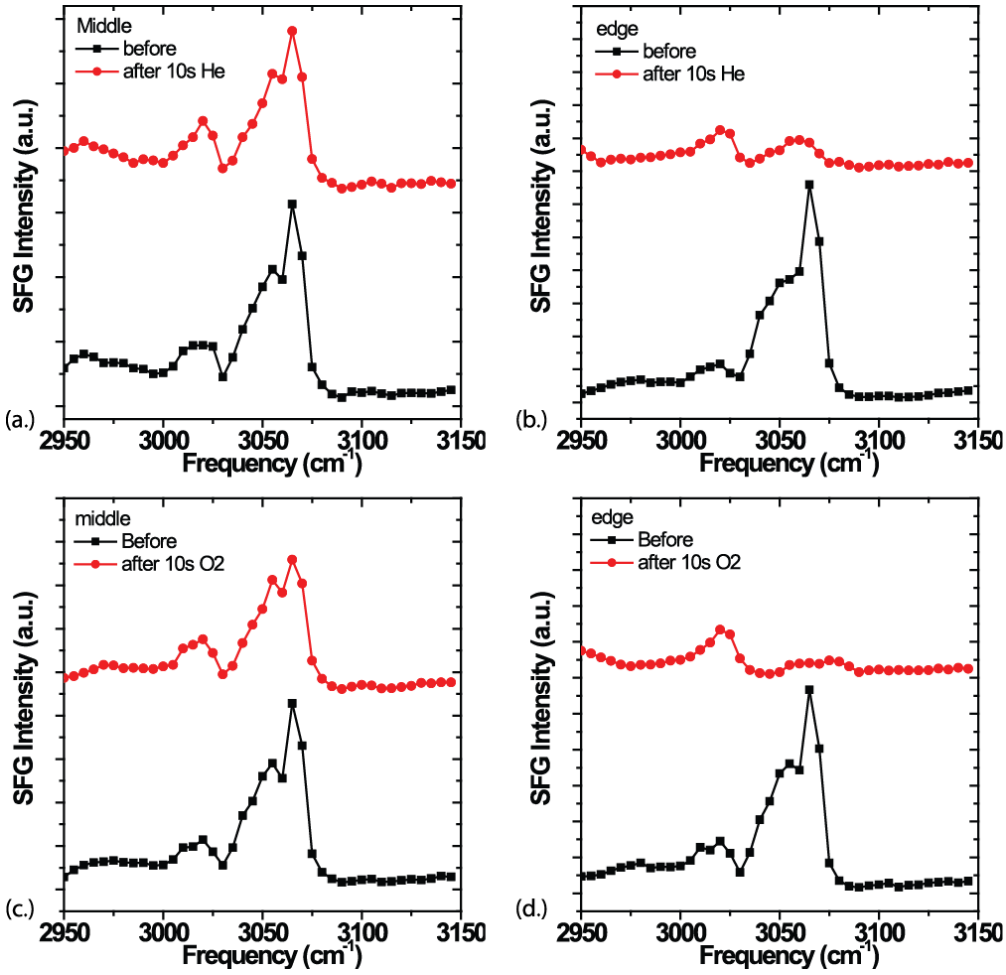

Figure 3.6: SFG spectra collected from (a.) The middle position, PS surface before and after 10 s He plasma (black plots are before and red plots are after), (b.) The edge position, PS surface before and after 10 s He plasma, (c.) The middle position, PS surface before and after 10 s O_2 plasma, (d.) The edge position, PS surface before and after 10 s O_2 plasma.

In order to analyze the PS film bulk structure, the samples were studied before and after 10 s of He or O_2 plasma treatment using FT-IR spectroscopy (Figure 3.7). In the FT-IR spectra, there are two peaks due to the CH_2 stretching: the symmetric at 2852 cm^{-1} and the antisymmetric at 2921 cm^{-1}, and four peaks due to the phenyl stretching modes: 3000 cm^{-1} combination band, 3025 cm^{-1} ν_{20b}, 3057 cm^{-1} ν_{7b}, 3066 cm^{-1} ν_2, and 3081 cm^{-1} ν_{20a}.[11, 12] It was found that the FT-IR spectra collected from the middle and edge positions of a pristine sample were identical to each other. After 10 s of He plasma, there was no detected spectral change in either the middle or the edge position. For the O_2 plasma experiment, the FT-IR spectra collected from both the edge and middle positions of the pristine surface were also identical to each other and showed no change after 10 s O_2 plasma. This shows that the bulk material is not affected by the plasma treatment. This conclusion was verified by the difference spectrum obtained by subtracting the FT-IR spectrum of plasma treated sample from the FT-IR spectrum of the pristine sample. The resultant spectral subtraction yields a flat line, which indicated that the two spectra are identical and this is the case for both the He and the O_2 plasma results. These results confirm that the plasmas do not remove a detectable amount of polymer and that the majority (if not all) of the polymer remains on the substrate. This result combined with the SFG spectral data presented above indicates that the plasma treatment changes the PS surface structure and the bulk of the material remains intact after treatment.

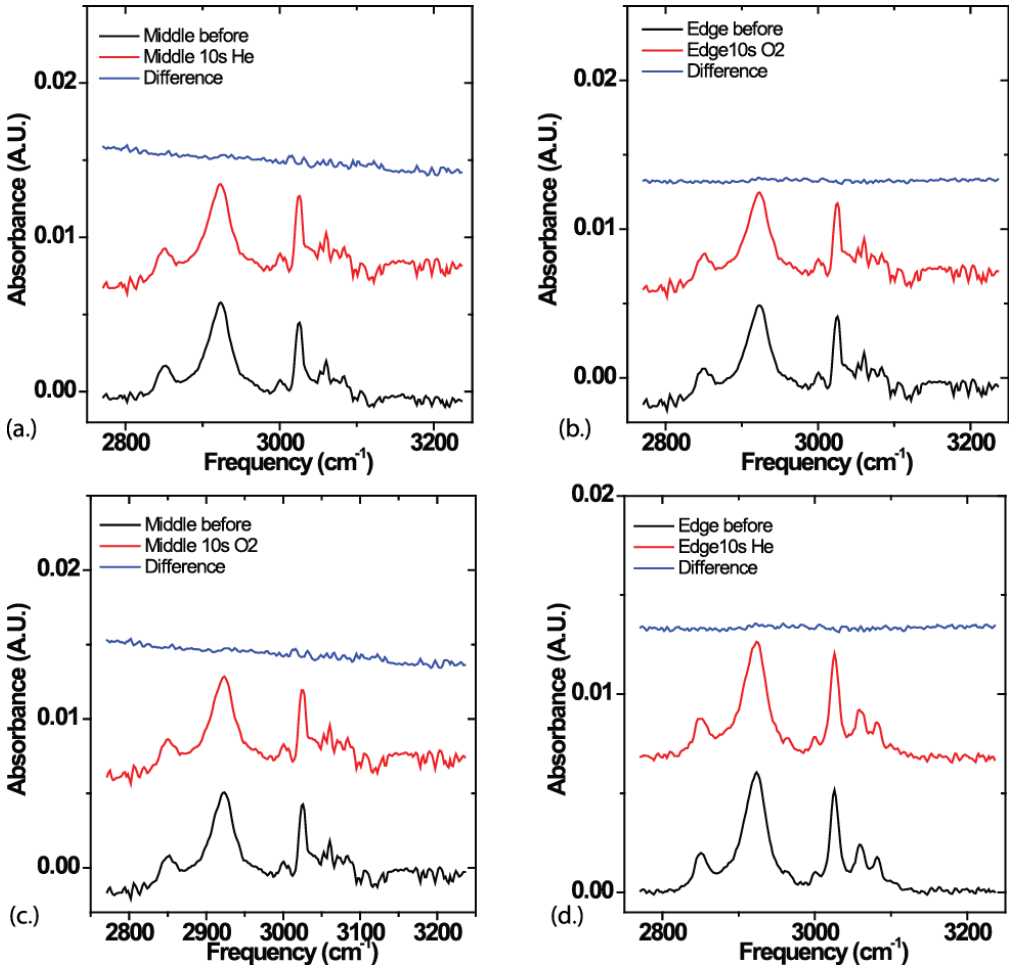

Figure 3.7: FT-IR spectra collected from (a.) The middle position, PS surface before and after 10 s He plasma (black spectra before, red spectra after, and the blue spectra are the subtracted results), (b.) The edge position, PS surface before and after 10 s He plasma, (c.) The middle position, PS surface before and after 10 s O_2 plasma, (d.) The edge position, PS surface before and after 10 s O_2 plasma.

Figure 3.4 shows that SFG C-H stretching spectra collected from the PS surface before and after the plasma treatment are dominated by the contributions from the phenyl groups. We believe that the PS surface is mainly covered by phenyl groups and we will deduce the phenyl orientation below. In order to accurately determine the orientation of surface phenyl groups on PS surfaces, SFG spectra were collected using two polarization combinations of the input/output beams, sps and ssp (Figure 3.8). Spectral analysis on the phenyl C-H stretching ν_2 and ν_{7b}vibrational modes were performed.[12]

Figure 3.3 shows the definition of axes for the lab-coordinate and molecule-fixed systems for a phenyl group, as well as schematic of phenyl C-H stretching vibrational modes. For simplicity, we

assume a delta orientation angle distribution for data analysis. To determine the orientation of a phenyl group on an isotropic surface, both tilt and twist angles need to be deduced. In the following we will perform analysis on two cases: (1) we will deduce the tilt angle by averaging the twist angle; (2) we will deduce both the tilt and the twist angles. We will study the SFG spectra collected from the center and edge positions before and after plasma treatment using ssp and sps polarization combinations of the input and output laser beams. From the fitting results of the SFG ssp and sps spectra, we could deduce χ_{yyz} and χ_{yzy} and then determine the phenyl orientation.

Figure 3.8 shows the ssp and sps SFG spectra with fitted results. The detailed phenyl orientation analysis methods based on the two vibrational modes (ν_2 or ν_{7b}) and SFG ssp and ppp spectra are presented in the introduction chapter (Equations 1-50 to 1-57). If we assume that the surface phenyl twist angle is random and can be averaged, the ratio of measured χ_{yyz} to χ_{yzy} from SFG ssp and sps spectra for each vibrational mode (e.g., ν_2 or ν_{7b} vibrational mode) can be used to determine an orientation (tilt) angle for the phenyl group. Thus, similar orientation angles deduced from two different modes would indicate that it is reasonable to average the twist angles.

The deduced phenyl tilt angles using each vibrational mode from SFG spectra collected from the middle or edge position before and after plasma treatment are listed in Table 3.2, Table 3.3, Table 3.4, and Table 3.5. It was found that before the plasma treatment, the deduced tilt angles for the SFG spectra collected from the middle and edge positions are identical, at 33° (from ν_2) or 40° (from ν_{7b}). Figure 3.8 shows that the SFG spectra and the fitting results for these two cases are very similar. This shows that the PS surface is homogenous before the plasma treatment. The phenyl tilt angles deduced from the two vibrational modes (33° from ν_2 and 40° from ν_{7b}) are not very different. This shows that the assumption about the random orientation of the twist angle is reasonable.

Table 3.2: Deduced phenyl tilt angles (assuming random twist angles) from the SFG spectra collected from the PS middle position before plasma

	strength and damping coefficients of v2	strength and damping coefficients of v7b
ssp	0.30/6.00	0.05/7.00
sps	0.04/6.00	-0.08/7.00
ratio of χ_{yyz}/χ_{yzy}	7.50	-0.63
phenyl tilt angle	33°	40°

Table 3.3: Deduced phenyl tile angles (assuming random twist angles) from the SFG spectra collected from the PS middle position after plasma

	strength and damping coefficients of v2	strength and damping coefficients of v7b
ssp	0.27/6.00	0.05/7.00
sps	0.04/6.00	-0.08/7.00
ratio of χ_{yyz}/χ_{yzy}	7.70	-0.63
phenyl tilt angle	31°	40°

Table 3.4: Deduced phenyl tilt angles (assuming random twist angles) from the SFG spectra collected from the PS edge position before plasma

	strength and damping coefficients of v2	strength and damping coefficients of v7b
ssp	0.30/6.00	0.05/7.00
sps	0.04/6.00	-0.08/7.00
ratio of χ_{yyz}/χ_{yzy}	7.50	-0.63
phenyl tilt angle	33°	40°

Table 3.5: Deduced phenyl orientation angles from the SFG spectra collected from the PS edge position after plasma

	strength and damping coefficients of v2	strength and damping coefficients of v7b
ssp	0.08/6.00	0.18/7.00
sps	0.028/6.00	-0.057/7.00
ratio of χ_{yyz}/χ_{yzy}	2.86	-3.16
phenyl tilt angle	74°	63°

After the plasma treatment, the deduced phenyl tilt angles from the SFG spectra collected from the middle position are similar to those before the plasma treatment, at 31° (from ν_2) or 40° (from ν_{7b}). Figure 3.8 shows that the spectra are similar to those collected from the PS before plasma treatment. This indicates that the plasma treatment does not affect the middle position of the PS surface (because the cover prevents the plasma from reaching the middle position). This result is well correlated to the results of the qualitative analysis on SFG signal intensity presented above. Differently, after the plasma treatment, the deduced phenyl tilt angles from the SFG spectra collected from the PS surface edge position are very different from those before the plasma treatment, at 74° (from ν_2) and 63° (from ν_{7b}) respectively. This shows that plasma treatment

greatly changes the surface structure of the PS at edge positions. The phenyl groups lie down more on the surface due to the plasma treatment at the edge. Figure 3.8 shows that the spectra collected from the edge position after plasma are different from those collected from the PS before plasma treatment. This result also matches the qualitative analysis result on SFG signal intensity presented above. The detailed analysis on the phenyl orientation at different sample positions before and after plasma treatment clearly demonstrated the inhomogeneous effect caused by the plasma treatment due to the cover. Since the phenyl tilt angles deduced using the two vibrational modes for each position are not very different, we believe that the assumption that the phenyl twist angle is random after plasma treatment at the same edge position is also likely correct.

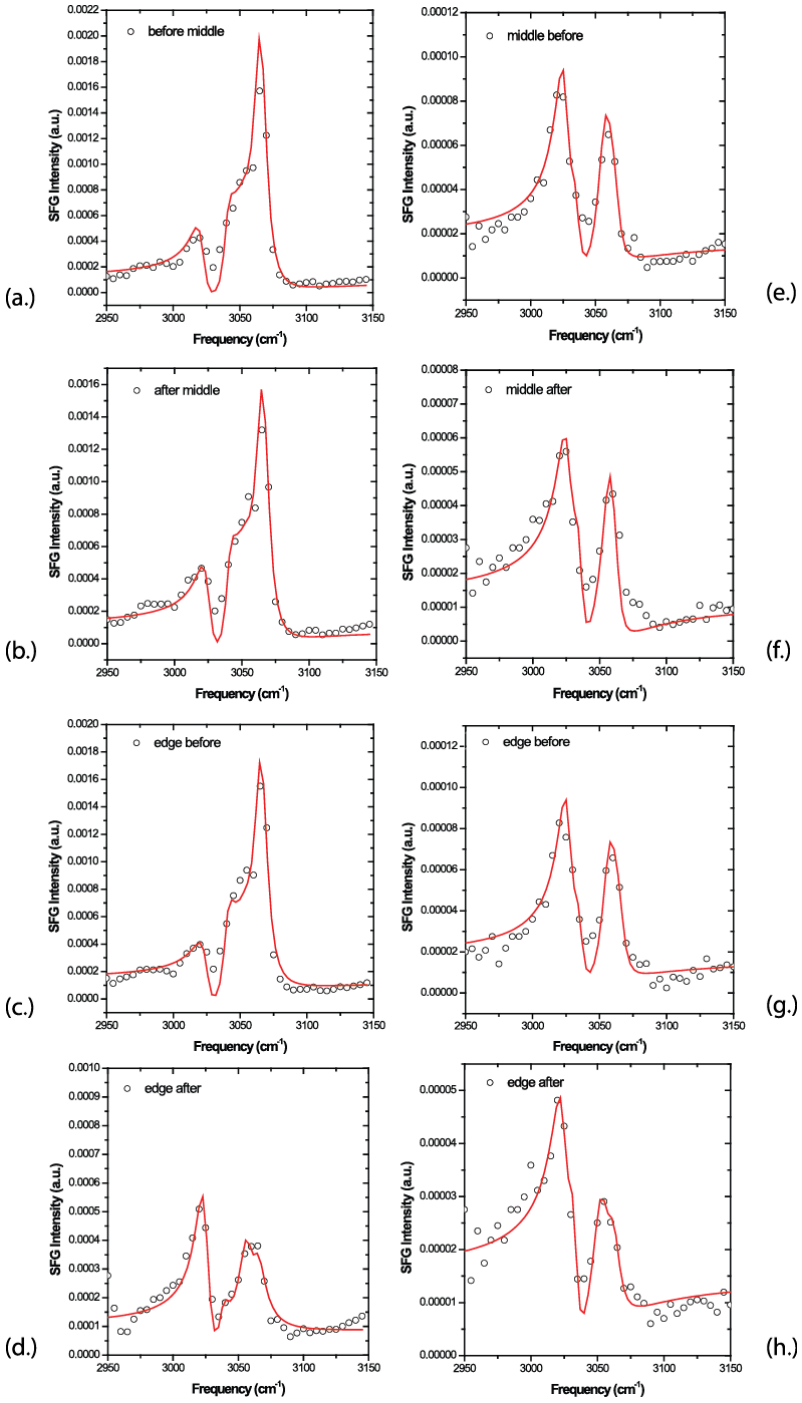

Figure 3.8: Collected spectra for the PS/air interface in the ssp (left) and sps (right) polarizations (multiplied by a factor of 10), before and after 10 s air plasma. (a.) middle position before (ssp). (b.) middle position after (ssp). (c.) edge position before (ssp). (d.) edge position after (ssp). (e.) middle position before (sps). (f.) middle position after (sps). (g.) edge position before (sps). (h.) edge position after (sps).

Since the two tilt angles deduced from two vibrational modes for each case by averaging the twist angle are not identical, it may be possible that the twist angle is not completely random. Here we also performed data analysis by combining the measured results from both vibrational modes to determine the phenyl tilt and the twist angles simultaneously (two measurements can be used to solve for two unknowns). We deduced the most likely tilt/twist angles numerically. Here the calculated ratios of χ_{xxz} to χ_{xzx} for the phenyl ν_2 and ν_{7b} vibrational modes are plotted as a function of the phenyl tilt and twist angles (Figure 3.9a and Figure 3.9b). By combining the experimentally measured $\frac{\chi_{yyz}}{\chi_{yzy}}$ ratio for the ν_2 (or ν_{7b}) mode and the above calculated plot, the most possible orientation angle regions which match the measured ν_2 (or ν_{7b}) mode data can be obtained and shown using a heat map.[72] Since the final orientation should satisfy experimentally measured data from both vibrational modes, the finally deduced orientation angle region should be the overlapped region(s) from the two maps obtained from the two vibrational modes. Figure 3.9 displays the four (final overlapped) heat maps showing the deduced orientation angle regions for the PS surfaces at middle and edge positions before and after plasma treatment. Considering other experimental errors and the possible fitting errors, a 20% error bar was included in the measured ratios for orientation analysis and the heat maps reflect this error bar. Interestingly, for the pristine PS surface in the middle/edge positions and the PS middle position after plasma treatment, the deduced orientation angle regions are very narrow and only one possible region was identified in each case. For the PS surface before plasma, again the tilt and the twist angles are identical, at 40° tilt and 30° twist. After the plasma treatment, the tilt and twist angles deduced from the phenyl groups at the middle position are 36° and 39°, respectively, which are not very different from those of the surface before plasma treatment. Again this result shows that the plasma treatment does not affect the PS surface structure much at the middle position. For the pristine PS surface in the edge position, after the plasma treatment, two possible orientation regions were found. We believe that the region with tilt angle at 90° is not reasonable, since we still can observe SFG signal from the ν_2 mode clearly. We therefore believe that the deduced tilt and twist angles should be 68° and 47°, respectively. This result again shows that the edge surface structure was substantially altered by the plasma treatment. The deduced tilt and twist angles are list in *Table 3.6*.

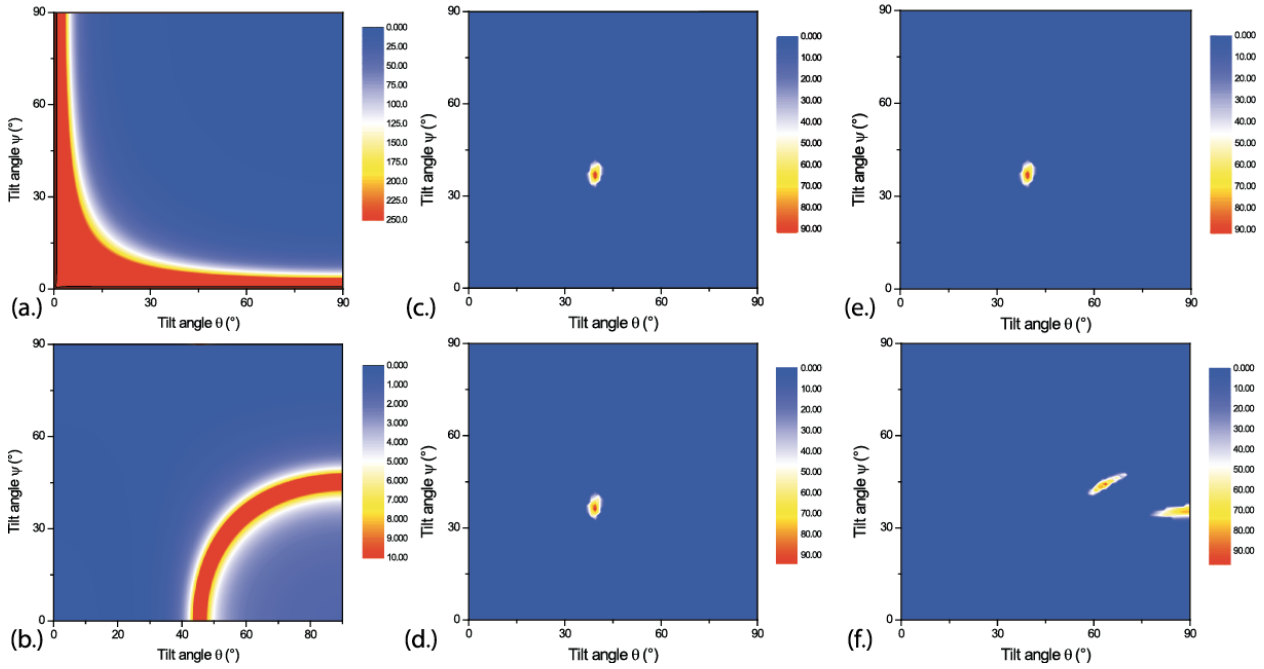

Figure 3.9: Contour plots and heat maps for the PS surface before and after 10s air plasma from the middle and edge positons. Contour plots of $\frac{\chi_{yyz,v_2}}{\chi_{yzy,v_2}}$ (a.) and $\frac{\chi_{yyz,v_{7b}}}{\chi_{yzy,v_{7b}}}$ (b.) plotted as functions of tilt (θ) and twist (ψ). Heats maps of (c.) middle position before plasma, (d.) middle position after plasma, (e.) edge position before plasma, and (f.) edge position after plasma.

Table 3.6: Deduced tilt and twist angles of the phenyl groups before and after plasma

Before plasma		Tilt	Twist
	Middle	40°	30°
	Edge	40°	30°
After plasma	Middle	36°	39°
	Edge	68°	47°

It is interesting to see that the phenyl tilt angle deduced by averaging the twist angle and the tilt angle deduced along with the twist angle are similar for each case. For the PS surface before plasma treatment, the averaged tilt angle measured using two modes by averaging the twist angle and the tilt angle measured along with the twist angle are ~37° (the mean value of the measurements using two modes) and ~40°, respectively. For the PS surface after plasma treatment at the middle position, these two angles are ~36° and ~36°, respectively. For the PS surface after plasma

treatment at the edge position, these two angles are ~69° and ~68°, respectively. This clearly demonstrated that regardless of the assumptions about the twist angles, the phenyl groups stand up more on the PS surface before plasma treatment (which agrees generally with the literature value for the tilt of PS on a Si wafer, which has been found to equal 33° from the surface normal [32]) and at the middle position after plasma treatment, while they lie down more after the plasma treatment at the edge position.

In summary, the orientation analysis shows that the edge position on PS is more affected than the middle position by the plasma treatment. In addition to the orientational changes of the phenyl moiety, there is also a strong decrease in SFG intensity for the edge position, to less than half the intensity of the pristine surface. There are several possibilities for the drop in SFG intensity: The number density of molecules at the surface has decreased, the orientation of the phenyl groups has changed, or the tilt and twist angle distribution has broadened. Previously some research reported that the number density of phenyl groups on the surface before and after air plasma is very similar,[13] others believed that surface phenyl densities decreased after plasma treatment.[14] We believe that the decrease in SFG intensity is due to both reasons: (1) the phenyl surface density decrease and (2) the phenyl orientation changes (as deduced above) and/or a broader distribution of tilt and twist angles. Due to the limited measurements, we could not quantify the orientation distribution here.

3.3.1.2 Investigation of the Polyimide Surface

After we examined the cover effect on the plasma treated PS surface, we carried out research to investigate the polyimide, PMDA/ODA surface. As we showed above, on the PS surface, edge and middle of the sample surface responded differently to plasma when there is a protective cover over the sample. Here we want to study whether PI surface has the same response when treated with He and O_2 plasmas. SFG spectra were collected from an edge and the middle position from both the pristine and post plasma treatment samples, which can be found in Figure 3.10. For each sample, there were three spots that were analyzed before and after 10 s plasma treatment: middle, edge 1, and edge 2. The edge 1 and edge 2 positions are opposite to each other (Figure 3.2, edge positions at 3-o'clock and 9-o'clock). For simplicity only SFG spectra collected from edge 1 are shown in the Figure 3.10 because they are identical to those collected from the edge 2 position, and we believe that they are representative of the data from the PI surface edge positions. All eight

SFG spectra are shown in Figure 3.10 and were fitted. The fitted spectra are displayed in Figure 3.11 and Figure 3.12 and fitting results in Table 3.7 and Table 3.8. There are two peaks in the spectra, one at 1740 cm^{-1} and the other at 1794 cm^{-1}, which can be assigned to the antisymmetric and symmetric stretching peaks contributed by the coupled C=O groups with imide ring, respectively.[15, 16]

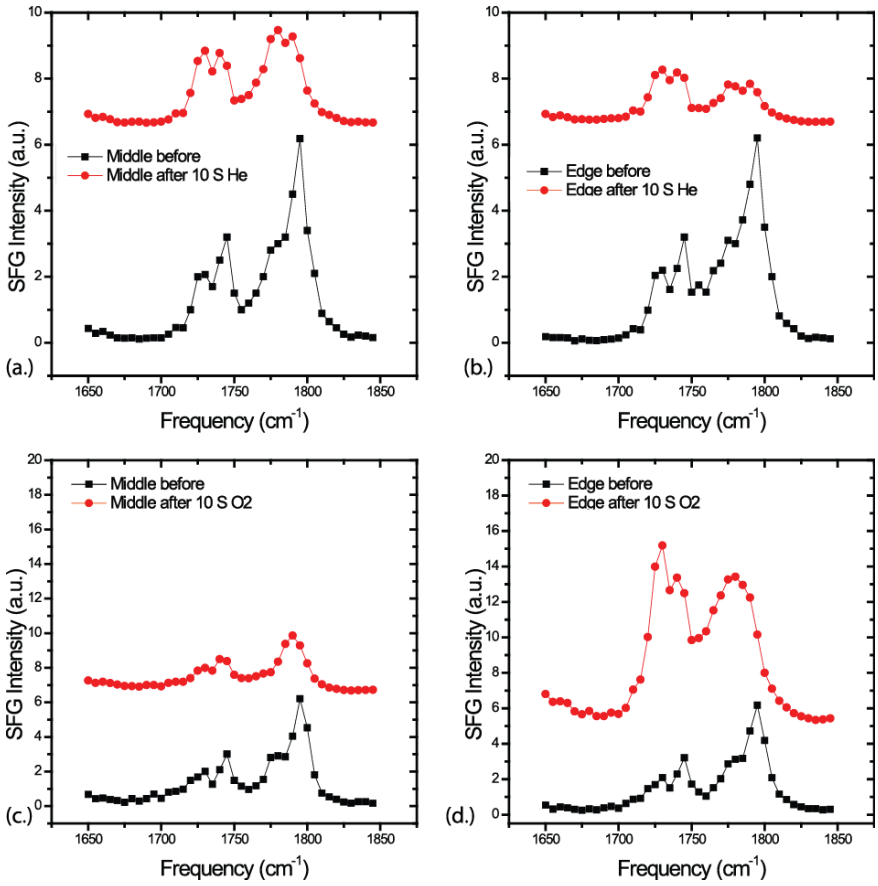

Figure 3.10: SFG spectra collected from (a.) The middle position, PI surface before and after 10 s He plasma (black spectra are before and red spectra are after), (b.) The edge position, PI surface before and after 10 s He plasma, (c.) The middle position, PI surface before and after 10 s O_2 plasma, (d.) The edge position, PI surface before and after 10 s O_2 plasma,

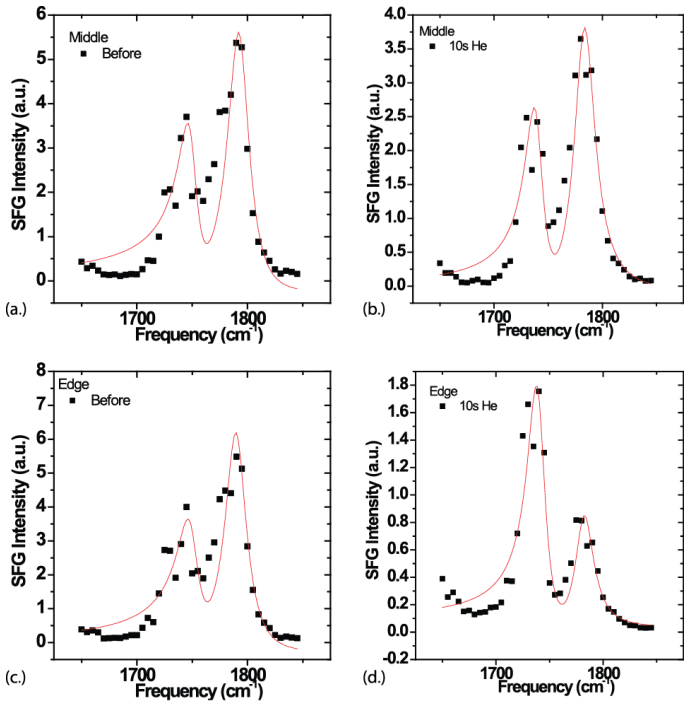

Figure 3.11: SFG spectra along with the results for the PI surface for (a.) the middle position, before, (b.) the middle position after 10 s He plasma, (c.) the edge position, before, (d.) the edge position, after 10 s He plasma.

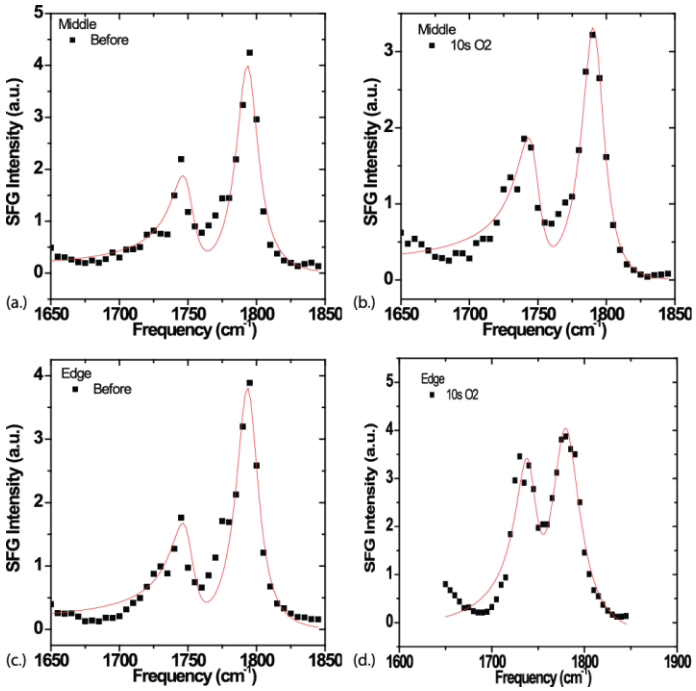

Figure 3.12: SFG spectra along with the results for the PI surface for (a.) the middle position, before, (b.) the middle position after 10 s O_2 plasma, (c.) the edge position, before, (d.) the edge position, after 10 s O_2 plasma.

Table 3.7: Fitting parameters for PI surface before and after He plasma treatment.

	ω_i (cm^{-1})	Γ_i (cm^{-1})	A_q (ssp)	A_q/Γ_i	X_{as}/X_s	Assign.
	1750±1	10.0±0.4	11.4±1.0	1.14±0.1		Asym.
middle before	1790±1	12.2±0.3	27.5±0.9	2.25±0.1	0.51±0.05	Sym.
	1744±1	10.0±0.8	9.9±0.9	0.99±0.1		Asym.
middle after	1784±1	12.5±0.4	21.4±0.7	1.71±0.1	0.58±0.07	Sym.
	1750±1	10.1±1.4	11.4±1.4	1.13±0.2		Asym.
Edge before	1793±1	12.5±0.5	28.9±1.0	2.31±0.1	0.49±0.09	Sym.
	1742±1	10.9±0.4	11.4±0.5	1.05±0.1		Asym.
Edge after	1784±1	12.2±0.9	12.9±0.6	1.06±0.1	0.99±0.11	Sym.

On the pristine PI surface, SFG spectra collected from the middle and edge regions are very similar, showing a homogenous PI film, similar to the PS data presented above. After 10 s He plasma treatment, the SFG spectrum detected from the middle position remains mostly unchanged, while the SFG signal from the edge position drastically changes. This observation is again similar to what we observed on PS surface. Here the intensities of the SFG signals collected from the PI edge position after plasma are drastically reduced for both peaks. The intensity of the peak at 1794 cm^{-1} is reduced by a factor of five, which has a larger reduction than the antisymmetric stretch (which is reduced by a factor of 2). For the O_2 plasma treated PI surface, the SFG spectrum collected from the middle spot changes slightly, but a larger difference is detected from the edge position. The intensity ratio of the two peaks changes dramatically: the symmetric stretch which dominated the pristine spectrum is now approximately the same size of the intensity of the antisymmetric stretching mode, which has interesting implications in the orientation analysis

(elaborated on further below). This same trend has been reported previously on PI surface after plasma treatment (without a cover).[17] In this study we can see that the edge region behaves like an unprotected surface and the middle position maintains its structure more or less with only slight changes following plasma treatment.

Table 3.8: Fitting parameters for PI surface before and after O_2 plasma treatment.

	ω_i (cm^{-1})	Γ_i (cm^{-1})	A_q	A_q/Γ_i	X_{as}/X_s	Assign.
	1749±1	8.9±1	10.1±0.7	0.88±0.15		Asym.
middle before	1794±1	12.0±0.3	27.0±0.4	0.44±0.07	0.50±0.07	Sym.
	1748±1	9.2±0.6	7.2±0.5	1.27±0.08		Asym.
middle after	1791±1	10.9±0.2	18.8±0.3	0.58±0.04	0.45±0.05	Sym.
	1750±1	9.1±1.2	10.1±0.7	0.90±0.17		Asym.
Edge before	1793±1	12.1±0.3	26.9±0.4	0.45±0.07	0.50±0.08	Sym.
	1738±1	15.2±0.8	35.4±0.8	0.43±0.13		Asym.
Edge after	1776±1	19.3±1.5	52.2±1.1	0.37±0.22	0.86±0.09	Sym.

Comparing the results obtained from the PI surfaces to those from the PS surfaces discussed above, similar trends could be observed for both surfaces. For both cases, the edges are affected greatly by the plasma and the middle positions are generally unaffected or only slightly affected by the plasma. A difference between the two systems is that the PS surface is affected mostly the same by the He and O_2 plasmas, while the PI system is affected differently by each plasma. This could be due to the O_2 plasma chemically reacting with the more reactive PI surface, while He plasma can only interact with the surface in a physical way. For the He plasma, the intensities of the SFG signals collected from the edge position for both peaks are reduced by the plasma, which could be

due to the surface reorienting and becoming more disordered. The O_2 plasma seems to be reorienting the PI surface, but there is still a high level of order on the surface that can be detected by SFG spectroscopy.

In addition to SFG spectroscopy, FT-IR was also used to study the bulk structure of the PI materials. FT-IR spectra were collected from the PI middle and edge positions before and after He or O_2 plasma treatment (Figure 3.13). Figure 3.13 shows that the precursors were successfully cross-linked and cured properly.[17] The signals contributed from the C-O-C antisymmetric stretch at 1239 cm^{-1}, CN stretch at 1373 cm^{-1}, phenyl C-C stretch at 1500 cm^{-1}, and imide CO stretches at 1726 cm^{-1} and 1780 cm^{-1} could be observed. [18, 19] Figure 3.13 shows that the FT-IR spectra collected from the edge and middle positions before and after plasma treatment were the same, which means that the bulk PI structure was unperturbed by plasma treatment. This confirms that the changes that are being detected by SFG spectroscopy originate from the surface and not from the bulk of the material. Both He and O_2 plasmas do not alter the PI bulk structure, regardless of the position on the sample, edge versus middle. This conclusion is well correlated to that observed from PS samples discussed above.

Similar to the studies on PS surfaces presented above, we also studied PI surface structure in more detail by SFG polarization analysis. An additional complexity for SFG data analysis for the PI system that is not found in the PS system exists: The two types of possible orientations lead to the contribution to the SFG signals from two pairs of C=O groups. The two carbonyls that are orthogonal to the polymer chain or the two carbonyls that are parallel to the chain can be exposed to the air and generate the detected SFG signal (The SFG signal generated from the C=O groups face to the bulk canceled out with those from the C=O groups in the bulk). Since there are two possible configurations, two separate orientation plots (relations between SFG measured signal strength ratio of the antisymmetric (AS) $\chi^{(2)}$ over the symmetric (SS) $\chi^{(2)}$ and PI imide ring orientation, e.g., the tilt angle (θ)) must be generated. Here the orientation analysis is based on the SFG ssp spectra. Detailed SFG orientation analysis methodology for PI has been developed and published in the literature:[15-17] For the high tilt angles, values of the hyperpolarizability components are: $\alpha_{asY'Y'Y'} = 1.13$, $\alpha_{asX'X'Y'}=1.00$, $\alpha_{ssY'Y'Y'}= 1.25$, and $\alpha_{ssX'X'Y'}=1.00$.[15-17] For the low tilt angles, the values of hyperpolarizability components are: $\alpha_{asX'Y'Y'}=1.80$, $\alpha_{ssX'X'X'}=1.00$, $\alpha_{ssY'Y'X'}=2.50$.[15-17]

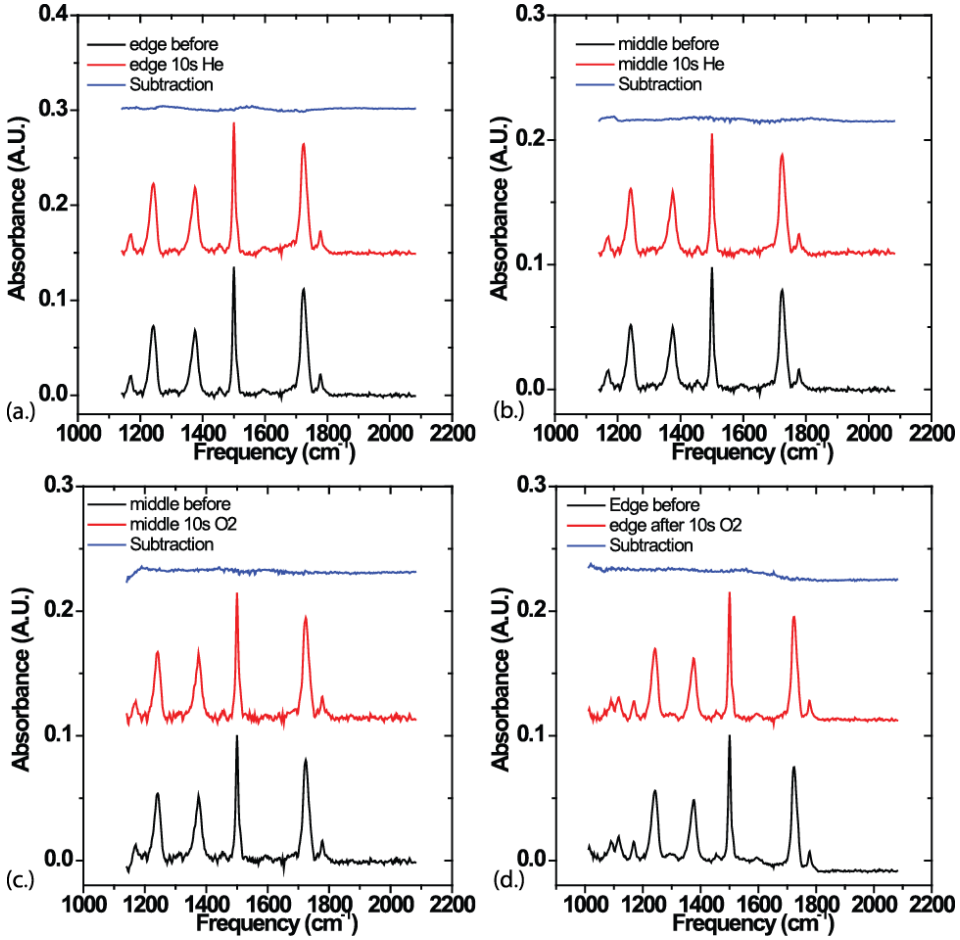

Figure 3.13: FT-IR spectra collected from (a.) The middle position, PI surface before and after 10 s He plasma (black plots before, red plots after, and the blue plots are the subtracted results) , (b.) The edge position, PI surface before and after 10 s He plasma, (c.) The middle position, PI surface before and after 10 s O_2 plasma, (d.) The edge position, PI surface before and after 10 s O_2 plasma,

Using the above known molecular hyperpolarizability components, the relationships between SFG measured signal strength ratio and the PI imide ring orientation can be plotted (Figure 3.14). The experimentally determined $\chi^{(2)}_{AS}/\ \chi^{(2)}_{SS}$ ratio for a pristine PI surface is 0.49±0.07. One measured ratio cannot determine both the tilt and twist angles of the imide ring. Here we deduce the imide ring tilt angle by assuming twist angle (ψ) to be 0°, 15°, 30°, or 45°, respectively. Figure 3.14 indicates that for a large tilt angle (60°-90°), the range of all the possible $\chi^{(2)}_{AS}/\ \chi^{(2)}_{SS}$ ratios is between 0.96 and 1.00. From our measured data (0.49±0.07), we know that the PI imide ring on the surface before plasma treatment does not have a tilt angle between 60° and 90°. We therefore should use the method for low tilt angle condition to perform data analysis. The range of possible values for the $\chi^{(2)}_{AS}/\ \chi^{(2)}_{SS}$ ratio for the lower tilt angle is from 0.00 to 2.00, and the experimental

value of 0.49 falls well within this range. The four determined tilt angles for the twist angles 0°, 15°, 30°, or 45°, are 33±4°, 34±4°, 38±5°, or 54±7°, respectively.

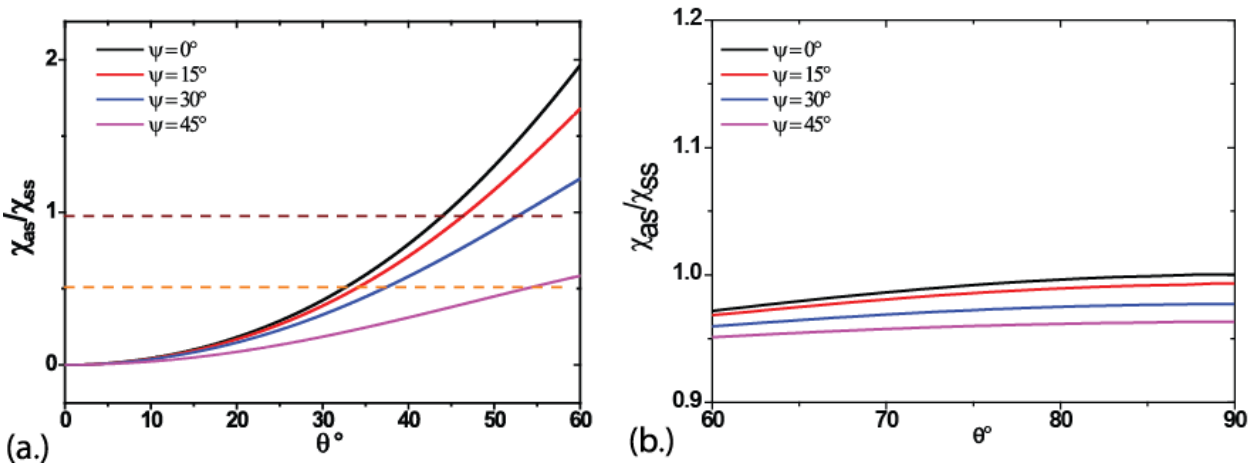

Figure 3.14: Orientation plot for the PI core. The y-axis is χ_{as}/χ_{ss} and the x-axis is the tilt angle. The black, blue, red, and pink curves assume a twist angle of 0°, 15°, 30°, and 45°.

For the SFG spectra collected from the PI middle position after the He and O_2 plasma treatment, the similar $\chi^{(2)}_{AS}/\chi^{(2)}_{SS}$ ratio was measured within the error bars. The measured $\chi^{(2)}_{AS}/\chi^{(2)}_{SS}$ ratios in the SFG spectra collected from the edge position greatly changed after both the He and the O_2 plasma treatments, going from 0.46±0.07 to 1.02±0.11 and 0.86±0.09, for the He and O_2 plasmas, respectively. What is worth noting, is that the He plasma treatment seems to have reduced the symmetric peak compared to that observed from the pristine PI surface, while the O_2 plasma seems to have increased the intensity of the antisymmetric peak. Both effects lead to the similar increase in the $\chi^{(2)}_{AS}/\chi^{(2)}_{SS}$ ratio, indicating that the tilt angle increases, which means the PI chain lies closer to the surface. The deduced tilt angle for the PI moiety after plasma treatment is 43±7° and 45±7°, for the twist angle of 0° and 15°, respectively. Due to the limited number of the independent measurements, we could not determine the tilt and twist angles at the same time. However, we believe that the tilt angle of the imide ring indeed increased on the PI surface after the plasma treatment, lying down more towards the surface.

Also due to the limited number of the independent measurements, we could not determine the orientation angle distribution. However, we believe that the stronger SFG signal detected from the O_2 plasma treated edge position is likely due to more ordered (narrower orientation distribution) surface structure compared to the pristine surface, while the weaker SFG signal detected from the

He plasma treated surface may be because the surface has a wider orientation distribution or more disordered.

In summary, the SFG results for PI surfaces treated with He and O_2 plasmas clearly demonstrated that the edge and middle regions behave differently when covered. In addition, it was found that the He and the O_2 plasmas affected the PI surface differently. The He plasma reduced the intensities of both the antisymmetric and the symmetric peaks in the SFG spectra, while the O_2 plasma increases the antisymmetric peak. We believe that the He plasma reduced the level of order at the interface, while the O_2 plasma made the surface more ordered. The FT-IR spectra show that the bulk structure remains the same throughout plasma treatment for the entire PI film, indicating that the plasma effects are seen exclusively on the surface. From the orientation analysis it is clear that the PI imide ring goes from a relatively small tilt (standing up) to a larger one (lying down), showing that the chain is adopting an orientation that is closer to parallel to the surface. By studying the PI surface, it was confirmed that the edge and middle positions behave differently when covered and exposed to plasma treatment, similar to the behavior of PS surface reported above.

3.3.2 Correlations to Industrially Prepared Flip-Chip Assemblies

The above study shows that when a covered polymer surface was exposed to plasma treatment, different surface positions could adopt varied surface structures. This implies that when adhesives adhere to such a plasma treated polymer surface, different positions at the adhesive/polymer interface may have different adhesion strengths, due to the different original structures on the different positions of the polymer surface after the plasma treatment. Such knowledge can be well correlated to the observations of device failures in industrial processes.

In industrial processes, flip-chip packages (Figure 3.15) were plasma treated prior to underfill dispensing step, and many samples were prepared simultaneously, which require loading many samples into the plasma chamber by utilizing trays and racks, see Figure 3.15(a.), (b.) and (c.). It is obvious that such an arrangement is similar to a case whether some of the sample surfaces are covered, which may lead to different adhesion with underfill and device failure.

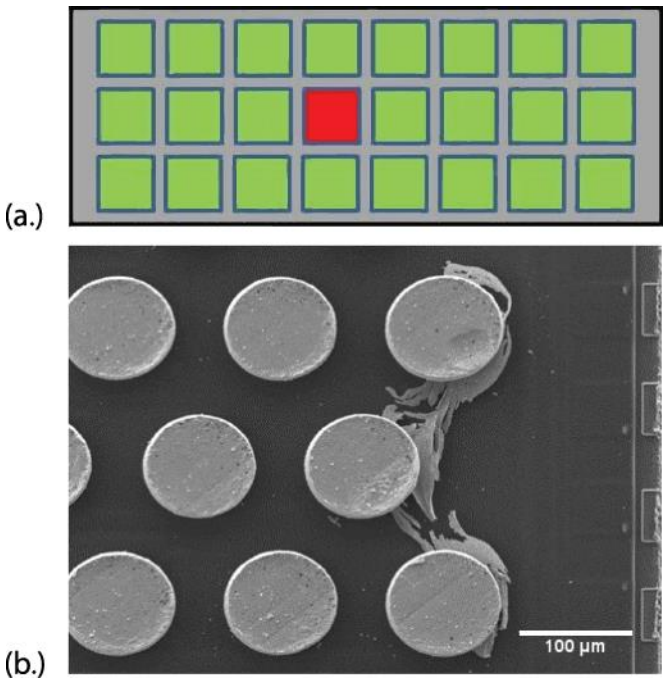

Figure 3.15: (a.) Tray fitting a 8x3 matrix in a plasma chamber. These trays are stacked vertically on top one another (i.e. 10-trays at a time) in a magazine cartridge. (b.) SEM image of flip chip assembly, plasma treated in the red position. The underfill has been chemically removed to reveal the electrical shorts.

To analyze the device failure, a die was isolated from the polymer substrate by side polishing off the polymer substrate layers to obtain images of the buried interface, which then exposed the flip-chip bumps. Region of failure was identified based on the test data, where failure was electrical shorts. It was found that flip-chip assemblies that are at the middle positions (the red square) have more electrical shorts (Figure 3.15 (a)), and thus fail more than the samples in the edge positions, indicating that the middle positions do not receive adequate plasma treatment. Figure 3.15 (d.) shows the SEM image of flip-chip assembly found in the middle position. The electric short can clearly be seen and this comes from the inhomogeneity of the plasma treatment. There is delamination at the underfill/polyimide interface, which enables a path for solder to extrude to adjacent bumps, causing an electrical short. In this image the underfill has been chemically removed to expose the solder bumps on the die surface. Solder extrusion formed in between the delaminated underfill and PI interface and migrated to adjacent bumps caused by plasma density differences at die edge and middle. Therefore, the reason for the delamination and solder material shorting to adjacent solder bumps was due to the plasma not activating the chip passivation layer (i.e. polyimide) at the middle part in the middle tray in the plasma chamber (due to its distance away from the electrodes to produce plasma). The root cause was due to poor plasma coverage as

a result of low plasma ion density, which impacted uniformity across the die. There are other physical processes that are involved including the depth of chamber size and electrode distance, but this example clearly shows that plasma has a diminishing effect from edge to middle in the plasma chamber, which has been shown previously in this work for both the PS and PI surfaces. For PI surface, the SFG results suggest plasma treatment causes the imide ring to lie parallel to the surface, leading to a higher electron density on the surface. This likely increases the bonding interaction between the PI surface and lone pair of electrons of underfill amine functionalities, facilitating the PI - underfill adhesion. The knowledge on polymer chain ordering and orientation at the surface will likely provide understanding on the mechanisms of why adhesion can be improved with plasma. Therefore we believe that our fundamental research on PS and PI surfaces before and after plasma treatment reported above provides important understanding on the sample failure observed in industrial processes.

3.3.3 Conclusions to Covered Plasma Effects

From this research it is clear that edge and middle positions of the covered PS and PI surfaces, behave very differently in the presence of plasma treatment. The bulk structure of both PS and PI films is generally unaffected by the plasma treatment, which means the changes that are being detected by SFG only occurred on the surface. This work shows that the plasma affects the edge of the sample surface more than the middle surface of a covered film. We believe that this is important knowledge and shows that sufficient plasma time is necessary for the treatment of surfaces relevant in the microelectronics industry to ensure that the entire surface is effectively treated by plasma.

Comparing the PS and PI films investigated in this research, the “cover effect” showing the different plasma effects on the edge and the middle of the sample was observed from both samples. However, for PS, the edge surface was greatly altered by plasma treatment, leading to much smaller SFG signal intensity likely due to the phenyl orientation change and/or disordering of the surface phenyl groups (with a broader orientation angle distribution). SFG polarization analysis shows that the phenyl groups tend to lie down more after the plasma treatment. Treatment results from different plasmas on PS are similar. Differently, O_2 plasma treatment leads to a more ordered structure on the PI edge surface, while He plasma treatment leads to a more disordered structure. In the next section, we will report the results of our studies on the buried interfaces between

polymer films and polymer adhesives to understand how different surface structures lead to varied interfacial structure, resulting in different interfacial properties such as adhesion.

3.4 Plasma Adhesion Promotion

3.4.1 Polystyrene Interface

The first system that will be discussed is the dPS/epoxy buried interface involving dPS before and after 100s He plasma. As shown above, plasma treatment can influence the PS surface structure. [9, 20] Here we will first show that the plasma effect on dPS is similar to that on regular PS. To determine how He plasma affects the dPS surface, polymer films were investigated before and after plasma, see Figure 3.16. Prior to the plasma treatment, the dPS surface generates very strong SFG signal, showing the surface is well ordered. There are two peaks in the SFG spectrum, at 2275 cm^{-1} and 2295 cm^{-1}, which can be assigned to the v_{20b} and the v_2 vibrational modes, respectively.[11] After the He plasma treatment, the SFG intensity from the dPS surface greatly decreases and the intensity is nearly zero. SFG signal is proportional to coverage, orientation, and orientation distribution, thus any of these three factors could be changing, which will decrease the SFG intensity. Our above study on regular PS indicated that plasma treatment changed the orientation of the surface phenyl group on PS surface, which led to SFG signal intensity decrease.[21] Here no SFG signal was detected after the plasma treatment, therefore we could not quantitatively deduce the orientation. No SFG signal detected may be due to the total loss of the surface phenyl groups, or the phenyl completely lying down geometry, or a broader distribution of orientation angles. We refer the latter two cases to “disordered” structure of dPS at the interface. We believe that in this case the dPS surface was more disordered after the plasma treatment, along with some surface phenyl group loss. It is worth mentioning that the plasma treatment time is longer than the covered plasma treatment effect reported in the previous section.

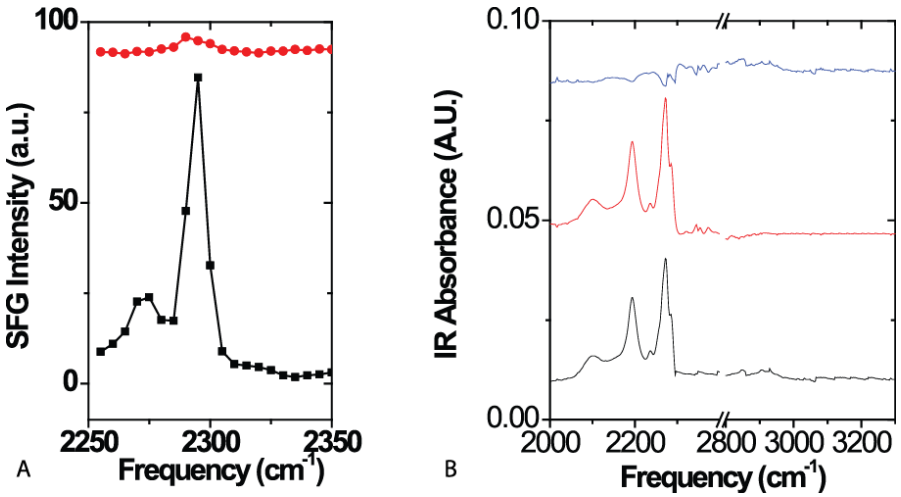

Figure 3.16: SFG (A) and ATR-FTIR (B) spectra of the dPS before (black) and after (red) 100s He plasma. (B) The difference of the ATR-FTIR spectra was taken and is displayed in blue.

For this system, we also applied ATR-FTIR spectroscopy to study the entire dPS film before and after He plasma treatment to see whether plasma treatment can remove the PS film or cause substantial bulk structural change (Figure 3.16). The theoretical penetration depth of the evanescent wave has been calculated previously as 800 nm, the dPS thin film is approximately 100 nm before plasma treatment,[22] therefore ATR-FTIR spectra can probe the entire dPS film. Figure 3.16 shows the ATR-FTIR spectra collected from the dPS polymer film before and after 100s He plasma, from which four peaks at 2193 cm^{-1}, 2236 cm^{-1}, 2272 cm^{-1}, 2285 cm^{-1} could be observed, assigned to the methylene sym, methylene asym, and two phenyl ring stretching modes, respectively.[23] The very similar ATR-FTIR spectra observed from dPS before and after He plasma treatment, shown by the subtraction results in Figure 3.16, indicate that the plasma treatment did not remove the dPS film and did not cause substantial bulk structural change. Therefore the plasma treatment could alter the dPS surface structure, but not the bulk structure.

We then probed the buried polymer/epoxy systems, first in the dPS C-D stretching frequency region and then in the epoxy C-H stretching region of the spectrum. SFG spectra were generated from the dPS/epoxy interface before and after 100s He plasma treatment on the dPS surface in the C-D stretching frequency region (Figure 3.17). The C-D stretching signals should be contributed from dPS because epoxy does not contain any C-D bonds. Prior to plasma treatment on dPS, there is a strong peak at 2290 cm^{-1} detected from the dPS/epoxy interface, attributed to the v_2 symmetric vibrational mode. After 100s He plasma treatment on dPS, this peak was no longer detected from the dPS (with plasma treatment)/epoxy interface. This shows that the dPS/epoxy interface is well

ordered prior to plasma treatment on the dPS surface. After plasma treating the dPS surface, dPS at the dPS/epoxy interface should change orientation and must be much less ordered (either lying down or having a broader orientation distribution or both) and the interface yields no SFG signal. After studying the dPS behavior at the dPS/epoxy interface, we then investigated the epoxy C-H stretching frequency region of the SFG spectra to determine if the change of the polymer surface causes the epoxy to also be less ordered.

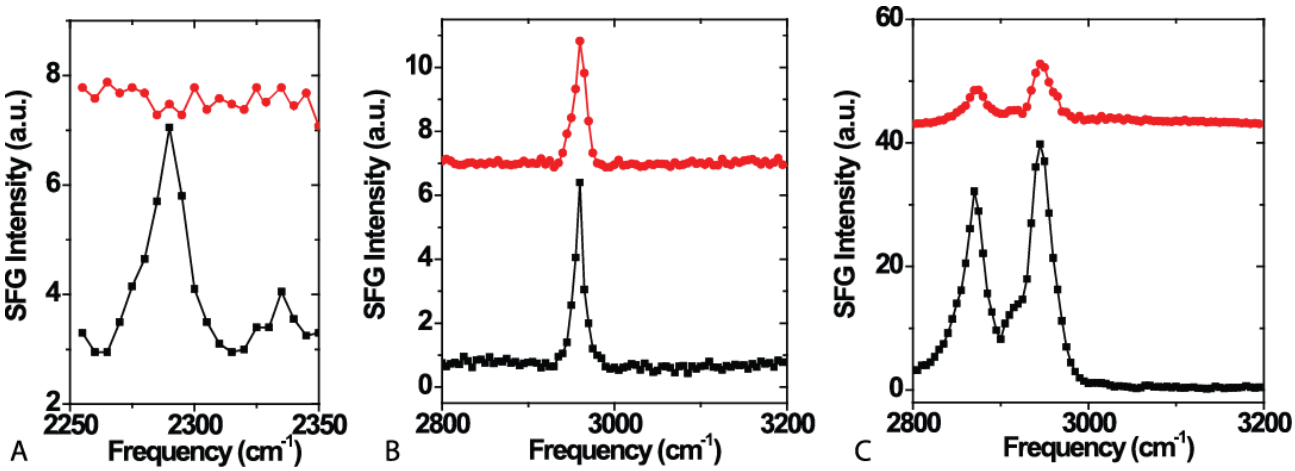

Figure 3.17: A: SFG ssp spectra of the dPS (before plasma treatment)/epoxy buried interface (black) and the dPS (after plasma treatment)/epoxy interface (red). SFG spectra of the dPS/epoxy buried interface in the sps (B) and ssp (C) before (black) and after (red) 100s He plasma treatment on dPS surface.

Figure 3.17 shows the sps and ssp SFG spectra collected from the dPS (before and after 100s He plasma)/epoxy buried interfaces in the C-H stretching frequency region. Such C-H signals should be contributed from epoxy, because dPS does not contain C-H bonds. As discussed above, plasma can alter the PS surface structure. Here Figure 3.17 clearly shows that the SFG spectra collected from the dPS/epoxy buried interfaces before and after plasma treatment are very different in the C-H stretching frequency region, indicating that the He plasma treatment of dPS surface influenced the behavior of epoxy at the buried dPS/epoxy interface.

The interface between epoxy and a pristine dPS sample yielded very strong SFG signals in both ssp and sps polarization combinations, while the interface between epoxy and the polymer surface exposed to 100s He plasma generated much lower SFG intensity. This is similar to what was observed for dPS before and after the He plasma treatment at the dPS/epoxy interface. In the sps spectrum from the dPS (before or after plasma treatment)/epoxy interface in the C-H stretching frequency region, there is one peak present at 2960 cm^{-1} that can be assigned to the methyl

antisymmetric stretch.[24] The ssp spectra can be fitted using five peaks, 2855 cm^{-1} (CH_2 sym), 2870 cm^{-1} (CH_3 sym), 2915 cm^{-1} (CH_2 asym), 2943 cm^{-1} (Fermi Resonance), and at 2970 cm^{-1} (CH_3 asym). In order to perform orientation calculations, all the sps and ssp spectra were fitted. The fitted spectra are plotted in Figure 3.18 along with the fitting parameters in Table 3.9.

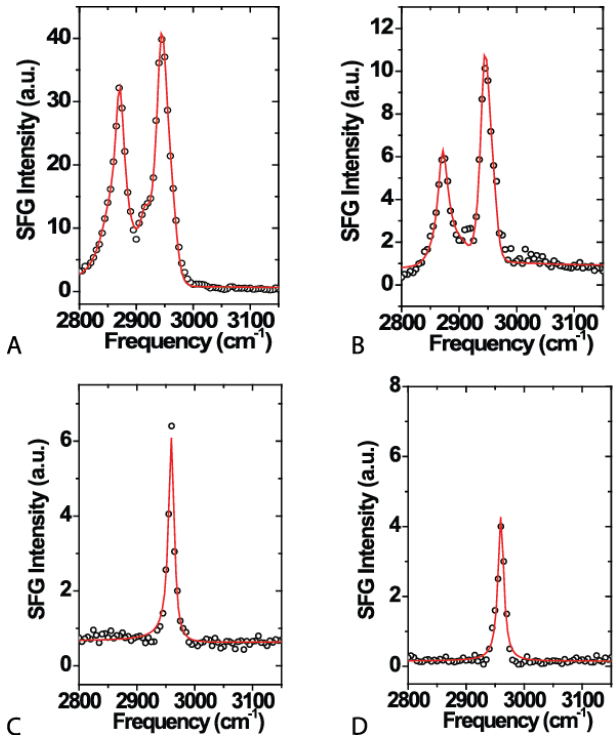

Figure 3.18: SFG spectra of the dPS/epoxy buried interface, in the ssp (top) and sps (bottom) polarization combinations before (left) and after (right) 100s He plasma treatment on dPS. The circles are the experimental data and the red curves are the fitted results. ssp before plasma (A), ssp after plasma (B), sps before plasma (C), sps after plasma (D).

Since SFG signal could be detected from C-H stretching modes of epoxy at the buried dPS/epoxy interface, we know that the epoxy molecules at the interface are ordered. SFG spectroscopy is sensitive to the interface coverage, orientation, orientation distribution (or ordering), therefore the structural change of the dPS surface caused by plasma treatment altered the interfacial epoxy coverage, orientation, or ordering. Plasma treatment is known to increase the strength of adhesion between polymers and underfill materials.[25-27] Such adhesion promotion must be induced by the structural change at the interface.

Table 3.9: Fitting parameters from the dPS/epoxy buried interface before and after 100s plasma treatment on dPS.

Pristine surface								
	ssp					sps		
Frequency	2855	2870	2915	2944	2965	2960		
Amplitude	26.0	54.0	-60.0	85.8	-60.0	13.9		
Width	15.0	10.9	12.9	10.5	13.1	6.0	$\chi_{yyz,sym}/\chi_{yzy,asym}$	5.7
Amplitude/Width	1.7	4.9	4.6	8.2	4.6	2.3		
Assignment	CH_2 sym	CH_3 sym	CH_2 asym	FR	CH_3 Asym	CH_3 Asym	$\chi_{yyz,asym}/\chi_{yzy,asym}$	2.0
100 s He plasma								
	ssp					sps		
Frequency	2855	2870	2915	2944	2965	2962		
Amplitude	4.3	23.7	-20.0	37.7	-15.0	12.2		
Width	15.0	10.9	12.9	10.5	13.1	6.0	$\chi_{yyz,sym}/\chi_{yzy,asym}$	2.8
Amplitude/Width	0.3	2.2	1.5	3.6	1.1	2.0		
Assignment	CH_2 sym	CH_3 sym	CH_2 asym	FR	CH_3 Asym	CH_3 Asym	$\chi_{yyz,asym}/\chi_{yzy,asym}$	0.6

To further understand the structural difference of the interfaces between pristine and plasma treated dPS and epoxy, we studied orientations of methyl groups of the epoxy at the interface based on the relationships between the SFG measured data and the $(CH_3)_2C$ group orientation (Figure 3.19). Here the experimentally measured $\chi_{yyz,sym}/\chi_{yzy,asym}$ and $\chi_{yyz,asym}/\chi_{yzy,asym}$ values were used to determine the methyl orientation angle (Figure 3.19).[28] The deduced orientation angles are listed in Table 3.10. It is feasible to deduce both the average orientation and orientation distribution (assuming a Gaussian distribution) of a surface functional group using SFG if the surface/interfacial coverage of the functional group is known.[29] Unfortunately here we do not know the interfacial coverage of the isopropyl group. Therefore, we utilize a delta orientation distribution and three Gaussian orientation distributions (with a width of 3°, 5°, and 10°) to deduce the average orientation of isopropyl groups at the dPS/epoxy interface. For measured $\chi_{yyz,sym}/\chi_{yzy,asym}$ value, the delta distribution shows that the $(CH_3)_2C$ groups at the pristine

dPS/epoxy interface have a tilt angle from the surface normal of 21.2±0.8°, and at the plasma treated PS/epoxy interface this angle is 50.6±2.3°. For the σ = 3° Gaussian distribution, 22.1±0.8° and 52.8±2.4° were found for the pristine dPS/epoxy and plasma treated dPS/epoxy interface, respectively. For the σ = 5° Gaussian distribution, 21.2±0.8 and 53.2±2.4° were deduced for the two interfaces. For the σ = 10° Gaussian distribution, 16.6±0.6 and 54.9±2.5° were determined. For measured $\chi_{yyz,asym}/\chi_{yzy,asym}$ value, the delta distribution shows that the $(CH_3)_2C$ groups at the pristine dPS/epoxy interface have a tilt angle from the surface normal of 21.0±0.8° and at the plasma treated dPS/epoxy interface, 46.8±8.4°. For the σ = 3° Gaussian distribution, 20.5±0.8° and 46.8±8.4° were found for the pristine dPS/epoxy and plasma treated dPS/epoxy interface, respectively. For the σ = 5° Gaussian distribution, 19.5±0.8 and 46.9±8.4° were deduced for the two interfaces, respectively. For the σ = 10° Gaussian distribution, 13.9±0.5 and 47.1±8.5° were determined. Since the results from the two independent measurements $\chi_{yyz,sym}/\chi_{yzy,asym}$ and $\chi_{yyz,asym}/\chi_{yzy,asym}$ led to similar results, we believe that the assumption of a narrow angle distribution is reasonable. For convenience, here the σ = 10° case will be used, and the average tilt angles measured from the $\chi_{yyz,sym}/\chi_{yzy,asym}$ and $\chi_{yyz,asym}/\chi_{yzy,asym}$ ratios will be used in the discussions below. Here the $(CH_3)_2C$ tilt angle at the dPS (prior to He plasma treatment)/epoxy interface is 15.3±0.8. After plasma treating the dPS surface, this tilt angle at the dPS (after plasma treatment)/epoxy interface is larger, 51.0±9.5°. This shows that the $(CH_3)_2C$ group tilts more at the dPS/epoxy interface after the dPS surface was plasma treated (Figure 3.19). It is interesting to note that prior to the plasma treatment that both methyl groups in $(CH_3)_2C$ are sticking mostly straight up at the interface, and then after plasma treatment one of the methyl groups is sticking more up and the other one is lying more down at the interface, the entire isopropyl group rotates by 40° after plasma treatment.

Such orientation changes may decrease the SFG signal intensity. As we presented above, SFG signals detected from epoxy at the dPS (after plasma treatment)/epoxy interface do decrease. The decrease of the SFG signal could also be due to a broader orientation distribution (i.e. a broader distribution of tilt angles) or a lower number density of methyl groups at the interface in addition to the average orientation angle effect. A broader distribution of tilt angles means a more randomly orientated or more disordered interface. The lack of order could come from interfacial diffusion, where there is no longer a well-defined boundary at the interface, which has been observed previously.[10, 22] The interfacial diffusion will increase the adhesion strength. Unfortunately

because we do not know the interfacial coverage of the $(CH_3)_2C$ group, we could not determine the orientation and orientation distribution at the same time. Therefore we could not discuss this effect quantitatively.

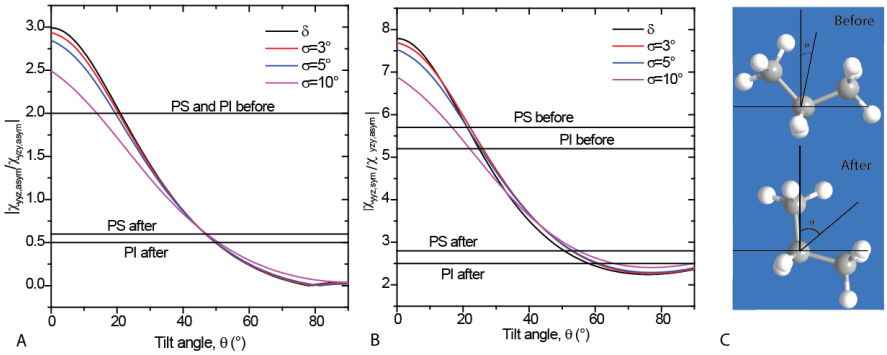

Figure 3.19: Orientation curves of the quasi-isopropyl methyl groups and illustration of the tilt angle before and after 100s He plasma. (A) the $\chi_{yyz,sym}/\chi_{yzy,asym}$ ratio as a function of the tilt angle θ and (B) the $\chi_{yyz,asym}/\chi_{yzy,asym}$ ratio. (C) The tilt angle before (top) and after (bottom) 100s plasma treatment, showing the increasing tilt angle after treatment.

Table 3.10: Tilt angles for the quasi-isopropyl methyl groups of the BADGE epoxy.

$\chi_{yyz,sym}/\chi_{yzy,asym}$				
	PS pristine	PS 100s He	PI pristine	PI 100s He
δ-distribution	21.2±0.8°	50.6±2.3°	24.9±0.9°	58.0±3.5°
σ =3°	22.1±0.8°	52.8±2.4°	26.1±1.0°	60.3±2.7°
σ =5°	21.2±0.8°	53.2±2.4°	25.4±0.9°	61.2±2.8°
σ =10°	16.6±0.6°	54.9±2.5°	22.1±0.8°	65.8±3.0°
$\chi_{yyz,asym}/\chi_{yzy,asym}$				
	PS pristine	PS 100s He	PI pristine	PI 100s He
δ-distribution	21.0±0.8°	46.8±8.4°	21.0±0.8°	49.8±5.0°
σ =3°	20.5±0.8°	46.8±8.4°	20.5±0.8°	49.9±5.0°
σ =5°	19.5±0.8°	46.9±8.4°	19.5±0.8°	50.0±5.0°
σ =10°	13.9±0.5°	47.1±8.5°	13.9±0.5°	50.7±5.1°

The SFG signal intensity decrease can also be caused by the reduction in number density of the methyl groups at the interface. The $\chi^{(2)}$ expressions contain N, which is the surface number density of a particular functional group. Using the known hyperpolarizability components and the deduced orientation (by assuming a certain distribution), by taking the ratio of $\chi^{(2)}_{After}$/ $\chi^{(2)}_{Before}$, the ratio of N_{After}/N_{Before} can be determined (Here "After" and "Before" mean after and before plasma treatment). Here two vibrational modes were used, the $\chi_{yyz,Sym}$ and $\chi_{yzy,Asym}$, to deduce this ratio, yielding 0.72 and 0.71 respectively. The two independent measurements lead to a similar result, showing that there is about a 30% decrease in the methyl group coverage at the interface (when assuming the same orientation distribution). This data suggests that the methyl interfacial coverage at the dPS/epoxy interface is indeed reduced at the dPS/epoxy interface after the dPS surface is plasma treated. From the above discussion, it is clear that the SFG signal intensity decrease at the dPS (after plasma treatment)/epoxy interface is due to the $(CH_3)_2C$ orientation change, a broader distribution, a smaller interfacial coverage, or a combination.

Our SFG studies on the dPS/epoxy interface demonstrated that after the plasma treatment on the dPS surface, dPS molecules exhibit varied orientations and ordering (more disordered) at the dPS/epoxy interface, which induces different epoxy orientation and a broader $(CH_3)_2C$ distribution or reduced $(CH_3)_2C$ coverage or both. As we reported previously, both interfacial disordering and less methyl coverage at the interface led to higher adhesion.[10] We therefore believe that the cause for plasma treatment on polymer to increase adhesion with epoxy is due to a more disordered interface and less methyl group presence of epoxy at the interface.

We also used ATR-FTIR to probe the epoxy bulk near the epoxy/dPS interface. As we discussed above, the ATR-FTIR probes ~800 nm into the sample, therefore it can probe 700 nm into the epoxy region.[22] The ATR-FTIR spectra collected from the sample of dPS polymer (before and after 100s He plasma) in contact with epoxy can be found in Figure 3.20. In addition to the four peaks from the dPS film, there are three peaks present in the C–H stretching frequency region at 2870 cm^{-1}, 2930 cm^{-1}, and 2965 cm^{-1}, which can be assigned to the epoxy methyl symmetric stretch, methylene antisymmetric stretch, and methyl antisymmetric stretch, respectively.[30] Before and after plasma treatment of dPS, the same signal was observed from the interfaces, showing that we could not observe any differences from the interfacial region (~800 nm) between dPS (before and after He plasma treatment) and epoxy. This demonstrated that if there is any

adhesion difference, it must be due to the interface effect, caused by the plasma treatment on the dPS surface.

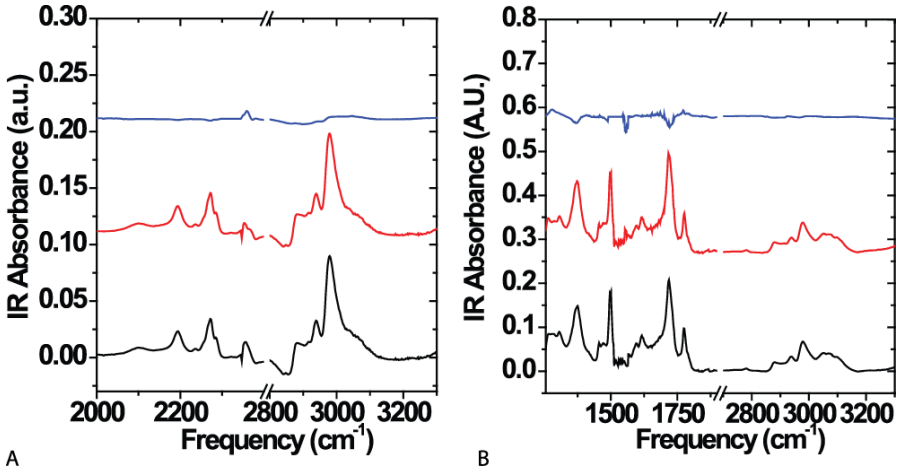

Figure 3.20: ATR-FTIR spectra of dPS (A) and PI (B) buried epoxy interfaces before plasma (black), after 100s He plasma (red), and the subtraction result (blue).

3.4.2 Polyimide Interface

The next system that will be discussed is the PI surface before and after 100s He plasma treatment. The PI polymer has no SFG signal in the CH stretching frequency region, but it has very strong signal in the C=O stretching frequency region due to the two carbonyl groups. The polymer PI has been well studied by SFG.[15-17] As presented in the previous section, we also studied plasma treatment effect on the PI surface. Here, to more clearly demonstrate the plasma treatment effect on adhesion, we used a much longer plasma treatment time.

Here, the PI surface was studied via SFG and ATR-FTIR (the spectra are in Figure 3.21). Similar to the PS surface, very strong SFG signal prior to plasma treatment was observed. There are two peaks in the SFG spectrum at 1735 cm^{-1} and 1775 cm^{-1}, which correspond to the antisymmetric and symmetric stretching modes for coupled C=O groups associated with each imide ring of the PI polymer, respectively. For the plasma treated PI surface there is no SFG signal detected, which is corroborated by previous plasma studies with Ar gas,[17] indicating a completely disordered surface or C=O groups completely lying down. There are six peaks present in the ATR-FTIR spectrum (Figure 3.21) that come from PI, 1776 cm^{-1}, ν(C=O) of imide; 1718 cm^{-1},ν(C=O) of imide; 1607 cm^{-1}, C-N/N-H coupled deformation of amide; 1505 cm^{-1}, breathing mode of aromatic ring; 1454 cm^{-1}, CH_2 asymmetric deformation; 1378 cm^{-1}, (C-N-C) of imide.[31] The ATR-FTIR

results show that there is PI before and after plasma treatment and there is negligible difference, as shown by the difference ATR-FTIR spectrum (Figure 3.21).

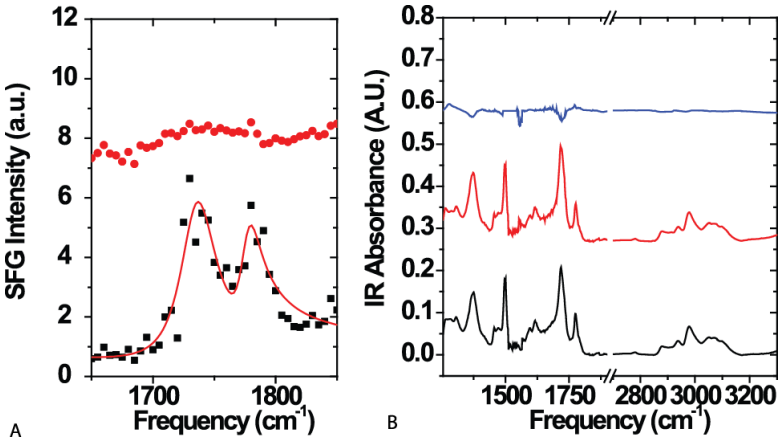

Figure 3.21: SFG (A) and ATR-FTIR (B) spectra of the PI surface before (black) and after (red) 100s He plasma. (A) The SFG experimental data was fit with a red curve to aid the eyes. (B) The difference of the ATR-FTIR spectra was taken and is displayed in blue.

After studying the PI surface, we investigated the buried PI/epoxy interface. SFG spectra were collected from epoxy/PI (before and after 100s He plasma) interfaces (Figure 3.22). As we discussed above, the 1735 cm^{-1} and 1775 cm^{-1} peaks from PI correspond to the antisymmetric and symmetric stretch modes for coupled CO groups associated with each imide ring of the PI polymer. Before plasma treatment for both the surface and buried interface the two peaks are very strong, after treatment there is no detected signal, which is corroborated by previous plasma studies with Ar gas.[17] The SFG spectra collected from the PI surface and buried pristine PI/epoxy interface have the same two peaks, but the spectral profiles are different, which could be due to the local environment of the PI/air versus the PI/epoxy interfaces, leading to different orientations of the C=O groups. The PI/air and PI/epoxy interfaces have been previously investigated with similar epoxies and it was found that the SFG spectra of PI at air interface and epoxy interface can be drastically different.[17] After the plasma treatment on PI, no SFG signal could be detected from the C=O groups on the PI surface in air or PI/epoxy interface. As our analysis on the dPS above, likely C=O groups lose surface coverage, or lie down completely or have a random distribution. Again we refer the latter two cases to disordering. Here we believe that the PI molecules are more disordered at the PI (after plasma treatment)/epoxy interface along with some loss the surface coverage.

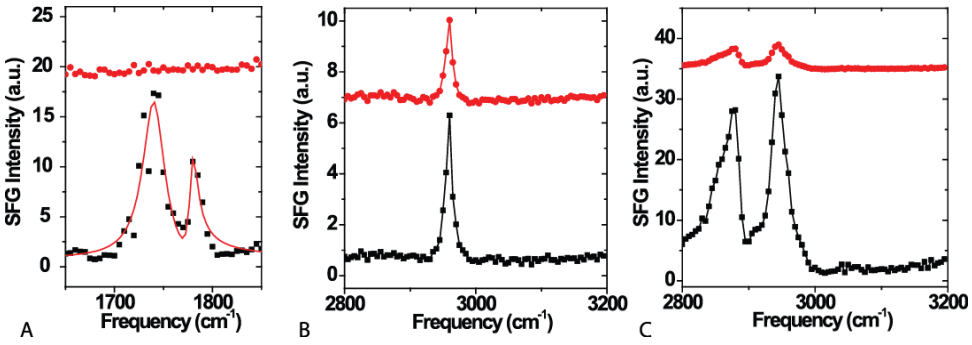

Figure 3.22: A: SFG ssp spectra in C=O stretching frequency region collected from the PI (before plasma treatment/epoxy buried interface (black) and the PI (after plasma treatment)/epoxy interface (red). SFG spectra in the C-H stretching frequency region collected from the PI (before plasma treatment)/epoxy buried interface (black) and the PI (after plasma treatment)/epoxy interface (red) in the sps (B) and ssp (C) polarization combinations.

In addition to the PI/epoxy spectra taken in the C=O stretching frequency region, SFG spectra were also taken in the C-H stretching frequency region, to verify that the epoxy molecules are more disordered at the buried interface after the PI surface was He plasma treated for 100s. Figure 3.22 displays these SFG ssp and sps spectra. As with the dPS/epoxy system, the PI (without plasma treatment)/epoxy interface yields very strong ssp and sps SFG signals, while SFG spectra collected from the PI (with 100s He plasma treatment)/epoxy interface have greatly reduced intensity. These C-H stretching SFG signals detected are solely due to the epoxy. In each sps spectrum there is one peak present at 2960 cm^{-1} that can be assigned to the methyl antisymmetric stretch.[24] The ssp spectrum can be fitted using five peaks at 2855 cm^{-1} (CH_2 sym), 2870 cm^{-1} (CH_3 sym), 2915 cm^{-1} (CH_2 asym), 2943 cm^{-1} (FR), and at 2970 cm^{-1} (CH_3 asym). In order to perform orientation calculations, all the sps and ssp spectra were fitted (Figure 3.23) along with the fitting parameters (Table 3.11).

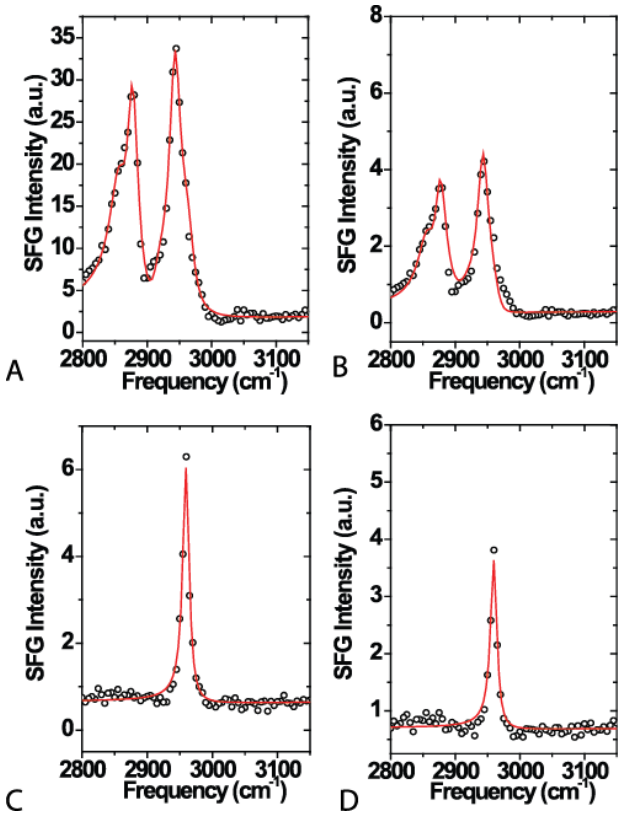

Figure 3.23: SFG spectra collected from the PI/epoxy buried interface, in the ssp (top) and sps (bottom) polarization combinations before (left) and after (right) 100s He plasma treatment on PI. The circles are the experimental data and the red curves are the fitted results. ssp before plasma (A), ssp after plasma (B), sps before plasma (C), sps after plasma (D).

Using the same method which we adopted above to study epoxy isopropyl group orientation at the dPS/epoxy interface, we could deduce the orientation of the epoxy isopropyl group at the PI/epoxy interface. Assuming different orientation distributions and using the detected $\chi_{yyz,sym}/\chi_{yzy,asym}$ ratios, the deduced tilt angles of epoxy isopropyl groups at the PI (without plasma treatment)/epoxy and PI (with 100s He plasma treatment)/epoxy interfaces are: (1) For delta distribution, 24.9±0.9° and 58.0±3.5°; (2) for the σ = 3° Gaussian distribution, 26.1±1.0° and 60.3±2.7°; (3) for the σ = 5° Gaussian distribution, 25.4±0.9 and 61.2±2.8°; (4) for the σ = 10° Gaussian distribution, 22.1±0.8 and 65.8±3.0°, respectively. Similarly, using the measured $\chi_{yyz,asym}/\chi_{yzy,asym}$ ratios, such tilt angles are: (1) For delta distribution, 21.0±0.8° and 49.8±5.0°; (2) for the σ = 3° Gaussian distribution, 20.5±0.8° and 49.9±5.0°; (3), for the σ = 5° Gaussian distribution, 19.5±0.8 and 50.0±5.0°; (4) for the σ = 10° Gaussian distribution, 13.9±0.5 and 50.7±5.1°, respectively.

Table 3.11: Fitting parameters from the PI/epoxy buried interface before and after 100s plasma treatment on PI

Pristine surface								
	ssp					sps		
Frequency	2859	2878	2915	2944	2965	2960		
Amplitude	34.6	52.1	-50.0	77.6	-60.0	13.9		
Width	15.0	10.9	12.9	10.5	13.1	6.0	$\chi_{yyz,sym}/\chi_{yzy,asym}$	5.2
Amplitude/ Width	2.3	4.8	3.9	7.4	4.6	2.3		
Assignment	CH_2 sym	CH_3 sym	CH_2 asym	FR	CH_3 Asym	CH_3 Asym	$\chi_{yyz,asym}/\chi_{yzy,asym}$	2.0
100 s He plasma								
	ssp					sps		
Frequency	2859	2877	2915	2944	2965	2962		
Amplitude	12.1	18.0	-17.0	27.0	-12.0	10.3		
Width	15.0	10.9	12.9	10.5	13.1	6.0	$\chi_{yyz,sym}/\chi_{yzy,asym}$	2.5
Amplitude/ Width	0.8	1.6	1.3	2.6	0.9	1.7		
Assignment	CH_2 sym	CH_3 sym	CH_2 asym	FR	CH_3 Asym	CH_3 Asym	$\chi_{yyz,asym}/\chi_{yzy,asym}$	0.5

Similar to the discussion on the dPS/epoxy interfaces presented above, here the average tilt angles measured with two ratios under the distribution of $\sigma = 10°$ will be used for comparison. The tilt angle of isopropyl groups at the PI (without plasma treatment)/epoxy interface is 18.0±1.0, more or less standing up at the interface. After the PI was treated by 100s He plasma, the epoxy isopropyl group tilt angle at the PI (plasma treatment)/epoxy interface is much larger, at 58.3±6.4°, lying down more at the interface (Table 3.10 has tilt angles listed). The same trend which is seen for the PI/epoxy systems was observed from the dPS/epoxy system, as reported above. Similar tilt angles of epoxy isopropyl group at dPS (without plasma)/epoxy interface (15.3±0.8) and PI (without plasma)/epoxy interface (18.0±1.0) were observed. Also similar tilt angles of epoxy isopropyl groups at dPS (after plasma)/epoxy interface (51.0±9.5°) and PI (after plasma)/epoxy interface

(58.3±6.4°) were observed. This shows that the epoxy isopropyl groups likely have a similar interaction with dPS and PI surface before plasma treatment. This is possible because both dPS and PI have aromatic ring structures. Then plasma treated dPS and PI surfaces alter the interaction with epoxy (that are both more disordered) at the polymer (after plasma treatment)/epoxy interface), so at the buried plasma treated polymer/epoxy interfaces, epoxy isopropyl groups lie down more.

Similar to the dPS case, the SFG signal collected from the PI (after plasma)/epoxy interface is weaker compared to that from the PI (before plasma)/epoxy interface. In addition to the orientation effect, orientation distribution can also influence the SFG signal intensity. Therefore the weak signal may indicate a more disordered interface. Certainly the signal decrease can be caused by less interfacial coverage of isopropyl groups. Similar to the dPS/epoxy system, here the number density of isopropyl groups can also be calculated for the PI/epoxy buried interface, assuming the signal change is caused by the different isopropyl interfacial coverages. It was found that the number density of isopropyl groups reduced to 0.57 (based on ssp sym intensity change) and 0.67 (based on sps asym intensity change) at the PI (after plasma)/epoxy interface (assuming 1.00 at the PI (without plasma treatment)/epoxy interface). The average number density of isopropyl group at the plasma treated PI/epoxy interface is 0.62. This indicates that the plasma treatment on PI caused a reduction of ~40% interfacial coverage of methyl groups at the polymer/epoxy interface, which is similar to the dPS/epoxy system where such a reduction is ~30%. A more disordered interface or an interface with less methyl coverage may lead to stronger adhesion, as we have published previously.[10, 22, 32]

For this system ATR-FTIR was also performed to verify no polymer loss and that the epoxy bulk structure is the same before and after plasma treatment. Figure 3.21 shows the ATR-FTIR spectra collected from the PI (without plasma)/epoxy and the PI (after plasma)/epoxy systems. As we discussed above, the ATR-FTIR method used here can detect signal within 800nm. Since the PI film thickness is about 100 nm, the ATR-FTIR probes the entire PI film and 700 nm into the epoxy bulk. Figure 3.21 shows that the ATR-FTIR spectra from the PI film and ~700 nm epoxy before and after plasma treatment on PI are similar. Therefore the bulk structures of the PI/epoxy system were not altered by the plasma treatment on PI. The difference detected by SFG discussed above due to the plasma treatment is purely the interfacial effect.

3.4.3 Lap Shear

The spectral data suggests that both dPS/epoxy and PI/epoxy interfaces may be more disordered and/or have less methyl groups after plasma treatment on the polymers, which should lead to a greater adhesion strength. To confirm this, adhesion strength between epoxy and polymers before and after plasma treatment was measured. Eight or more samples were prepared for lap shear testing for each of the four systems: PS (before plasma)/epoxy, PS (after plasma)/epoxy, PI (before plasma)/epoxy, and PI (after plasma)/epoxy. Figure 3.24 shows the measured adhesion data for these samples. For the PS/epoxy system, before plasma treatment the adhesion strength is 6.8±0.2 MPa and after 100s of He plasma treatment on PS, the strength increases to 8.8±0.3 MPa (a 20% increase). The PI/epoxy system prior to plasma treatment on PI has an adhesion strength of 11.0±0.4 MPa, and after plasma treatment on PI it increases to 14.4±0.9 (also an increase of 20%). This adhesion testing data shows that if a polymer surface is plasma treated, the adhesion strength between this surface and epoxy will increase. As we stated above, we can correlate this increase in adhesion strength to the more disordered interfacial region and/or less interfacial methyl coverage (as shown by the SFG data). It is also interesting to note that the more hydrophilic polymer, PI has a stronger adhesion strength than the more hydrophobic polymer, PS, which corresponds well to the trend that more polar polymers have stronger adhesion strength than more nonpolar polymers.[22] This could be due to hydrophilic polymers having better wettability which have been shown to have better adhesion strength.[2, 3]

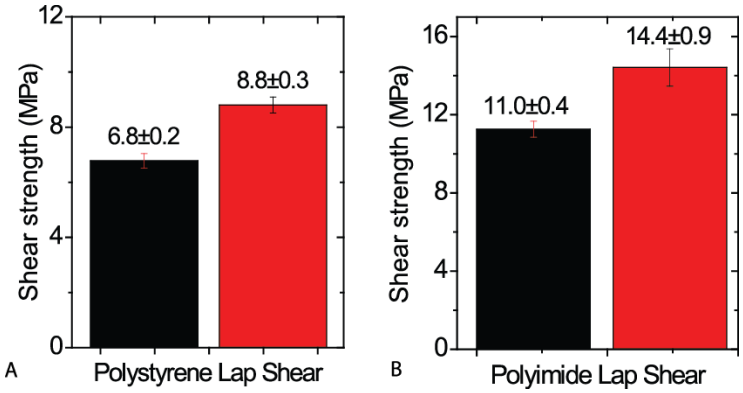

Figure 3.24: Lap shear results for PS (A) and PI (B) before (black) and after (red) 100s He plasma exposure with epoxy.

3.4.4 Contact Angle Measurements

Contact angle measurements were performed to see if the polymer surface wettability changes as a function of He plasma treatment. The PS surface was measured first and it was found that the

pristine PS surface has a contact angle of 115°, 47° after 5s of He plasma, 37° after 10s He plasma, and 26° after 30s He plasma treatment (see Table 3.12). The PI surface was measured next and it was found that the pristine PI surface had a contact angle of 87°, 32° after 5s He plasma, 21° after 10s, and too hydrophilic to measure after 30s He plasma treatment (Table 3.12). This data shows that as the polymer surface is plasma treated it becomes more hydrophilic and has better wettability, which we believe is related to the surface ordering/disordering.

Table 3.12: Contact angles measure with and without He plasma treatment on the PS and PI polymer surfaces

Time (s)	PS	PI
0	115°	87°
5	47°	32°
10	37°	21°
30	26°	too hydrophilic

3.4.5 Literature findings on surface modification via plasma

In addition to the measured data, there is also evidence in the literature that as PS is treated with He plasma, the contact angle decreases and, in addition, there is more oxygen present at the polymer surface.[33] In this reference the contact angle goes from 92° to 36° after 10s He plasma and 34° after 25s plasma, which is a similar trend that was found in our work. Differences in the values could be due to different PS samples, e.g., different Mw and Mn. In addition to contact angle, they also collected XPS data and found that the O/C ratio of the PS surface went from 0.07 before plasma to 0.26 after 10s He plasma, which stayed the same after 25s He plasma treatment, showing that even He plasma can increase the O/C ratio of the PS. Because helium is an inert gas, the plasma is not capable of directly reacting with the free radicals generated at the surface of the PS. Thus, all active radicals go unreacted until they are exposed to the ambient atmosphere, at which time reaction with oxygen, carbon dioxide, water and other species can occur.[34] Therefore the observed adhesion increase may also contributed by the increase oxygen content on the polymer surface in addition to the surface disordering and less coverage of interfacial methyl groups, which will be investigated further in the future. Other literature studies also found that the surface oxygen content increased. For example, PS surface O content goes from 2 to 10%,[35] PI goes from an O/C ratio of 23% to 26% after 90 s of He plasma. It is clear that the surface has more

oxygen after plasma, but is far from the domination of oxygen after the plasma.[36] The C content decrease may be related to the phenyl group loss, but no reference states so explicitly, and no quantitative correlation can be established.

Surface modification with plasma treatment is a complex process, involving surface group reorientation, and free radicals and polar groups created by the plasma (which can then recombine to trigger branching and crosslinking).[37] It is generally held that pendant groups at the surface of a polymer will re-orient toward or away from the bulk in order to minimize the interfacial free energy.[38] It was also reported that the surface modification, in the presence of He plasma, can be due to oxidation and/or crosslinking caused by the radicals created on the surface. Oxidation can be proved with XPS, but crosslinking cannot.[33] In one study it was found that the oxygen and nitrogen tend to bond to common carbon atoms, to form amide groups on the PS surface when He plasma is used.[35] In this study, as we discussed, we focused on the He plasma effect on the orientation/ordering change of surface groups

3.4.6 AFM measurements of Polymer Surfaces

It was reported that the plasma treatment may change the surface roughness.[6] AFM measurements were performed on the PS and PI surfaces before and after 100 s He plasma treatment (Figure 3.25). It was found that the RMS for PS went from 0.49 nm to 1.34 nm; and the PI went from 0.28 nm to 2.83 nm. This generally agrees with the trend of the polymer film becoming slightly rougher following He plasma. In the literature, one study found that the roughness ranged from 2.3 to 4.1 after He plasma, by varying different parameters, but the bottom line is the PI roughness increases by nanometers following He plasma.[39] Such a small roughness change would not decrease SFG signal because of the diffused reflection instead of the specular reflection. In the SFG experiment, the input and output beams have wavelengths of hundreds or thousands of nanometers. Specular reflection will occur even if the roughness is in the order of tens of nanometers or even larger.

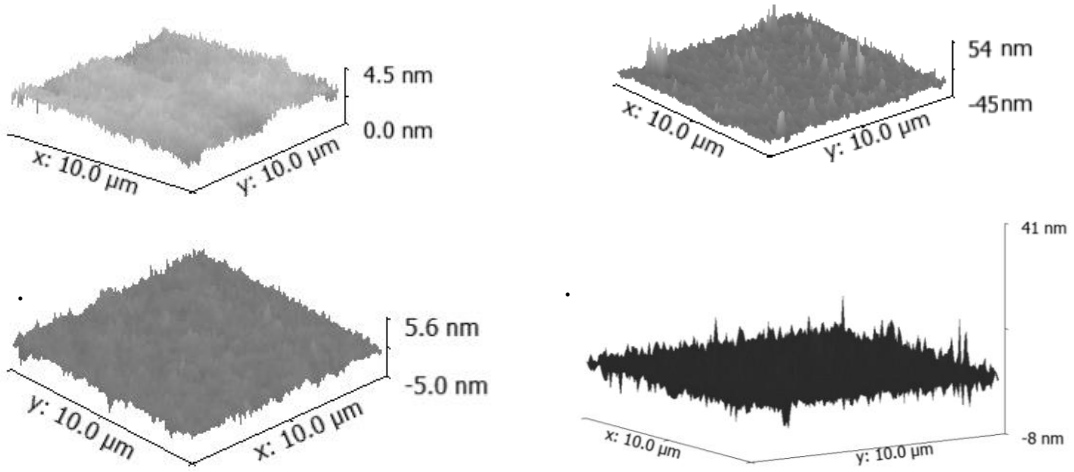

Figure 3.25: A. PI pristine (Rms=0.28 nm), B. PI after plasma (Rms=03.47) nm, C. PS pristine (Rms=0.49 nm), and D. PS after plasma (Rms=1.34 nm).

3.4.7 Summary of Plasma Adhesion Promotion

In this study, molecular structures at buried polymer/epoxy interfaces were studied in situ and noninvasively, with SFG and ATR-FTIR spectroscopy, before and after He plasma treatment on the polymer surfaces. Two polymers, dPS and PI, were studied in this research. PS was investigated as a model polymer and PI as a more industrially relevant polymer that has been widely used in microelectronics. For adhesion failure, we believe that it is important to probe the buried interface in situ instead of studying the exposed separated surfaces because the buried interfacial structure likely will be different after the interface is broken, and the interfacial interaction was destroyed when separating the materials at the interface.

For both the dPS/epoxy and PI/epoxy systems, SFG detected strong polymer signals (dPS C-D stretching signals or PI C=O stretching signals) and epoxy signals at the pristine polymer/epoxy interfaces, showing that the interfaces are very ordered. Differently, for both dPS and PI cases, after the polymer surface was plasma treated, the SFG signals collected from polymer (after plasma treatment)/epoxy interfaces exhibit no polymer signals and much weaker epoxy signals. We showed that such signal decreases are caused by interfacial disordering, interfacial functional group orientation change and/or reduced coverage of methyl groups at the interfaces. Such structural changes lead to interfacial adhesion strength increase, shown by our adhesion testing data. Our ATR-FTIR results demonstrated that the bulk interfacial region (polymer film + hundreds of nanometers into the epoxy material) did not change after plasma treating the polymer surface. Therefore the varied adhesion was solely caused by the interfacial change. In this study,

we also quantitatively analyzed the SFG data and deduced the epoxy isopropyl group orientation at both polymer/epoxy interfaces before and after plasma treating the polymer surfaces. For both the dPS and PI cases, epoxy isopropyl tilt angle (vs. the surface normal) became much larger at the polymer (after plasma treatment)/epoxy interface compared to that of the polymer (before plasma treatment)/epoxy interface. In addition, water contact angle measurements were also performed and it was found that the polymer surfaces have better wettability after He plasma and this could also promote the adhesion strength.

As we discussed above, adhesion is a complex phenomenon and many factors could contribute to interfacial adhesion. It is believed that interfacial structure greatly influences adhesion. SFG is a unique and powerful technique which can probe the molecular structures at buried interfaces in situ, without the need to break the interfaces. Here we indeed observed the structural differences of both polymer and epoxy at the buried polymer/epoxy interface before and after the polymer was plasma treated. We believe that such structural differences caused by polymer plasma treatment led to different adhesion between polymer and epoxy.

3.5 Overall Conclusions

In this chapter, SFG was utilized to investigate plasma effects *in situ* and noninvasively, which has not previously been done. Covered surfaces and plasma-based adhesion promotion were both investigated at the PS and PI surfaces. It was found that covered polymer surfaces behave differently than exposed surfaces and the plasma effects are heterogeneous. This finding has implications to industrial processing conditions and will facilitate better surface modification from plasma treatment. The mechanism for adhesion promotion via He plasma treatment was primarily found to be disordering of the polymer surface, which translates to a more disordered buried interface. The disordered (plasma treated) system gave an adhesion increase of 20%. This work has provided valuable information to real industrially relevant problems, which shows the capabilities of SFG to provide useful data to complicated problems.

3.6 References

[1] F. Awaja, M. Gilbert, G. Kelly, B. Fox, and P. J. Pigram, "Adhesion of polymers," *Prog. Polym. Sci.,* vol. 34, pp. 948-968, **2009**.

[2] S. Bhattacharya, A. Datta, J. M. Berg, and S. Gangopadhyay, "Studies on surface wettability of poly(dimethyl) siloxane (PDMS) and glass under oxygen-plasma treatment and correlation with bond strength," *Journal of Microelectromechanical Systems,* vol. 14, pp. 590-597, 2005.

[3] D. Hegemann, H. Brunner, and C. Oehr, "Plasma treatment of polymers for surface and adhesion improvement," *Nuclear Instruments and Methods in Physics Research Section B: Beam Interactions with Materials and Atoms,* vol. 208, pp. 281-286, 8// 2003.

[4] M. A. Uddin, M. O. Alam, Y. C. Chan, and H. P. Chan, "Adhesion strength and contact resistance of flip chip on flex packages—effect of curing degree of anisotropic conductive film," *Microelectronics Reliability,* vol. 44, pp. 505-514, 3// 2004.

[5] Y. C. Chan and D. Y. Luk, "Effects of bonding parameters on the reliability performance of anisotropic conductive adhesive interconnects for flip-chip-on-flex packages assembly II. Different bonding pressure," *Microelectronics Reliability,* vol. 42, pp. 1195-1204, 8// 2002.

[6] S. H. Kim, S. W. Na, N. E. Lee, Y. W. Nam, and Y.-H. Kim, "Effect of surface roughness on the adhesion properties of Cu/Cr films on polyimide substrate treated by inductively coupled oxygen plasma," *Surface and Coatings Technology,* vol. 200, pp. 2072-2079, 12/21/ 2005.

[7] C. Wu, Y. Li, M. R. Baklanov, and K. Croes, "Electrical Reliability Challenges of Advanced Low-k Dielectrics," *ECS Journal of Solid State Science and Technology,* vol. 4, pp. N3065-N3070, January 1, 2015 2015.

[8] D. Shamiryan, M. R. Baklanov, S. Vanhaelemeersch, and K. Maex, "Comparative study of SiOCH low-k films with varied porosity interacting with etching and cleaning plasma," *Journal of Vacuum Science & Technology B,* vol. 20, pp. 1923-1928, 2002.

[9] C. Zhang, J. Wang, A. Khmaladze, Y. Liu, B. Ding, J. Jasensky, *et al.*, "Examining surface and bulk structures using combined nonlinear vibrational spectroscopies," *Optics letters,* vol. 36, pp. 2272-4, 2011.

[10] C. Zhang, J. Hankett, and Z. Chen, "Molecular Level Understanding of Adhesion Mechanisms at the Epoxy/Polymer Interfaces," *ACS Appl. Mater. Interfaces,* vol. 4, pp. 3730-3737, 2012.

[11] X. Lu, J. N. Myers, and Z. Chen, "Molecular Ordering of Phenyl Groups at the Buried Polystyrene/Metal Interface," *Langmuir,* vol. 30, pp. 9418-9422, 2014/08/12 2014.

[12] K. A. Briggman, J. C. Stephenson, W. E. Wallace, and L. J. Richter, "Absolute Molecular Orientational Distribution of the Polystyrene Surface," *The Journal of Physical Chemistry B,* vol. 105, pp. 2785-2791, 2001/04/01 2001.

[13] A. R. Calchera, A. D. Curtis, and J. E. Patterson, "Plasma Treatment of Polystyrene Thin Films Affects More Than the Surface," *ACS Applied Materials & Interfaces,* vol. 4, pp. 3493-3499, 2012/07/25 2012.

[14] D. Zhang, S. M. Dougal, and M. S. Yeganeh, "Effects of UV Irradiation and Plasma Treatment on a Polystyrene Surface Studied by IR−Visible Sum Frequency Generation Spectroscopy," *Langmuir,* vol. 16, pp. 4528-4532, 2000/05/01 2000.

[15] J. Sung, D. Kim, C. N. Whang, M. Oh-e, and H. Yokoyama, "Sum-Frequency Vibrational Spectroscopic Study of Polyimide Surfaces Made by Spin Coating and Ionized Cluster

Beam Deposition," *The Journal of Physical Chemistry B,* vol. 108, pp. 10991-10996, 2004/07/01 2004.
[16] D. Kim, M. Oh-e, and Y. R. Shen, "Rubbed Polyimide Surface Studied by Sum-Frequency Vibrational Spectroscopy," *Macromolecules,* vol. 34, pp. 9125-9129, 2001/12/01 2001.
[17] J. N. Myers and Z. Chen, "Surface plasma treatment effects on the molecular structure at polyimide/air and buried polyimide/epoxy interfaces," *Chin. Chem. Lett.,* vol. 26, p. 449, 2015.
[18] G. D. Hietpas, J. M. Sands, and D. L. Allara, "Formation of A Molecularly Reconstructed Surface Layer during Unidirectional Rubbing of Polyimide Films," *Macromolecules,* vol. 31, pp. 3374-3378, 1998/05/01 1998.
[19] K. Sakamoto, R. Arafune, N. Ito, S. Ushioda, Y. Suzuki, and S. Morokawa, "Determination of molecular orientation of very thin rubbed and unrubbed polyimide films," *Journal of Applied Physics,* vol. 80, pp. 431-439, 1996.
[20] K. S. Gautam, A. D. Schwab, A. Dhinojwala, D. Zhang, S. M. Dougal, and M. S. Yeganeh, "Molecular Structure of Polystyrene at Air/Polymer and Solid/Polymer Interfaces," *Physical Review Letters,* vol. 85, pp. 3854-3857, 10/30/ 2000.
[21] X. Lu, C. Zhang, N. Ulrich, M. Xiao, Y.-H. Ma, and Z. Chen, "Studying Polymer Surfaces and Interfaces with Sum Frequency Generation Vibrational Spectroscopy," *Analytical Chemistry,* vol. 89, pp. 466-489, 2016.
[22] N. W. Ulrich, J. N. Myers, and Z. Chen, "Characterization of polymer/epoxy buried interfaces with silane adhesion promoters before and after hygrothermal aging for the elucidation of molecular level details relevant to adhesion," *RSC Advances,* vol. 5, pp. 105622-105631, 2015.
[23] D. A. Condirston and J. D. Laposa, "Vibrational spectra of styrene-H8, -D3, -D5, and -D8," *Journal of Molecular Spectroscopy,* vol. 63, pp. 466-477, 1976/12/01 1976.
[24] A. V. Vázquez, B. Holden, C. Kristalyn, M. Fuller, B. Wilkerson, and Z. Chen, "Surface and buried interfacial structures of epoxy resins used as underfills studied by sum frequency generation vibrational spectroscopy," *ACS Appl. Mater. Interfaces,* vol. 3, pp. 1640-51, 2011.
[25] M. J. Shenton, M. C. Lovell-Hoare, and G. C. Stevens, "Adhesion enhancement of polymer surfaces by atmospheric plasma treatment," *Journal of Physics D: Applied Physics,* vol. 34, p. 2754, 2001.
[26] M. J. Owen and P. J. Smith, "Plasma treatment of polydimethylsiloxane," *Journal of Adhesion Science and Technology,* vol. 8, pp. 1063-1075, 1994/01/01 1994.
[27] M. Tatoulian, F. Arefi-Khonsari, I. Mabille-Rouger, J. Amouroux, M. Gheorgiu, and D. Bouchier, "Role of helium plasma pretreatment in the stability of the wettability, adhesion, and mechanical properties of ammonia plasma-treated polymers. Application to the Al-polypropylene system," *Journal of Adhesion Science and Technology,* vol. 9, pp. 923-934, 1995/01/01 1995.
[28] S. Kataoka and P. S. Cremer, "Probing molecular structure at interfaces for comparison with bulk solution behavior: Water/2-propanol mixtures monitored by vibrational sum frequency spectroscopy," *J. Am. Chem. Soc.,* vol. 128, pp. 5516-5522, 2006.
[29] J. Wang, Z. Paszti, M. A. Even, and Z. Chen, "Measuring Polymer Surface Ordering Differences in Air and Water by Sum Frequency Generation Vibrational Spectroscopy," *Journal of the American Chemical Society,* vol. 124, pp. 7016-7023, 2002.

[30] B. Stuart, *Infrared spectroscopy fundamentals and applications*. Chichester, Eng.; Hoboken, N.J.: J. Wiley, 2004.
[31] W. S. Li, Z. X. Shen, J. Z. Zheng, and S. H. Tang, "FT-IR Study of the Imidization Process of Photosensitive Polyimide PMDA/ODA," *Applied Spectroscopy,* vol. 52, pp. 985-989, 1998/07/01 1998.
[32] J. N. Myers, C. Zhang, K.-W. Lee, J. Williamson, and Z. Chen, "Hygrothermal Aging Effects on Buried Molecular Structures at Epoxy Interfaces," *Langmuir,* vol. 30, pp. 165-171, 2014.
[33] I. Luciana Punga and G. Borcia, "Surface modification and stability of polymers treated by atmospheric-pressure helium plasma," *Journal of Advanced Research in Physics,* vol. 4, pp. 011305-011309, 2013.
[34] J. W. Chin and J. P. Wightman, "Adhesion to Plasma-Modified LaRC-TPI I. Surface Characterization," *The Journal of Adhesion,* vol. 36, pp. 25-37, 1991/11/01 1991.
[35] R. W. Paynter, "XPS studies of the ageing of plasma-treated polymer surfaces," *Surface and Interface Analysis,* vol. 29, pp. 56-64, 2000.
[36] S. M. Kang, W. J. Park, and D. H. Yoon, "Surface Characteristics of a Polimide Film Treated with a Dielectric Barrier Discharge Plasma," *Journal of the Korean Physical Society,* vol. 54, pp. 1156-1160, 2009.
[37] C. Borcia, G. Borcia, and N. Dumitrascu, "Surface treatment of polymers by plasma and UV radiation," *Romanian Journal of Physics,* vol. 56, pp. 224-232, 2011.
[38] T. Yasuda, K. Yoshida, T. Okuno, and H. Yasuda, "A study of surface dynamics of polymers. III. Surface dynamic stabilization by plasma polymerization," *Journal of Polymer Science Part B: Polymer Physics,* vol. 26, pp. 2061-2074, 1988.
[39] B. Tae Joon, K. Sung Il, K. Youn Joon, C. Yoon Suk, C. In Sik, S. Yuichi, *et al.*, "Surface Modification of Polyimide for Improving Adhesion Strength by Inductively Coupled Plasma," *Japanese Journal of Applied Physics,* vol. 48, p. 08HL01, 2009.

Chapter 4: Probing Molecular Structures of Buried Interfaces in Thick Multi-layered Microelectronic Packages

4.1 Introduction

In this study, SFG spectroscopy was utilized to investigate real FCOL devices. Vibrational spectra were collected from three interfaces, air/MC, MC/LF, and PI/MC interfaces. For a buried interface in a thick device, the input laser beams could not reach the interface, and therefore SFG signal could not be detected. To facilitate data collection, the FCOL were milled down so that the top layer material thickness was ~1 μm, which enables the laser to access the buried interface. We can mill down further and access the MC/LF or less and access the PI/MC interface (Figure 4.1, more details will be presented below). This work shows the capability and power of SFG to study buried interfaces in multi-layered, real-world devices, using this new method of data collection. The new and innovative metrology developed in this paper can be applied to other systems that previously have not been accessible to SFG spectroscopy.

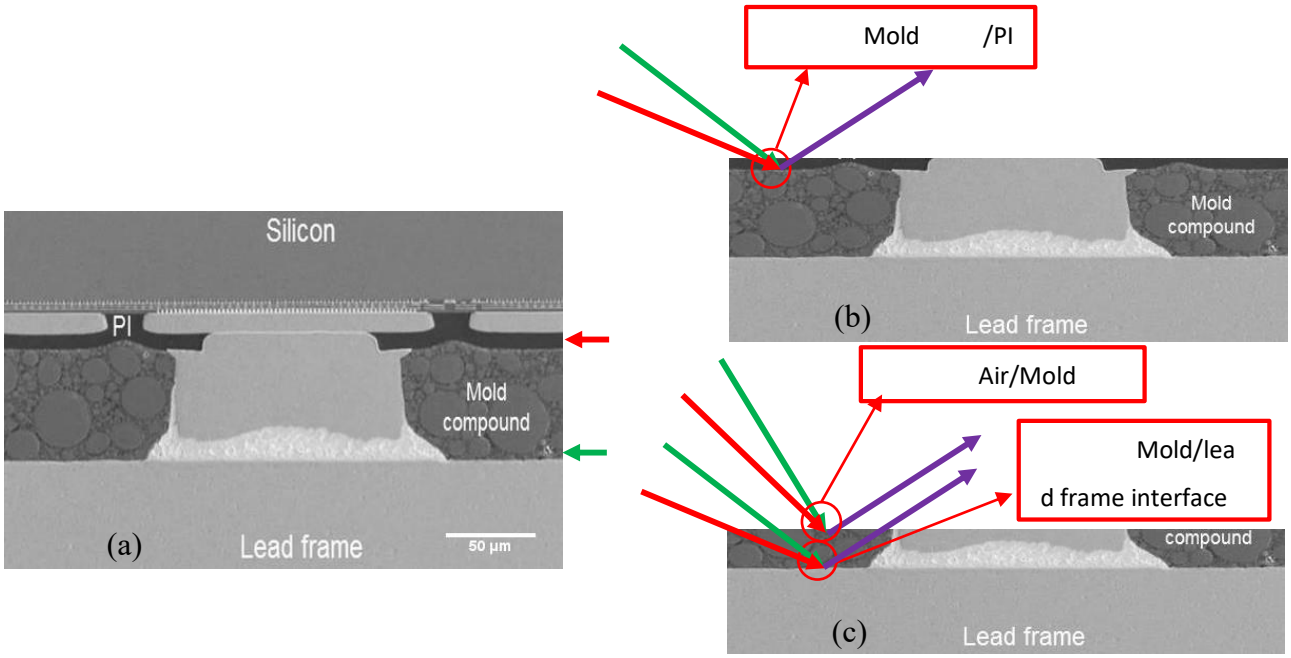

Figure 4.1 (a) SEM image of a FCOL device. The red and green arrows are pointing to the PI/MC and MC/LF interfaces respectively. (b) By milling down just the Si chip and some of the PI, the PI/MC interface can be analyzed. (c) By further milling through the MC, the MC/LF interface can be probed. It is worth noting that (b) and (c) are not the SEM images of the milled down samples. They are just the schematics obtained by modifying the image shown in (a).

4.2 Materials and Methods

4.2.1 Clean Silica Substrates

IR grade fused silica right angle prisms (12.7x12.7x12.7 mm) and IR grade round fused silica flat windows (25.4 mm in diameter and 3.0 mm in thickness) were bought from Altos Photonics (Bozeman, MT) and used to collect SFG spectra. They were cleaned with sulfuric acid saturated with potassium dichromate (SigmaAldrich, St. Louis, MO), followed by rinsing with DI water, and air plasma treatment for 3 minutes.

4.2.2 Sample Preparation

FCOL devices were prepared by Texas Instruments. Figure 4.1a shows FCOL SEM image. The FCOL device has many buried interfaces and is a multi-layered unit. Here we want to probe the buried PI/MC interface (indicated by the red arrow in Figure 4.1a) and the MC/LF interface (indicated with the green arrow in Figure 4.1a). These two interfaces cannot be accessed by laser beams because the input beams could not penetrate the top silicon and the lower lead frame materials to reach to these interfaces. To probe these two interfaces, sample preparation is needed. In order to do so, polishing was performed. By milling down just the Si chip and some of the PI,

the PI/MC interface can be analyzed (Figure 4.1b). By further milling through the MC, the MC/LF interface can be probed (Figure 4.1c).

4.2.3 SFG

SFG spectra were collected with the ssp (s-polarized signal beam, s-polarized visible beam, and p-polarized IR beam) and ppp polarization combinations of the input and signal beams using both window and prism geometries (Figure 4.2). The prism only generates SFG signal from the exposed surface and the window generates signal from both the exposed and buried interfaces (see more details below).

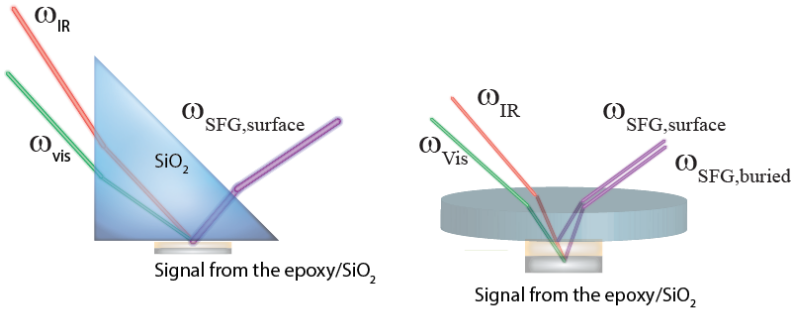

Figure 4.2: SFG experimental geometry utilized to collect spectra

4.2.4 Orientation Analysis

SFG peaks can be fit with the following equation:

$$\chi_{\mathrm{eff}}^{(2)} = \chi_{\mathrm{nr}}^{(2)} + \sum_{\mathrm{q}} \frac{\mathrm{A_q}}{\omega_2 - \omega_{\mathrm{q}} + \mathrm{i}\Gamma_{\mathrm{q}}} \qquad \text{Equation 4-1}$$

where $\chi_{nr}^{(2)}$ is the nonresonant term of $\chi_{eff}^{(2)}$ and is not dependent on the infrared light frequency. A_q, ω_q, and Γ_q are the strength, resonant frequency, and damping coefficient of the qth vibrational mode, respectively. This equation was used for fitting the spectra collected with the prism geometry, and the window geometry for the PI/MC interface. For the SFG spectra collected from the MC/LF interface using the window geometry, signals originate from both the surface and the buried interface. For such spectra, equation 4.2 applies:

$$\chi_{\mathrm{eff,window}} = |\mathrm{F'_{window}}\chi_{\mathrm{surface}} + \mathrm{F_{window}}\chi_{\mathrm{buried}}|^2 \qquad \text{Equation 4-2}$$

Here we have $\chi^{(2)}_{eff}$ from the surface and the buried interface. The $\chi^{(2)}_{surface}$ was determined from the SFG signals collected using the prism geometry. Different experimental geometries yield different Fresnel factors for the surface signals collected. This gives the new equation:

$$\chi_{eff,window} = \left| \frac{F'_{window,surface}}{F'_{prism,surface}} \chi_{surface} + F_{window} \chi_{buried} \right|^2 \quad \text{Equation 4-3}$$

Then the $\chi^{(2)}_{buried}$ can be fit using equation 4.1, adding in the Fresnel ratio, and adding in the peaks from the surface. This results in a ten peak fitting function, where half of the peaks come from the surface and half come from the buried interface.

4.2.5 Thickness Determination

MC Film on LF

To measure the mold compound (MC) thickness on the LF in our samples, laser confocal microscopy was utilized. The Olympus OLS 4000 LEXT was used to take high resolution 3D images by acquiring successive images of the sample between two heights. It then recombined the laser acquired images to produce a 3D projection that could be used to measure the thickness of films (Figure 4.3). The samples received from Texas Instruments (TI) were analyzed without further preparation. It was found that there are exposed metal regions and MC regions (the majority of the surface is covered by MC and SFG spectra were collected from the MC regions). By measuring an area with different regions, it enables us to determine the film thickness. There were

seven measurements made (Figure 4.3), which resulted in an average film thickness of 1.165 μm. This result was used for all Fresnel calculations.

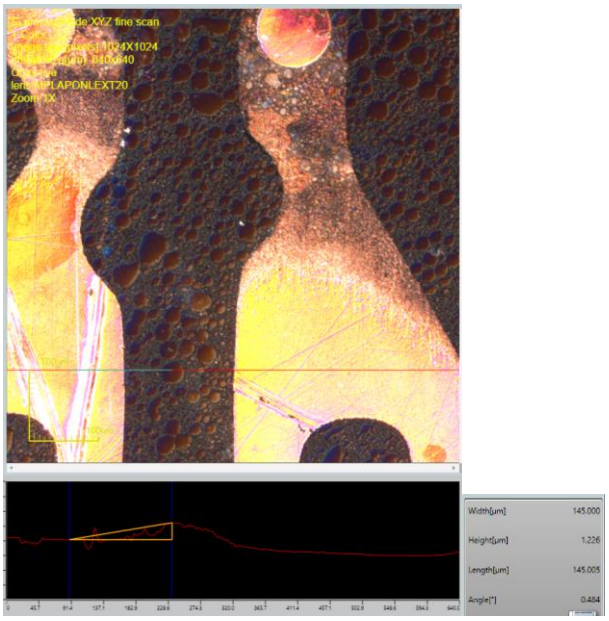

Figure 4.3: Laser confocal microscopic image of MC film on LF.

Table 4.1: Thickness measurement values for multiple sites of MC film on LF

Thickness	Ave.
0.924	1.165 μm
1.162	
0.611	
1.391	
1.558	
1.281	
1.226	

4.2.6 MC PI Film on MC

The thickness of the PI film on MC was more difficult to measure as the PI film was completely homogenous. To measure the thickness, a cross section was prepared by cutting the FCOL-PI device with a diamond coated circular saw. Once the sample was prepared, a Hitachi SU8000

In-line FE-SEM was utilized to image the cross section (Figure 4.4). The PI film was found to be 1.2 μm thick.

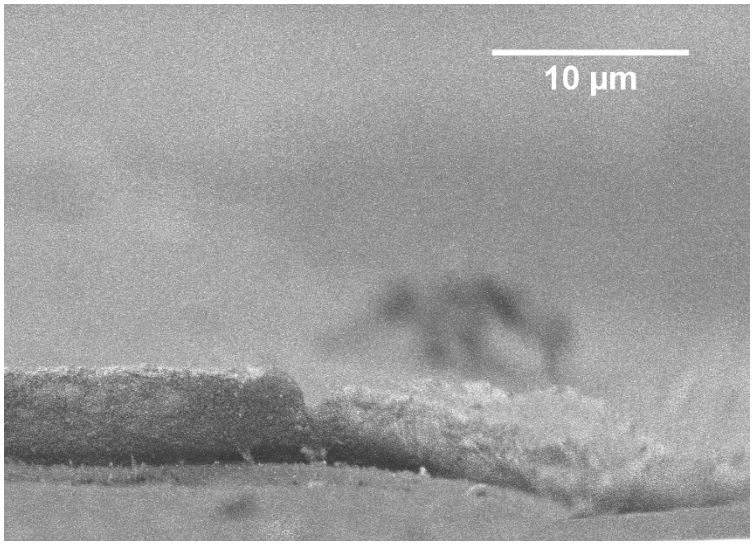

Figure 4.4: SEM cross-sectional image of PI on MC.

4.2.7 XRD Measurements

To determine if the Cu at the MC/LF interface was pure copper or a Cu oxide, XRD experiment was performed. The XRD spectar were collected at ambient temperature on a PANalytical Empyrean diffractometer in Bragg–Brentano geometry using Cu-Kα radiation (1.54187 Å) operating at 45 kV, 40 mA. The incident beam was equipped with a Bragg-Brentano HD X-ray optic using fixed slits/soller slits. The detector was a silicon-based linear position sensitive X'Celerator Scientific operating in 1-D scanning mode. Data were collected from 25° to 60° 2θ using a step size of 0.0167° 2θ and a count time of at least 10 s per step. Two peaks were observed and identified as Cu_2O at 30° and 43° (Figure 4.5).[1] Two peaks were observed and assigned to the Cu metal, 44.1° and 50.6°.[1] The Cu_2O should be on the surface and for this reason, the refractive index of Cu_2O was used for the Fresnel factor calculations.

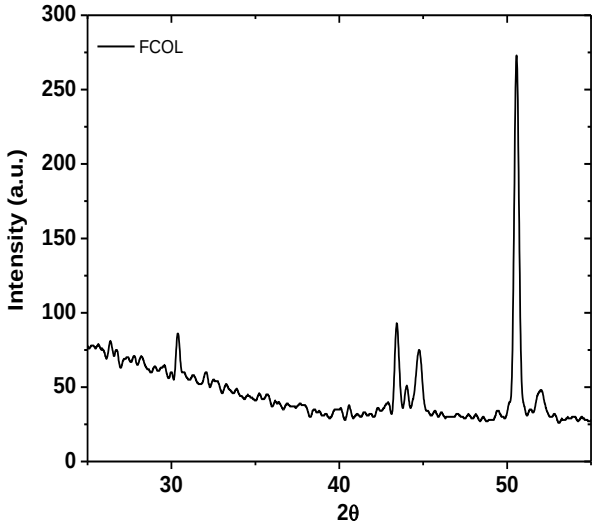

Figure 4.5: XRD data collected from a FCOL sample.

4.3 Results and Discussion

4.3.1 Probing Buried Interfacial Structure

Figure 4.1a shows that a flip chip device is composed of many interfaces. Here we want to probe the molecular structures of the buried PI/MC interface and the MC/LF interface. As shown in Figure 4.1b, to study the buried PI/MC interface, we can polish the device to prepare the sample with the PI/MC interface with a thin PI layer on top. As shown in Figure 4.1c, to study the MC/LF interface, we can further polish the device to prepare the sample with the MC/LF interface with a thin MC layer on top. For both cases, the interfaces can be accessed by the input laser beams because the top films (either PI or MC films) are thin. Also because the two films on top are thin, it is impossible to separate the SFG signals generated from the thin surface in air and the buried interface. To elucidate the structure from the buried interface, we collected SFG spectra using both the prism and window geometries (Figure 4.2). The SFG spectra collected using the prism geometry with total reflection only contains the contribution from the top surface, or surface in air, because the evanescent beam cannot reach the buried interface to generate signal (see below for more details). The SFG signals collected using the window geometry contain both the signals from the surface and the buried interface. After analyzing these two types of spectra carefully, the signals from the buried interface can be deduced, from which the structural information of the buried interface can be obtained.

4.3.2 MC/LF and Air/MC Interfaces

To better present the methodology we adopted in this research to study the buried interface of thick samples, we first discuss the results on the sample with Air/MC and MC/LF interfaces. As discussed above, by utilizing prism and window geometry, we can selectively look at both the exposed and buried interfaces *in situ*, noninvasively. Figure 4.6 shows the SFG spectra collected from the sample in Figure 4.1c using the prism geometry with the ssp (Figure 4.6 left) and ppp (Figure 4.6, middle) polarization combinations, respectively. There are five peaks present in each SFG spectrum: 2855 cm^{-1} (CH_2 ss), 2880 cm^{-1} (CH_3 ss), 2915 cm^{-1} (CH_2 as), 2945 cm^{-1} (Fermi Resonance), and 2965 cm^{-1} (CH_3 as) (fitting parameters in Table 4.2). These signals originate solely from the MC at the air/MC interface, through the total internal reflection process, which greatly limits the penetration depth of the input beams. The thickness of the MC is ~1 μm (as discussed above), thus the only interface probed is the air/MC as the evanescent wave cannot probe the buried interface. The penetration depth is on the order of hundreds of nanometers. To confirm we have total internal reflection, we collected spectra using the prism geometry, plasma treated the samples, and then attempted to collect SFG spectra again. There was no signal detected after the plasma treatment on the sample surface, indicating that after the plasma treatment the surface was completely disordered and originally with the same experimental geometry SFG signal was only generated from the surface (before the plasma treatment). If the SFG signal was a function of both the surface and buried interface, we would expect to see SFG signal from the buried interface after the plasma treatment, but this was not what was observed. This result suggests that the prism geometry signal comes solely from the surface of the sample and not a combination of surface and buried interface. Clearly the MC/air interface is covered by mainly methyl and methylene signals. The methylene signal is much stronger than that of the methyl signal, which may indicate that methylene has a higher coverage on the MC/air interface. The orientation of the methyl group could be deduced from the SFG spectra collected using the ssp and ppp polarization combinations or the symmetric and asymmetric stretching signals in the same spectrum, as discussed in more detail later.

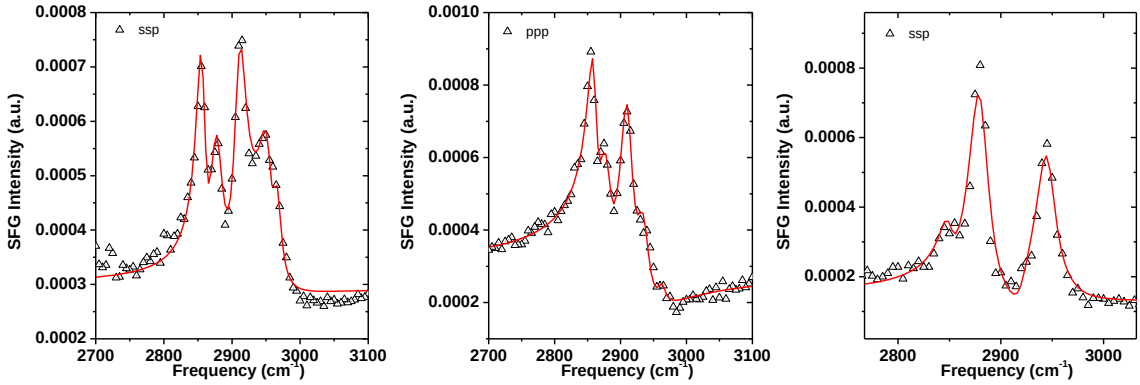

Figure 4.6: SFG ssp prism (left), ppp prism (middle), and ssp window (right) spectra collected from the MC layer on LF.

Table 4.2: Fitting parameters of SFG spectra collected from MC film on LF. Please note that the fitting parameters for window/surface spectra are the same as those of prism/surface spectra.

		Prism/surface		Window/buried	
ωi (cm^{-1})	Γi (cm^{-1})	Aq (ssp)	Aq (ppp)	Aq (ssp)	assignment
2855	8	0.1112	0.0854	-0.01421	CH_2 (ss)
2880	12	0.216	0.1165	0.1804	CH_3 (ss)
2915	11	-.28	0.20	0.01217	CH_2 (as)
2945	12	0.313	0.1326	0.10058	FR
2965	7	-0.2	0.0292	0.100	CH_3 (as)

The SFG spectrum collected using the window geometry with a silica window on top of the sample was contributed from both the surface and the buried interface (Figure 4.6 right). The same peaks are present in the ssp spectrum collected using the window geometry as those found in the spectrum collected using the prism geometry. Therefore the spectrum collected using the window geometry was fitted with 10 peaks, 5 peaks using the fitting parameters obtained from those used to fit the spectrum collected using the prisms geometry (contributed from the surface) and 5 additional peaks from the buried interface. From the fitting parameters of the signals contributed from the buried interface, we could deduce the structural information of the buried MC/LF interface. We

can see that at the buried interface, both methylene and methyl groups are present. In this research, we will only focus our spectral detection/analysis for methyl and methylene groups to demonstrate the feasibility of our approach to study buried interface in real devices with multilayers and thick samples. In the future, many other functional groups will be probed (as we will discuss in the conclusion section).

4.3.3 4.2.3 PI/MC Interface

We then applied SFG to study the PI/MC interface with a thin layer of PI on MC. No SFG C-H stretching signals were observed from the PI/MC sample using the prism geometry, indicating that no ordered C-H groups (e.g., methyl or methylene groups) are present on the PI surface. Therefore the SFG signal collected from the PI/MC sample using the window geometry should be solely contributed from the buried PI/MC interface. Figure 4.7 shows the fitted SFG spectrum from the PI/MC interface collected with the window geometry. Table 4.3 has the fitting parameters. The same five peaks were used for spectral fitting, with varied intensities. The presence of methyl and methylene peaks indicates that the PI/MC interface is well ordered, with both the methyl and methylene presence at the interface.

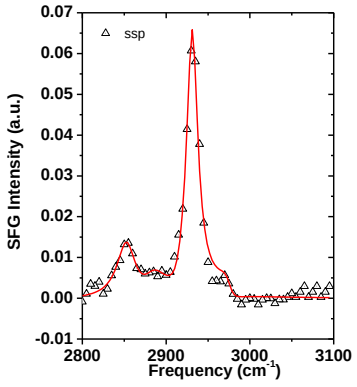

Figure 4.7: SFG spectrum of the PI/MC interface using the window geometry, ssp.

Table 4.3: Fitting parameters of SFG spectra collected from the PI/MC interface

ωi (cm^{-1})	Γi (cm^{-1})	Window/buried Aq (ssp)	Assignment
2855	13	1.467	CH_2 (ss)
2880	16	0.901	CH_3 (ss)
2915	12	-2.00	CH_2 (as)
2931	8	2.468	FR
2975	8	-0.35	CH_3 (as)

4.3.4 Methyl Orientation

SFG has been extensively applied to study methyl orientation on surfaces and at interfaces.[2-4] We have shown that the presence of methyl groups at epoxy interfaces may greatly influence the adhesion of the interface.[5-7] Since adhesion is very important for the PI/MC and MC/LF interfaces, here we want to study more detailed structural information of methyl groups at these two buried interfaces. More specifically, we hope to measure the orientations of methyl groups at the buried PI/MC and MC/LF interfaces using SFG.

It is well known that a methyl group can be treated as having C_{3v} symmetry. The orientation of a methyl on the surface can be defined by a tilt angle θ, which is the angle between the methyl main axis and the surface normal. Using SFG, the methyl orientation can be deduced either by the ratio of different components (e.g., $\chi_{yyz,ss}$ vs. $\chi_{zzz,ss}$) of the second order nonlinear optical susceptibility defined in the lab fixed coordinate frame of the same vibrational mode or the ratio of the same component of the susceptibility of different methyl C-H stretching vibration modes (e.g., $\chi_{yyz,s}$ vs. $\chi_{yyz,as}$). The detailed relationships between the different χ components and the methyl tilt angle θ have been extensively reported.[8-10] For example, for the symmetric C-H stretching mode of a methyl group, we have

$$\chi_{xxz}^{(2)} = \chi_{yyz}^{(2)} = \frac{1}{2} N_s \beta_{ccc}^{(2)} [\langle cos\theta \rangle (1+R) - \langle cos^3\theta \rangle (1-R)]$$

Here N_s, $\beta^{(2)}_{ccc}$, "< >", θ, and R, are the number of oscillators, a component of molecular hyperpolarizability tensor, ensemble average, methyl tilt angle, and the ratio of the two hyperpolarizability components $\beta^{(2)}_{aac}/\beta^{(2)}_{ccc}$, respectively.

$\chi^{(2)}$ (or χ for simplicity here) is the second order nonlinear optical susceptibility. As discussed above in this thesis, the above different χ components defined in the (xyz) lab frame can be related to the measured susceptibility terms (χ_{eff}) using SFG experiments with polarized beams (e.g., ssp or ppp). For example, we can measure χ_{yyz} using χ_{ssp}. For a spectrum collected using the prism geometry, we only detected the signal from the surface, we have:

$$\left(\chi_{eff,prism,ssp}\right)^2 = \left(F_{prism}\chi_{surface,yyz}\right)^2$$

For a spectrum collected using the window geometry, we have:

$$\left(\chi_{eff,window}\right)^2 = \left|F'_{window}\chi_{surface} + F_{window}\chi_{buried}\right|^2$$

The F or F' terms are Fresnel factors, which are local field correction terms that take into account reflection, transmission, and the refractive indices. The Fresnel factors can be calculated (Table 4.4). The above presented SFG spectra (Figure 4.6 and Figure 4.7) were fitted and the fitting parameters are listed in Table 4.2 and Table 4.3.

Figure 4.8 shows the relationship of measured $\frac{\chi^{(2)}_{as}}{\chi^{(2)}_{ss}}$ in ssp SFG spectra and $\frac{\chi^{(2)}_{ss,ppp}}{\chi^{(2)}_{ss,ssp}}$ as a function of methyl orientation angle. The methyl tilt angle at different interfaces can be determined by the signal strength ratio of asymmetric and symmetric vibrational mode in the ssp polarization combination, or $\frac{\chi^{(2)}_{as}}{\chi^{(2)}_{ss}}$. We obtained such ratios for the air/MC, MC/LF, and PI/MC from the spectra fitting, using the ratios of A/Γ values for the methyl symmetric and asymmetric modes listed in in Table 4.2 and Table 4.3. The measured χ_{yyz} ratios (same as χ_{ssp} ratios) were 0.65, 0.61, and 0.12, respectively for the above three interfaces, leading to the methyl tilt angles of 46°, 44°, and 20° from the surface normal, respectively (Figure 4.8a). In addition to the use of the χ_{yyz} asym/sym ratio, the methyl orientation can also be deduced from the ratio of the signal strength of the same

vibrational mode detected using two different polarization combinations. Here we used $\frac{\chi^{(2)}_{ss,ppp}}{\chi^{(2)}_{ss,ssp}}$ measured from the air/MC interface with the prism geometry. For the ppp signal detected using the prism geometry, the contribution is dominated by the zzz term. Therefore using the $\frac{\chi^{(2)}_{ss,ppp}}{\chi^{(2)}_{ss,ssp}}$ ratio, it is easy to calculate the $\frac{\chi^{(2)}_{ss,zzz}}{\chi^{(2)}_{ss,xxz}}$ ratio with the calculated Fresnel factors. With the relationship between $\frac{\chi^{(2)}_{ss,zzz}}{\chi^{(2)}_{ss,xxz}}$ and the methyl orientation, the relationship between $\frac{\chi^{(2)}_{ss,ppp}}{\chi^{(2)}_{ss,ssp}}$ and methyl orientation can be deduced (Figure 4.8b). Using the fitting parameters listed in Table 4.2, we found that $\frac{\chi^{(2)}_{ss,ppp}}{\chi^{(2)}_{ss,ssp}}$ ratio is 0.47, leading to the measured tilt angle of 41°. This result is similar to the one previously deduced (46°). It can be seen from the above discussion that the methyl orientation determination involves spectra collection, spectra fitting, Fresnel factor calculation, each of the above processes could induce errors. Our two independent measurements lead to similar results, indicating that the errors introduced in the above process are small. For the air/MC interface, the average of the above two values for methyl tilt angle will be used in the subsequent discussion (43.5°). We did not perform orientation analysis of spectra collected using different polarization combinations with the window geometry, because the window ppp spectra are a contribution of multiple terms (χxxz, xzx, zzz, zxx), which may induce more errors (e.g., in Fresnel factor calculations).

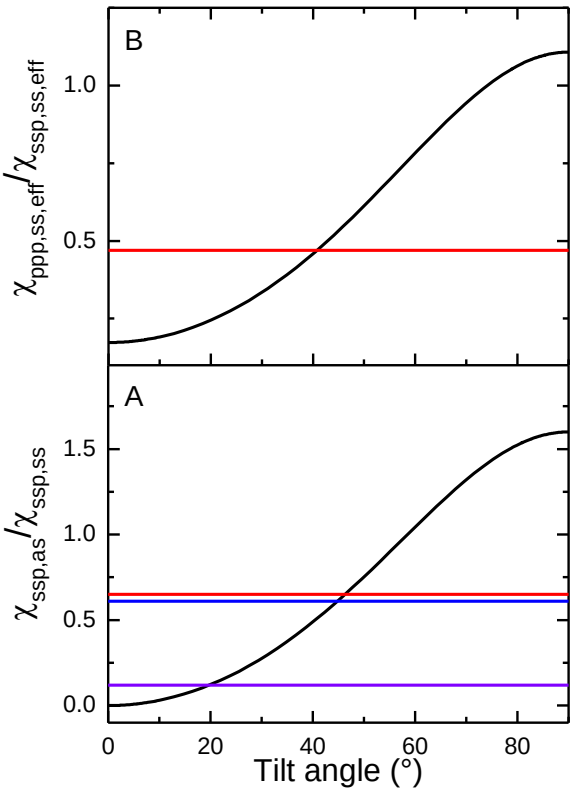

Figure 4.8: Orientation curves for the methyl tilt angle, B shows the $\frac{\chi^{(2)}_{ss,ppp}}{\chi^{(2)}_{ss,ssp}}$ ratio and A shows the $\frac{\chi^{(2)}_{as,ssp}}{\chi^{(2)}_{ss,ssp}}$ ratio. The horizontal lines are the experimentally measured ratios found using SFG, the red line in B comes from the $\frac{\chi^{(2)}_{ss,ppp}}{\chi^{(2)}_{ss,ssp}}$ (0.47) measured from the air/MC interface with the prism geometry, leading to the measured tilt angle of 41°. In A, the three lines come from the air/MC, MC/LF, and PI/MC interfaces: The measured χ_{yyz} ratios were 0.65, 0.61, and 0.12, leading to methyl tilt angles of of 46°, 44°, and 20° from the surface normal, respectively.

Table 4.4: Fresnel Factors

	Prism surface	Window surface	Window "buried"
$F_{ssp\ xxz}$	0.472	0.23	0.0532
$F_{ppp\ zzz}$	0.423	0.159	0.0189

The methyl functional group is typically considered to be rather hydrophobic, thus they will lie down more at hydrophilic interfaces (due to unfavorable interactions) and stand up more at hydrophobic interfaces (due to favorable interactions). This has been shown previously, where methyl groups lie down more at the epoxy/PI interface and stand up more at the epoxy/PS interface.[11] For the PI/MC and MC/LF interfaces studied here, the PI is a polymer which is much more hydrophobic than the LF. The LF is composed of metals and metal oxides. Our results demonstrated that the methyl groups mostly stand up at the PI/MC interface, with a tilt angle of 20° from the surface normal. While at the MC/LF interface, the tilt angle is 44°, lying down more than at the PI/MC interface. This is due to the minimization of energy; it is more energetically favorable for methyl groups to lie down more at hydrophilic interfaces. An orientation schematic diagram is depicted in Figure 4.9.

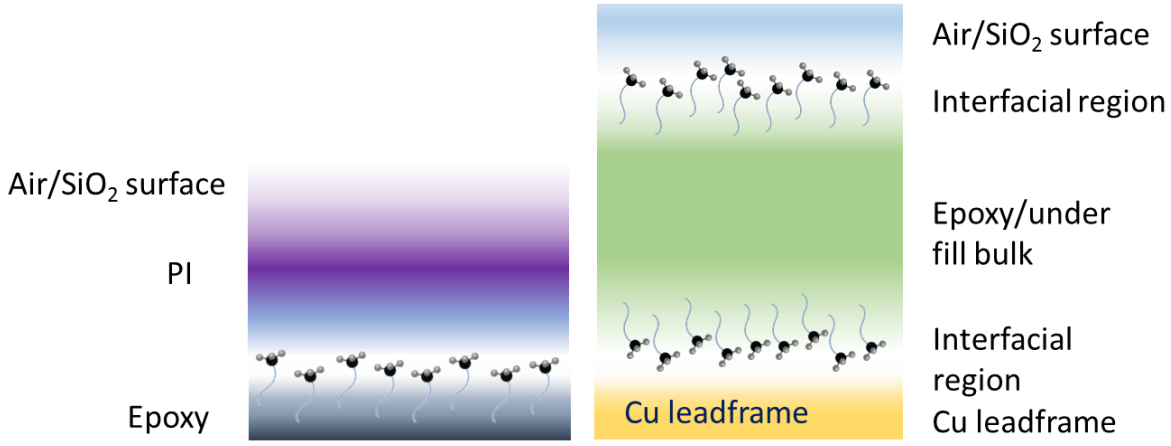

Figure 4.9: Tilt angles of the methyl groups from the PI/MC interface (left), and air/MC and MC/LF interfaces (right)

Air is also a more hydrophobic mixture, the surface methyl groups should stand up more on the MC surface in air. However, our results in this study indicated that methyl groups tilted at 44° from the surface normal. This may be due to the fact that the MC material was milled down to prepare the sample. In the milling process, the methyl group orientation may be altered. Also, the surface methyl groups in air could have more freedom, leading to a broader orientation distribution including some more tilted and even lying down orientations.[4]

4.3.5 Further Discussion

In this work we have collected the SFG spectra from the surface and the buried interface, and then deconvoluted the spectra using the above presented approach to separate the signal contribution from the surface and the interface to deduce their structures respectively. We have to deconvolute the spectra from the surface and interface because the layer separating the surface and interface is very thin, therefore SFG signals from the surface and the interface could not be spatially separated. Another method could be used to eliminate the contribution from the surface, i.e. plasma treatment. Plasma treatment typically causes the surface to be completely disordered, thus generating no SFG signal. The SFG signals detected from the sample would then, exclusively come from the buried interface. However, there are two issues with this method: 1) The plasma treatment may not completely disorder the surface for every sample, therefore this method is not generally applicable; 2) since the layer between the surface and interface is thin, plasma may penetrate the thin film to alter the buried interfacial structure. We believe that the method we have utilized in the above research is less invasive and should provide more accurate information from the unperturbed system.

As mentioned in the introduction, buried interfaces involving polymers are important in microelectronics and delamination at any of the interfaces can cause device failure. It is extremely difficult to investigate buried interfaces using traditional surface sensitive techniques, because many of these important interfaces are between solids. However, breaking an interface, especially a strongly adhered interface, may alter or even destroy the original interfacial structure. SFG has been shown to be a unique tool to reveal molecular structures of buried solid/solid interfaces. Methyl group orientation of polymers have been studied extensively,[3, 10-14] and can be used to show the level of order at buried interfaces. By studying methyl group orientation we have a better understanding of the structure at buried interfaces. It has been shown that ordered methyl groups can indicate poor adhesion,[15] and the more ordered they are, the worse the adhesion.

4.4 Conclusions

To the best of our knowledge, this is the first time to apply SFG to investigate molecular structures of buried solid/solid interfaces in real microelectronic devices *in situ*, in real time. Using the milling down approach, SFG has been successfully used to obtained signals from individual buried interfaces in multilayer thick microelectronic device samples. With the different SFG spectra

collection geometry (e.g., prism vs. window), we have successfully deconvoluted the SFG signals collected from two interfaces and deduced the molecular structures (e.g., the presence of functional groups and the orientation) of individual buried interfaces. More specifically, methyl and methylene groups are present at the Air/MC, MC/LF, and PI/MC interfaces, and the methyl tilt angles at these three interfaces were found to equal 43.5°, 44°, and 20°, respectively. Methyl groups are hydrophobic so we expect them to lie down more in contact with Cu at the MC/LF interface and stand up more at the PI/MC interface.

This work is just the beginning to apply SFG to probe buried interfacial structures of thick multilayer samples in microelectronics. In the future, more functional groups, other than methyl and methylene, will be probed. In addition to the presence and orientation of interfacial functions, interfacial chemical reaction, interfacial ordering, interfacial hydrogen bonding, and interfacial diffusion will all be probed.

Buried interfaces are incredibly important in the microelectronics industry and there are few analytical tools that are capable of nondestructively probing them. This work outlines the strength and power of SFG as an analytical tool to probe buried interfacial structures nondestructively, which the microelectronics industry can greatly benefit. From the buried interfacial structure we could understand the structure-property relationships of buried interfaces, which enables us to develop a better understanding of how the interfaces behave with various processing steps and guide the optimization of the processing procedures.

The methodology developed in this research is generally applicable, which can be used to study buried interfaces of many polymer materials and devices involving polymer materials, ranging from adhesives, glues, and tapes for everyday use to polymer composite materials and polymer coatings to semiconducting polymers used for solar cells.

4.5 References

[1] S.-L. Cheng and M.-F. Chen, "Fabrication, characterization, and kinetic study of vertical single-crystalline CuO nanowires on Si substrates," *Nanoscale Research Letters,* vol. 7, p. 119, February 13 2012.

[2] N. Akamatsu, K. Domen, and C. Hirose, "SFG study of two-dimensional orientation of surface methyl groups on cadmium arachidate Langmuir-Blodgett films," *The Journal of Physical Chemistry,* vol. 97, pp. 10070-10075, 1993.

[3] J. Wang, C. Chen, S. M. Buck, and Z. Chen, "Molecular chemical structure on poly(methyl methacrylate) (PMMA) surface studied by sum frequency generation (SFG) vibrational spectroscopy," *J. Phys. Chem. B,* vol. 105, pp. 12118-12125, 2001.

[4] J. Wang, Z. Paszti, M. A. Even, and Z. Chen, "Measuring Polymer Surface Ordering Differences in Air and Water by Sum Frequency Generation Vibrational Spectroscopy," *Journal of the American Chemical Society,* vol. 124, pp. 7016-7023, 2002.

[5] N. W. Ulrich, J. N. Myers, and Z. Chen, "Characterization of polymer/epoxy buried interfaces with silane adhesion promoters before and after hygrothermal aging for the elucidation of molecular level details relevant to adhesion," *RSC Advances,* vol. 5, pp. 105622-105631, 2015.

[6] C. Zhang, J. Hankett, and Z. Chen, "Molecular Level Understanding of Adhesion Mechanisms at the Epoxy/Polymer Interfaces," *ACS Appl. Mater. Interfaces,* vol. 4, pp. 3730-3737, 2012.

[7] J. N. Myers, C. Zhang, K.-W. Lee, J. Williamson, and Z. Chen, "Hygrothermal Aging Effects on Buried Molecular Structures at Epoxy Interfaces," *Langmuir,* vol. 30, pp. 165-171, 2014.

[8] A. J. Moad and G. J. Simpson, "A unified treatment of symmetry relations and selection rules in sum-frequency and second harmonic spectroscopies," *J. Phys. Chem. B,* vol. 108, pp. 3548-3562, 2004.

[9] C. Zhang, J. N. Myers, and Z. Chen, "Soft Matter interfaces and biological interfaces using sum frequency generation vibrational spectroscopy," *Soft Matter,* vol. 9, pp. 4738-4761, 2013.

[10] X. Lu, C. Zhang, N. Ulrich, M. Xiao, Y.-H. Ma, and Z. Chen, "Studying Polymer Surfaces and Interfaces with Sum Frequency Generation Vibrational Spectroscopy," *Analytical Chemistry,* vol. 89, pp. 466-489, 2016.

[11] N. W. Ulrich, J. Andre, J. Williamson, K.-W. Lee, and Z. Chen, "Plasma treatment effect on polymer buried interfacial structure and property," *Physical Chemistry Chemical Physics,* vol. 19, pp. 12144-12155 2017.

[12] J. Xu, Y. Liu, J. He, R. Zhang, B. Zuo, and X. Wang, "Surface structures of poly(methyl methacrylate) films influenced by chain entanglement in the corresponding film-formation solution," *Soft Matter,* vol. 10, pp. 8992-9002, 2014.

[13] H. Zhu, K. C. Jha, R. S. Bhatta, M. Tsige, and A. Dhinojwala, "Molecular Structure of Poly(methyl methacrylate) Surface. I. Combination of Interface-Sensitive Infrared–Visible Sum Frequency Generation, Molecular Dynamics Simulations, and ab Initio Calculations," *Langmuir,* vol. 30, pp. 11609-11618, 2014.

[14] K. C. Jha, H. Zhu, A. Dhinojwala, and M. Tsige, "Molecular Structure of Poly(methyl methacrylate) Surface II: Effect of Stereoregularity Examined through All-Atom Molecular Dynamics," *Langmuir,* vol. 30, pp. 12775-12785, 2014/11/04 2014.

[15] C. Zhang, J. Myers, and Z. Chen, "Elucidation of molecular structures at buried polymer interfaces and biological interfaces using sum frequency generation vibrational spectroscopy," *Soft matter,* vol. 9, pp. 4738-4761, 2013.

Chapter 5: Nondestructive Analysis of Buried Interfacial Behaviors of Flux Residue and Their Impact on Interfacial Mechanical Property

5.1 Introduction

One type of substrate that dies can be connected to are lead frames, which utilize Cu posts to connect the circuit board to the die. In processing, after the lead frame is fabricated, flux material is spray jetted on the substrate. The flux material is typically a proprietary blend, composed of dicarboxylic acids and/or amines. Flux can remove copper oxides from the Cu posts leading to better wetting and electrical contact to the solder and subsequently the die.[1] One potential problem from flux application is the residues that can form, which can cause underfill void formation or solder bridging between Cu posts when performing highly accelerated stress testing (HAST). [2-4]

The flux mechanism has been studied previously using adipic acid as a model flux.[5] The free acid in solution binds to the copper oxide surface and forms a copper salt by deprotonating both carboxylic groups in the acid: the hydrogen ions react with the copper oxide layer to form water, and the charged oxygen on the flux coordinates with the Cu. The actual fluxes used in the microelectronics industry may vary, but this is the most general theory as to how the flux removes copper oxides from the substrate surface.

In this study, SFG spectroscopy was implemented to probe the flux behavior on Cu and SiO_2 surfaces and at the corresponding buried interfaces between Cu or SiO_2 and bisphenol A diglycidyl ether (BADGE, scheme 1). In this research various washing procedures were used (5s, 4 hours) to study if the flux residue could be removed. In addition to spectroscopic analysis, adhesion testing experiments were performed to measure the adhesion strengths between epoxies and substrates to understand if the flux treatment changed the adhesion strength. The adhesion measurement data can be interpreted by the molecular structures of the buried interfaces deduced from the SFG results. In this work we set out to answer how easily flux residue can be removed from surfaces,

whether the residue changes the buried interface, and how adhesion strength varies as a function of flux residue.

5.2 Materials and Methods

5.2.1 Materials

BADGE, 4,4'-Diamino- diphenylmethane (DDM) (≥97%), and glutaric acid (99%) were obtained from Sigma-Aldrich (St. Louis, MO) Figure 5.1). CaF_2 prisms and windows were purchased from Altos Photonics (Bozeman, MT). A layer of 100 nm SiO_2 was deposited onto each CaF_2 prism by an electron-beam deposition process using an SJ-26 Evaporator system at a pressure below 10^{-5} Torr. The deposition rate was 5 Å/s. The CaF_2 windows and SiO_2 coated CaF_2 prisms were treated with air plasma for 2 min in a PE-25-JW plasma cleaner (Plasma Etch, Carson City, NV). Cu substrates for SFG measurements were prepared by depositing 100 nm of Cu onto silicon wafers using E-beam evaporation at 10 $Å s^{-1}$ (Cooke evaporator and Cooke Vacuum Products).

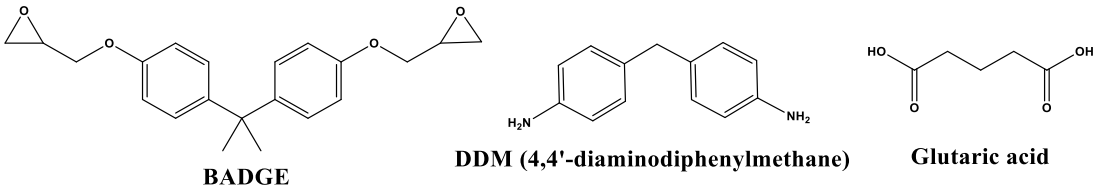

Figure 5.1: Molecules used in this work

5.2.2 Sample Preparation

Four types of samples were prepared: 1. SiO_2 surface, 2. Epoxy/SiO_2 buried, 3. Cu surface, and 4. Epoxy/Cu buried. For each of these samples there was a control (no flux), flux, flux wash 5s, and flux wash 4 hours. The flux surfaces were prepared by spincasting a 1.5% (by mass) glutaric acid/water solution on either SiO_2 or Cu at 2500 RPM for 30s. These prepared surfaces were analyzed directly for the surface characterization or contacted with epoxy for the buried analysis. To wash the surfaces, a hot water bath (500 mL of deionized water) was stirred and heated to 70°C and the prepared fluxed surfaces were submerged for either 5s or 4 hours. To prepare the Cu buried epoxy interfaces, epoxy thin films were first prepared by spin coating a toluene solution of BADGE and DDM on fused silica windows (Speedline Technologies P-6000). A stoichiometric mole ratio of two BADGE to one DDM was used, shows all molecules used in this study. The solution concentration was ~60 gL^{-1}, which resulted in a film thickness of approximately 200 nm.[6] Samples were initially cured at room temperature and pressure for 1 h after which they were held under vacuum to remove residual solvent. Following the vacuum treatment, the epoxy coated SiO_2

substrates were put in contact with the Cu surfaces, which were prepared previously. All vapor deposited Cu substrates were used within 24 h of Cu deposition. Next, the samples were cured for 1 h at 50°C, 45 min at 75°C, and 30 min at 110°C.[6] To prepare the SiO_2 buried epoxy samples, prisms were coated with flux and then a mixture of melted BADGE:DDM (2:1 mol ratio) was applied to the surface and cured as described previously.

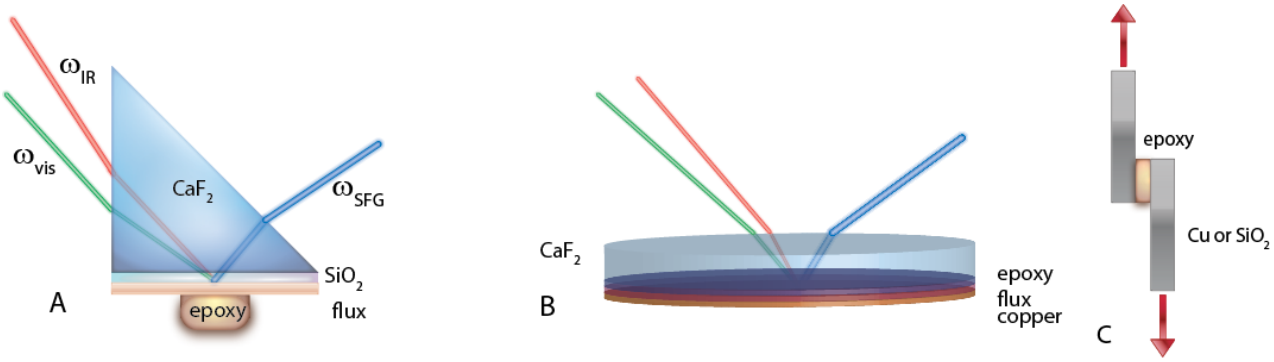

Figure 5.2: Experimental geometry used in this study: (A) SFG prism geometry to collect spectra on SiO_2 surfaces or at SiO_2 interfaces, (B) SFG window geometry to collect spectra on Cu surfaces and at Cu interfaces, (C) Lap shear analysis.

5.2.3 Lap Shear Adhesion Testing

Adhesion lap shear tests were performed at room temperature using a method based on ASTM D3163, with the Instron 5544 (Figure 5.2). When the adherents were completely separated, an abrupt drop in adhesion strength was observed. The maximum adhesion strength observed before the sudden drop in force was utilized for all reported adhesion strength measurements. The adherents utilized were made of SiO_2 slides or Cu sheets. All results are the average data measured from eight or more samples.

5.3 Results and Discussion

5.3.1 Flux on SiO_2 surface

SFG ssp and ppp spectra were first collected from the SiO_2 surface coated with flux without washing (Figure 5.3). Here, both the SFG ssp and ppp spectra are dominated by three peaks at 2865 cm^{-1} (CH_2 symmetric stretching (d+)), 2920 cm^{-1} (CH_2 asymmetric stretching (d-)), and 2940 cm^{-1} (CH_2 Fermi resonance) (Figure 5.3).[7] The flux was then washed by hot water for 5s, and SFG spectra were collected from the SiO_2 surface with flux after washing for 5s (Figure 5.3). The spectra are similar to those collected from the SiO_2 surface with flux without washing. For both the SiO_2 surfaces with flux without and with short washing, flux molecules on the surface are very

ordered, and the SFG signals from the flux can be easily seen. SFG spectra were then collected from the SiO_2 surface with flux after washing for 4 hours. After such a long washing step, the SFG flux C-H signals decreased substantially (Figure 5.3). However, in addition to the ordered flux, very strong water signal was observed in the spectrum. This is interesting because the samples were dried with N_2 after the washing steps, indicating that water could be strongly adsorbed to the silica surface. The weaker flux signal detected may be due to a less ordered interface or less flux material on the surface. The main conclusion from the SFG studies on the silica surface with flux before and after washing is that flux molecules could be very ordered on the surface and it is difficult to remove. Even after a long time of washing (4 hours), there is still some signal from flux detected and ordered water adsorbs to the surface.

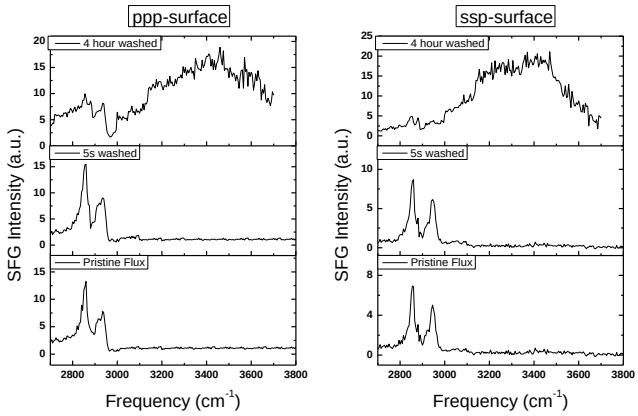

Figure 5.3: SFG spectra of the Silica surface collected in the ppp (left) and ssp (right) polarization combinations. SFG spectra collected from pristine flux on SiO_2, 5s wash, and 4 hours wash are shown from bottom to top, respectively.

5.3.2 SiO_2/Flux Buried Interfaces

The next system that was investigated with SFG spectroscopy, was the SiO_2/epoxy buried interface. The same three systems with epoxy plus a control (no flux, the SiO_2/epoxy interface) were probed (Figure 5.4). For the control SiO_2/epoxy interface, no SFG signal was detected, indicating a disordered interface, or epoxy molecules at the interface are disordered. The SiO_2/epoxy interfaces often do not give any SFG signal,[8] which is due to the disordered interface. For the three SiO_2/epoxy interfaces with flux added to the SiO_2 surface with and without washing, strong SFG signals were detected in all of them. There are five peaks in most of these SFG spectra: 2860 cm^{-1} (CH_2 symmetric stretching (d+)), 2885 cm^{-1} (CH_3 symmetric stretching), 2920 cm^{-1}, CH_2 (asymmetric stretching (d-)), 2950 cm^{-1} (CH_3 Fermi), and 3065 cm^{-1} (phenyl v_2).[9] SFG spectra collected from the SiO_2 (with flux without washing)/epoxy interface has the highest signal.

SFG spectra collected from the SiO_2 (with flux with 5 s washing)/epoxy interface have decreased intensities, due to the fact that some of the flux could be washed off. For the SFG spectra collected from the SiO_2 (with flux with 4 hours of washing)/epoxy interface, SFG signal intensities further decreased substantially, with some water signal detected. The SFG spectra collected from the buried epoxy interfaces are well correlated to the SFG spectra collected from the SiO_2 surfaces discussed above.

From the SFG data obtained from the buried epoxy interfaces, it can be inferred that flux is still at the interface after washing, because if it was removed then no signal would be detected. There is a very high level of order of the flux molecules at the SiO_2/epoxy interface without washing the flux. A 5 s washing of the flux only changed the SFG spectra slightly, indicating a change in the amount and/or orientation of the methyl/methylene groups (from flux and epoxy) at the interface, but they should still be very ordered. After the long washing step of 4 hours, we see water signal, just like the surface measurements. Water adsorbs on the flux surface and remains even after the epoxy curing step. Much smaller intensities of SFG spectra of flux were detected from the buried interface, which is also well correlated to the surface study data presented above.

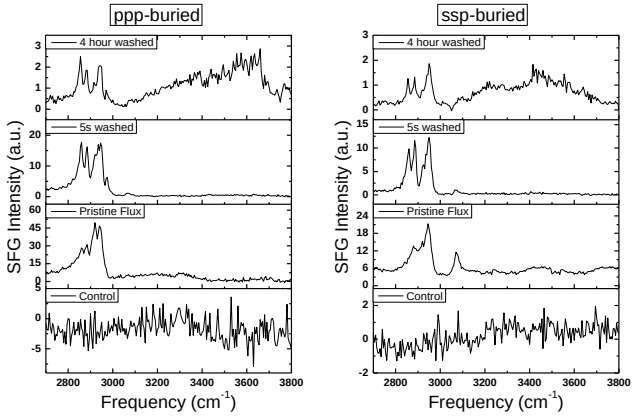

Figure 5.4: SFG spectra of the SiO_2/epoxy buried interface collected in the ppp (left) and ssp (right) polarization combinations. The SFG spectra collected from the interfaces between epoxy and SiO_2 (Control), SiO_2 with flux, SiO_2 with flux after 5 s wash, and SiO_2 with flux after 4 hour wash are shown from bottom to top, respectively.

5.3.3 Flux on Cu Surface

Next, the Cu surface with flux was investigated (Figure 5.5). For the SFG ppp spectrum collected from flux on Cu, there are two peaks present at 2860 cm^{-1} (CH_2 ss) and 2920 cm^{-1} (CH_2 as). The peak at 2860 cm^{-1} is more resolved after the short 5s washing, but the overall spectral intensities are only slightly lower, showing that 5s washing cannot remove the flux from the Cu surface. No

resolved peaks following the long washing of 4 hours were observed, which may indicate the complete removal of the flux from the Cu surface. Here the reason the peak is negative comes from the phase term and is a result of interference from the non-resonant SFG signal from the metal surface. The long washing sample also has very high non-resonant SFG signal, which could be from the flux removing the metal oxides on the surface and leaving a more conductive surface.

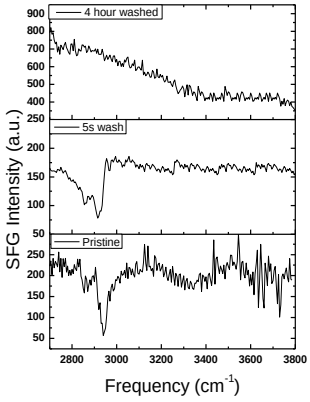

Figure 5.5: SFG spectra (ppp) of the Cu surface with flux (control), with flux and after 5s wash, and with flux and after 4 hour wash are shown from bottom to top, respectively.

5.3.4 Cu/Flux Buried Interface

The final system investigated with SFG was the Cu/epoxy buried interfaces (Figure 5.6). As we have demonstrated previously, for SFG ppp spectra collected from a thin polymer film on metal, signals are mainly from the buried polymer/metal interface.[10, 11] For the control Cu (with no flux)/epoxy interface, there are two peaks that resolve at 2860 cm^{-1} (CH_2 ss) and 2965 cm^{-1} (CH_3 as), contributed from the epoxy at the Cu/epoxy interface. For the SFG ppp spectrum collected from the Cu (with flux)/epoxy interface the peaks are similar with the addition of a new peak at 3080 cm^{-1} which is due to the phenyl in BADGE. The peak at ~2860 cm^{-1} becomes wider, containing a contribution from flux at the interface. The overall spectra intensity decreased substantially, which indicated that the presence of flux at the interface made the interfacial epoxy more disordered. For the SFG ppp spectrum collected from the Cu (with flux after 5s washing)/epoxy interface, the spectrum is considerably different than the former two, with peaks at 2870 cm^{-1} (CH_3 ss), 2920 cm^{-1} (CH_2 as), 2950 cm^{-1} (CH_3 Fermi), and a very broad peak around 3400 cm^{-1}, which can be assigned to water. The different spectrum that was collected from the control sample shows that the flux molecules are ordered at the interface. The SFG spectrum

collected from the Cu (with flux and after 4 hour washing)/epoxy interface contained no C-H signal, indicating that there was no detected flux at the interface, and strong water peaks were detected.

For the buried interface between Cu (with or without flux, before and after wash), SFG spectra collected from the control Cu (with no flux)/epoxy and the Cu (with flux no wash)/epoxy buried interfaces look very similar to each other, indicating the epoxy is dominating the signal. The broadened ~2860 cm^{-1} peak indicated the presence and ordering of the flux molecules at the Cu (with flux no wash)/epoxy interface. Interestingly, after 5s wash, the spectrum collected from the Cu (with flux after 5s wash)/epoxy interface greatly changed and more methylene peaks were detected, which could be from either the flux or the epoxy. After long washing the only detected signal comes from ordered water at the Cu/epoxy interface. This indicates that the flux is removed or disordered and the epoxy has become very disordered as well at the Cu (with flux after 4 hour wash)/epoxy interface. By studying both the surface and buried interface we can determine that after long washing there is no flux on the Cu surface or at the Cu/epoxy interface.

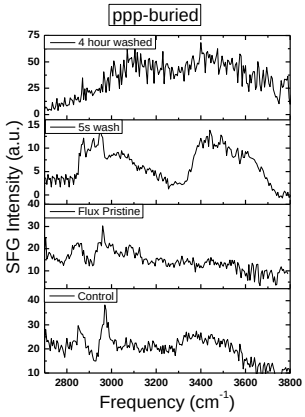

Figure 5.6: SFG spectra (ppp) of the control Cu (no flux)/epoxy, Cu (with flux and no wash)/epoxy, Cu (with flux and after 5s wash)/epoxy, and Cu (with flux and after 4 hour wash) buried interfaces are shown from bottom to top, respectively.

5.3.5 Discussion of SFG Results

The SiO_2 and Cu surfaces are both industrially relevant and unique in how each interacts with the fluxing agent. The interactions with silica and flux should predominantly be physical, while the Cu surface can react chemically and the flux can remove metal oxides from the surface. The SFG spectra for both Cu and silica surfaces are similar in the sense that they show well-ordered interfaces and the methylene functional groups from the flux were detected in both. There is not

much detectable difference between unwashed flux on the surface and the short washing systems, indicating that this washing does little to perturb or remove the flux residue. The long washing systems are quite different, where the silica shows both flux and water, while the Cu only shows water and a very high non-resonant SFG signal due to the high degree of polarizability of the metal (with initial surface metal oxide removed). This is reasonable as the silica surface cannot chemically react with the flux, while the Cu surface can chemically react with the flux and the byproducts can be easily removed with the washing step. The chemical reaction between copper oxides and flux produces water and the copper salt.[5]

The buried control interfaces between epoxy and SiO_2 or Cu without flux show different SFG spectra, where the epoxy at the silica interface is disordered and at the Cu interface has order. This could be due to intrinsic differences between the silica and Cu, which determine the level of order of epoxy at the buried interface. After adding the flux to the silica or Cu surface, the silica/epoxy interface became very ordered and the Cu interface remained mostly the same and the interfacial functional groups potentially reoriented slightly. After the short washing step on the surface, flux was still detected at both interfaces, but no water was detected at the silica interface, while at the Cu interface water was detected. After the long washing step, the silica interface showed water and much less flux, while the Cu/epoxy interface showed just water. This shows that it is more difficult to remove flux residue from the silica surface and is easier to remove flux residue from the Cu surface. The results obtained from the buried epoxy interfaces can be well correlated to those obtained from the SiO_2 or Cu surfaces. By studying the exposed surface and buried interface we can better understand how flux behaves at various interfaces.

The spectral data shows how flux behaves at silica and Cu surfaces and their interfaces with epoxy. At the silica surface, the flux was more difficult to remove and did not change the chemistry of the surface, while at the Cu interface the flux could be removed with longer washing and it did change the Cu surface, removing the copper oxides. Previous work showed that adipic acid at 100° has an oxide etch rate of 1 nm/s.[5] Our system has Glutaric acid and was heated at 70°, we believe that under our experimental conditions, copper oxide on the surface can be removed.

5.3.6 Lap Shear Analysis

In order to better understand how flux residue can affect the reliability of packaging, we performed lap shear analysis (Figure 5.7). This method of testing can indicate how the flux residue changes

the bonding strength of the two surfaces and ultimately, how reliable a package is. **(1) Silica:** For the interfaces between epoxy and silica with no flux, the measured adhesion (MPa) is 1.22±0.10; silica with flux but no wash 0.97±0.06; silica with flux after 5s washing, 0.95±0.08; and silica with flux after the 4 hour wash, 1.26±0.10. The control and the long washing systems have the same adhesion when accounting for the error bars. The interface between silica and epoxy (with flux at the interface) and the interface between silica and epoxy (with flux on the silica surface and with 5s wash) also have similar adhesion strength. The lower adhesion of the silica (with flux)/epoxy interface than the control sample indicates that the interfacial flux reduced the adhesion between silica and epoxy, therefore it is necessary to remove the flux at the interface. The similar adhesion of the silica (with flux)/epoxy and silica (with flux after 5s wash)/epoxy interfaces indicates that the short washing for 5s does not significantly remove flux residue from the SiO_2 surface. The longer washing step does remove flux, leading to the similar adhesion at the silica (with no flux)/epoxy and silica (with flux after the 4 hour wash)/epoxy interfaces. **(2) Copper:** For the interface between epoxy and Cu surface with no flux (control), the measured adhesion (MPa) is 2.70±0.18; Cu with flux no wash, 2.26±0.28; Cu with flux after 5s washing, 3.09±0.34; and Cu with flux after the 4 hour wash, 4.64±0.40. Apparently, the control sample of the Cu (no flux)/epoxy interface has a higher adhesion strength than the Cu (with flux)/epoxy interface, again indicating that the interfacial flux reduced adhesion at the Cu/epoxy interface. Both washing treatments improve the adhesion of the Cu/epoxy interfaces. The long washing step has an increase in adhesion of 40%, which should be due to the oxides being removed from the metal surface.

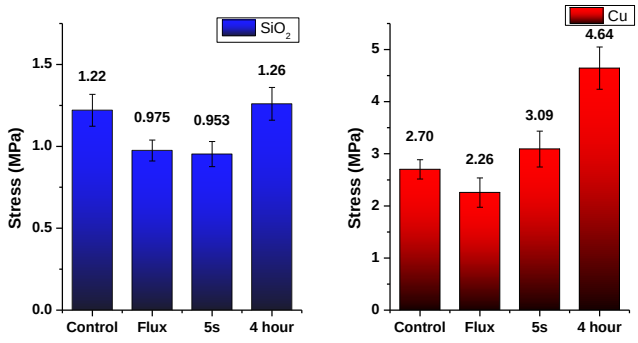

Figure 5.7: Lap shear analysis results, SiO_2 interfaces on the left and Cu interfaces on the right. Plots show the measured adhesion results from interfaces between epoxy and silica or Cu without flux (control), with flux, with flux and after 5s wash, and with flux and after 4 hour wash.

Here the lap shear results are well correlated to SFG data presented above. The flux cannot chemically react with the silica surface, thus the original decrease in adhesion with flux was due to the flux residue film on the surface, where the epoxy was partially sticking to the flux film and the silica surface. This was confirmed by our SFG study presented above. Short washing time 5s could not remove the flux from the SiO_2 surface, as indicated by SFG results. Therefore, similar low adhesion was measured at the silica (with flux)/epoxy and silica (with flux after 5s wash)/epoxy interface. SFG data showed that long washing time of 4 hours could effectively remove the flux on SiO_2, leading to similar adhesion strength at the silica (with flux after the 4 hour wash)/epoxy interface and the control system. Therefore SFG results can easily interpret the measured adhesion strengths: The adhesion decreases once flux is applied and then after long washing the adhesion returns to the same strength as the control. But there is still flux remaining, as determined by SFG, so there must be considerably less flux, but a residue still remains after the long washing step.

It is expected that the adhesion on the Cu surface can be increased by fluxing, and this is what we observed. The fluxed surface has lower adhesion to epoxy, which indicates the surface has not been cleaned by the flux and the residue is preventing the epoxy from making good contact, confirmed by SFG data presented above. After short washing the adhesion increases to a little more than the control, the SFG spectrum was markedly different at the interface of Cu (with flux after 5s wash)/epoxy compared to that detected from the Cu (with flux)/epoxy interface. The long washing shows an increase of 40% as compared with the control. This is a very high increase and shows that the Cu surface has much higher adhesion following fluxing and long washing. Our SFG data showed that such a long time washing removed flux from Cu surface after flux removed Cu oxides. The adhesion at the interface between epoxy and Cu (after Cu oxides removed) is higher than that at the Cu (with oxides)/epoxy interface.

5.4 Conclusions

In this work, molecular behaviors of a flux molecule, glutaric acid, on silica and Cu surfaces and their interfaces with epoxy were investigated using SFG spectroscopy. The effects of short and long washing treatments were also examined. It was shown that at the silica surface, the flux is difficult to remove and persist even after long washing. The Cu surface is easier to clean, with the long washing removing the flux. The buried SiO_2/epoxy interface is very disordered, but by adding

flux, the interface becomes very ordered. After washing, there is water detected at the interface. The Cu/epoxy buried interface is ordered and after adding flux it is still ordered. After washing there is water that is detected in the spectra and after long washing the flux is removed. The SFG results can be correlated to the lap shear data, which showed with the flux at the interface, the adhesion was lower for both the silica/epoxy and Cu/epoxy interfaces. After the long washing for flux on silica, even though not all the flux can be removed, the SFG signal drop indicated that some flux could be removed, and the adhesion at the silica (with flux after long time washing)/epoxy interface returned to the original silica/epoxy interface. Differently, for Cu (with flux after long time washing)/epoxy interface, the adhesion is larger than the original Cu/epoxy interface. This is because the flux can react with the Cu oxide layer and after a long time of washing, flux could be removed, therefore the Cu (without oxide)/epoxy interface has a stronger adhesion. At this interface, SFG non-resonant signal increased. We believe that this is because of the removal of Cu surface oxides by flux, which also increased adhesion by 40% after the long washing step.

This work provides important insight into the real problem faced in industry: how flux materials behave at silica and Cu surfaces and their interfaces with epoxy. Fluxes are ubiquitous in the microelectronics industry and a better understanding of them will hopefully provide knowledge needed to improve package reliability. Fluxes can be very difficult to remove from surfaces and the surface itself has a large role in how easily the flux can be removed. The flux greatly changes the silica buried interfaces, while the Cu interface is still dominated with the epoxy signal, which implies that the surface has a large role in mediating interfacial interactions, resulting in varied buried interface structures. For the silica surface the main decrease in adhesion strength comes from the flux residue preventing good contact with the silica surface and following long washing the adhesion returns to that of the control. For the Cu surface, just flux residue (with no wash) decreased the adhesion with epoxy, but after short and long washing the Cu surface, the adhesion with epoxy greatly increases because flux removed the surface oxides.

This work illustrates the power of SFG spectroscopy as an analytical tool to investigate important buried interfaces at the molecular level for the microelectronics industry. SFG has sub-monolayer sensitivity, can operate at standard temperature and pressure, and is noninvasive for buried interface investigation. There are few techniques that can provide this level of detail with such

little sample preparation, and none that can investigate buried solid/solid interfaces in situ in real time.

5.5 References

[1] C.-L. Chung, K.-S. Moon, and C. P. Wong, "Influence of flux on wetting behavior of lead-free solder balls during the infrared-reflow process," *Journal of Electronic Materials,* vol. 34, pp. 994-1001, 2005.

[2] J. C. Lin and C. L. Huang, "Bump structural designs to minimize package defects," ed: Google Patents, 2017.

[3] B. Tunaboylu, "Testing of Copper Pillar Bumps for Wafer Sort," *IEEE Trans. Compon. Packag. Manuf. Technol.*, vol. 2, pp. 985-993, 2012.

[4] T. Muto, "ome reliability problems of surface-mounted devices,," *IEEE Circuits and Devices*, vol. 4, pp. 9-13, 1988.

[5] G. Qua, S. S. S. Veguntaa, K. Maia, C. J. Weinmanb, T. Ghoshb, W. Wub*, et al.*, "Copper Oxide Removal Activity in Nonaqueous Carboxylic Acid Solutions," *Journal of The Electrochemical Society*, vol. 160, pp. E49-E53, 2013.

[6] S. Onard, I. Martin, J.-F. Chailan, A. Crespy, and P. Carriere, "Nanostructuration in Thin Epoxy−Amine Films Inducing Controlled Specific Phase Etherification: Effect on the Glass Transition Temperatures," *Macromolecules,* vol. 44, pp. 3485-3493, 2011.

[7] N. A. Valley, P. G. Blower, S. R. Wood, K. L. Plath, L. E. McWilliams, and G. L. Richmond, "Doubling Down: Delving into the Details of Diacid Adsorption at Aqueous Surfaces," *The Journal of Physical Chemistry A,* vol. 118, pp. 4778-4789, 2014.

[8] J. N. Myers, C. Zhang, K.-W. Lee, J. Williamson, and Z. Chen, "Hygrothermal Aging Effects on Buried Molecular Structures at Epoxy Interfaces," *Langmuir,* vol. 30, pp. 165-171, 2014.

[9] G. P. Harp, H. Rangwalla, M. S. Yeganeh, and A. Dhinojwala, "Infrared-Visible Sum Frequency Generation Spectroscopic Study of Molecular Orientation at Polystyrene/Comb-Polymer Interfaces," *J. Am. Chem. Soc.*, vol. 125, pp. 11283-11290, 2003.

[10] X. Lu, G. Xue, X. Wang, J. Han, X. Han, J. Hankett, *et al.*, "Directly Probing Molecular Ordering at the Buried Polymer/Metal Interface 2: Using P-Polarized Input Beams," *Macromolecules*, vol. 45, pp. 6087-6094, 2012.

[11] J. N. Myers, X. Zhang, Y. Xiu, Y. Wei, J. M. Williamson, K. W. Lee, *et al.*, "Nondestructive Characterization of Molecular Structures at Buried Copper/Epoxy Interfaces and Their Relationship to Locus of Failure Analysis," *IEEE Transactions on Components, Packaging and Manufacturing Technology*, vol. 5, pp. 1432-1440, 2015.

Chapter 6: Conclusions and Outlook

The primary goal of this dissertation work was to further develop SFG spectroscopy into a powerful tool to probe buried interfaces and advance the understanding of interfacial structures of common materials and variations of interfacial structures with common methods utilized in the microelectronics industry. The SFG techniques utilized enabled us to nondestructively probed buried solid/solid interfaces *in situ* at the molecular level, which cannot be done with other analytical techniques. Several treatments were performed on polymer and inorganic surfaces to see how they change the structures and thus properties of surfaces and the surface/epoxy buried interfaces. This work focused on understanding the structure-property (e.g., adhesion) relationships at interfaces, adhesion mechanisms, and how to improve adhesion. Specifically, we investigated the effects of SAPs, plasma treatment, and flux treatment on the interfacial structures and their impacts on interfacial properties. In addition to adhesion improving methods, which were all model systems, new metrology was also developed to enable probing of real flip-chip (FC) devices, something that has never before been done with SFG. In chapter 2, SAPs were added to epoxy mixtures and then exposed to hygrothermal aging. It was found that SAPs migrate to the interface and can greatly change the interfacial molecular orientation/ordering to prevent the adhesion loss after hygrothermal aging. Chapter 3 focused on plasma treatment of polymer films to determine, A. if covered surfaces are heterogeneously affected by plasma, and B. how plasma treatment can increase adhesion between polymers and adhesives. Chapter 4 studied real systems, using SFG to probe various buried interfaces found in FC devices. Chapter 5 focused on flux treatment of surfaces and how it changes the buried interfacial structure and macroscopic properties. Detailed results from each of the above chapters will be presented below.

In chapter 2, the molecular structures at buried polymer/epoxy interfaces were probed before and after hygrothermal aging, to see how the interface is affected by the aging process and to determine if ordered interfacial water forms. As determined by SFG spectroscopy, the hydrophobic interface was well ordered and no ordered water formed following hygrothermal treatment. In contrast, at

the hydrophilic polymer/epoxy buried interface, highly ordered water was detected. This shows how the polarity of the polymer greatly influences the buried interfacial structure at the polymer/epoxy interface. In addition to these two controls, small amounts of SAPs were added to the epoxy mixture to see how they would change the interface and if they can prevent any ordered water from forming. There were small differences seen in the SFG spectra for the hydrophobic interface, but the hydrophilic interface was greatly changed, and no detected water was found, indicating that SAPs can prevent interfacial water. Interestingly, bulk water was detected in all eight systems, while interfacial water was only detected at the hydrophilic control. Mechanical testing was performed on the above systems to determine the changes in adhesion strength caused by hygrothermal aging and if SAPs can prevent any adhesion loss. It was found that a very small amount of SAPs can greatly decrease the adhesion loss. Particularly, it was found that there was less adhesion loss at the hydrophilic interface than the hydrophobic interface. By combining studies on interface, bulk, and mechanical properties, a comprehensive understanding on the effects of hygrothermal aging on adhesion can be obtained.

Preventing water at buried interfaces is very important to mitigate moisture induced failure modes. This study provides a better understanding of polymer/epoxy interfaces with SAPs added and how they interact with hygrothermal aging. By understanding these systems better we can design more resilient epoxy systems and use the best additives to prevent moisture induced failure.

In chapter 3, plasma effects were investigated to show how covered polymer surfaces behave and to determine how plasma treatment increases adhesion strength. It was found with SFG that covered polymer surfaces are affected heterogeneously, with the edge becoming greatly disordered following treatment. It was determined that the orientation of functional groups of polymers changes greatly at the edge position, while the middle position remains constant through plasma treatment. The mechanism for plasma-based adhesion was found to primarily come from the disordering of the polymer surface, which was qualitatively and quantitatively determined using SFG spectroscopy. The adhesion strength, as measured with lap shear, increased by 30%, following He plasma treatment. These results provide valuable insight into plasma treatment of polymers and how it can disorder and reorient polymer surfaces.

Delamination at polymer/epoxy interfaces due to weak interfacial adhesion continues to be a reliability concern in microelectronic packaging. Plasma treatment is widely used to increase the

adhesion strength of polymer to epoxy underfill materials, however, the adhesion mechanism is not well understood and must be investigated further. This research indicates that buried interfacial molecular structures are strongly affected by plasma treatment, which should be considered in adhesion mechanisms and such structures should be correlated to adhesion strength measurements. Relationships between adhesion strength and interfacial molecular orientation at buried adhesive/polymer interfaces can then be used to design interfacial structures with predicted adhesion properties in microelectronic packages that can withstand accelerated stress testing.

In chapter 4, new SFG metrology was developed to probe real FC devices. This is the first time SFG has been utilized to probe real microelectronic samples. Typically model systems are used to simplify the data collection. This work drastically propels SFG capabilities forward and demonstrates the power of SFG as an analytical technique. Texas Instruments supplied us with FC devices and polished them to varying thicknesses to expose three interfaces that generate SFG signal: PI/MC, MC/air, and MC/LF. Quantitative orientation was determined for the methyl groups of the MC. It was found that the hydrophobic methyl groups lie down more at the more hydrophilic LF interface and stand up more at the, more hydrophobic PI interface. At the exposed MC/air interface, the methyl groups partially stand up at the surface. This research shows the power of SFG and its noninvasive capabilities. Determination of detailed orientation at buried solid/solid interfaces is impossible with traditional techniques, especially when probing real electronic devices.

In chapter 5, flux characterization was performed at the surface and buried interface in an effort to better understand device failure due to flux residue. Cu and SiO_2 surfaces and buried epoxy interfaces were probed with SFG and mechanical testing. Washing the fluxed surfaces was performed to determine how easily the flux material can be removed from the surface. By studying both the exposed surface and buried interface we can understand how easily flux can be removed, and how the flux changes the buried interfacial structure when contacted with epoxy. Flux material greatly changes the structure of the buried interface, causing it to be more ordered. It was found that flux material is very difficult to remove from the SiO_2 surface and easier to remove from the Cu surface, which may be due to fluxes ability to react with Cu more readily than with SiO_2. In addition to SFG analysis, lap shear testing was also performed. It was determined that the flux residue reduces adhesion strength. Following extended washing, the SiO_2 system has similar

adhesion as the control, while the Cu system has higher adhesion strength after extended washing, indicating that the flux is actually improving the adhesion by removing CuO_x's from the surface. This is very important work that attempts to elucidate a common industry problem, where flux residue can cause premature failure of devices.

The general nature of the methodology developed in this thesis will enable it to be directly utilized by the growing number of research groups that use SFG for interface characterization. The information generated by studying adhesion promoting treatment is directly valuable to the microelectronics industry. This thesis work focuses on investigating surfaces and solid/solid buried interfaces and correlating them to interfacial molecular structure properties. We have elucidated general interfacial structure-property relationships and correlated them to surface and epoxy mixture modification. Predicting interfacial properties in microelectronic packaging models is very challenging and the structure-property relationships derived herein can be directly used by the microelectronics industry. The work in this thesis contains fundamental scientific research, but the implications have broad applications to surface treatment and adhesion promotion. Moreover, the structure-property relationships elucidated in this thesis are general and can be applied in many technical areas where polymer/solid interfaces play an important role, e.g. polymer composites, optical fibers, paints, and anti-corrosion coatings.

There are several ways to extend the work presented in this research. The work in chapter 2 can be extended by looking at more polymers, using more SAPs, and different epoxy materials. By using more polymers we could confirm the trends that we saw with our hydrophobic and hydrophilic polymers, and see if the polarity of the polymer determines the amount of interfacial water that forms after hygrothermal aging. We could investigate more epoxy materials to see if there are any that prevent interfacial water from forming without SAPs. By studying even more SAPs, one may be found that can completely prevent any loss of adhesion following hygrothermal aging.

The work in chapter 3 can be extended by varying the height of the protective cover and using more plasmas. By changing the height of the protective we can see at what height the plasma effects begin to be more homogeneous. At some height, the time dependent plasma effects that were observed should no longer appear. For the plasma-base adhesion promotion, more reactive plasmas could be used to see if the adhesion could be improved even more. By using He, an

increase in adhesion of 30% was measured, but O_2 or Ar may improve the adhesion to a greater degree.

The work in chapter 4 can be extended by directly looking at more real FC devices. More FC devices could be manufactured, polished, and probed with SFG to see how the orientation of methyl groups change with different devices. By probing FCOL devices with different processing conditions we could determine trends and correlate the interfacial molecular structures with macroscale properties.

The work in chapter 5 can be extended by looking at more fluxes and epoxy materials. By looking at more fluxes, we can determine which ones are most easily removed and increase the adhesion of Cu the most. It would be interesting to see if certain epoxy materials could solubilize the flux material and reduce adhesion loss. Using real fluxing agents would also be an excellent way to extend this research. By using the same flux materials that industry uses we can more directly probe relevant systems and our conclusions would be more valid.